TITANIA: Model Free Interpretation of Residual Dipolar Couplings in the context of Organic Compounds

Felix A. Roth, Volker Schmidts, Christina M. Thiele*

Clemens-Schöpf-Institut für Organische Chemie und Biochemie, Technical University of Darmstadt, Alarich-Weiss-Str. 16, 64287 Darmstadt (Germany), E-mail: cthiele@thielelab.de

NMR spectroscopy, configuration determination, residual dipolar couplings, model-free, vector orientation

ABSTRACT: Residual dipolar couplings (RDCs) become increasingly important as additional NMR parameter in the structure elucidation of organic compounds, but are usually used in fitting procedures to discriminate between (computed) structures that are in accordance with RDCs and others that can be ruled out. Thus determination of configurations requires prior structural information. The direct use of RDCs as restraint to construct structures based on RDCs has only recently begun also in organic compounds. No protocol has been published though, which uses the vector and dynamics information available in multi alignment data sets directly for the joint determination of conformation and configuration of organic compounds. This is proposed within the current manuscript. We show that employing these data even a flat or random start structure converges into the correctly configured structure when employing multiple alignment data sets in our iterative procedure. The requirements in terms of number of RDCs and alignment media necessary are discussed in detail.

INTRODUCTION

Nuclear magnetic resonance spectroscopy (NMR) provides a wealth of spectroscopic observables encoding the molecular structure and dynamics of the investigated compounds. Complementary information is accessible from chemical shifts, isotropic scalar *J* coupling constants and the nuclear Overhauser effect (nOe).[1-4] Additionally, anisotropic observables of compounds aligned with respect to the magnetic field like residual dipolar couplings (RDCs) have proven to be a reliable tool for the determination[5-10] and refinement[11-15] of both small molecules and biomolecular structures. Standard protocols for RDC-based structure determination assume rigid structure models and a single tensor (e.g. the alignment tensor **A**) describing the molecular alignment following the classical formalism by Saupe.[16-17] This tensor is generally unknown and calculated by a fitting procedure utilizing e.g. singular value decomposition (SVD) as introduced for RDC order matrix analyses by Losonczi in 1999.[18] Discrimination of structure models is based on correlation of experimental RDCs D_{exp} and RDCs back-calculated from the order matrix model, D_{calc} (see Figure 1). The description of conformational flexibility or other forms of intramolecular dynamics is often modeled by ensemble averaging of rigid equilibrium geometries [10, 19-20] thus limiting the information from experimental RDCs by the choice or parametrization of the models employed in fitting.

For the interpretation of RDCs in biomacromolecules, the so called "direct interpretation of dipolar couplings" (DIDC)[21-22] and "model free approach" (MFA)[23-24] have been proposed, which do not rely on a strict definition of an alignment tensor and a molecular geometry but rather directly express the experimental RDCs as a function of dynamically averaged vector orientations.

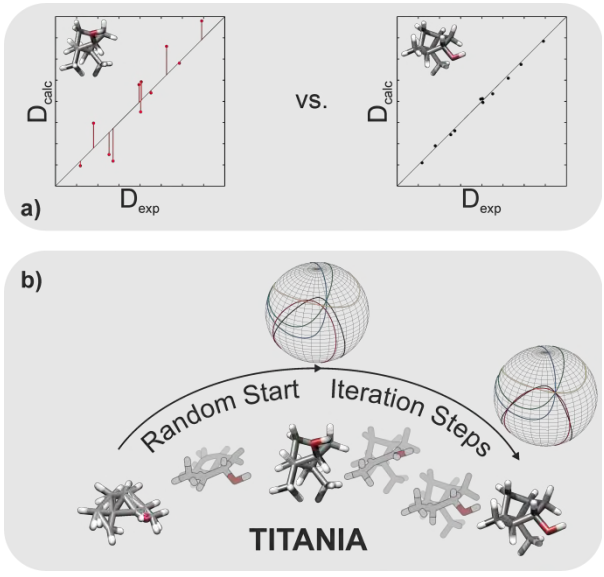

Figure 1. Conventional RDC analyses validate experimental data by correlating them with back calculated data (see top **a**). TITANIA directly interprets RDC data to derive RDC vector orientation and dynamic information to determine the correct stereochemistry of the compound (see bottom **b**).

The DIDC minimizes the RDC vector motion needed to explain the experimental data while the MFA uses spherical harmonics, as proposed by Lipari and Szabo for the interpretation of relaxation data,[25-26] to describe internal motion. The underlying algorithms were extended to iterative schemes to improve robustness and quality of results.[27-29]

At the core of these methods is the requirement for at least five linearly independent sets of experimental RDCs (alignment conditions) and a large amount of RDC vectors,[30] to simultaneously evaluate the corresponding relative vector orientations and their respective distribution(s). The wealth of RDC data experimentally accessible in labelled biomacromolecules enabled the development and broad application of these methods in that field. Modern developments in alignment media[31-39] compatible with small organic molecules, introducing different alignment conditions combined with new NMR pulse sequences[40-49] designed to give easier access to crucial long-range $^{n}D_{XH}$ and $^{n}D_{HH}$ RDCs may now finally allow to extend the model free approach also to organic compounds. This is investigated within the current manuscript. The crucial linear independence of alignment conditions is assessed here by methods based on principle component analysis, like the self-consistency of dipolar couplings analysis (SECONDA) protocol by Hus and Brüschweiler.[50-51]

When applying the model free approach to small molecule RDC analysis, the additional challenge stems from the fact that the relative configuration of stereogenic centers is introduced as additional unknown, the determination of which is coupled to the determination of unknown conformation. Recent approaches for organic compounds focused on alternative algorithms employing (pseudo) force fields (FF). Cornilescu *et al.* introduced progressive stereo locking (PSL) in combination with FF methods in 2017 to resolve the relative configuration and conformation of small molecules in Xplor-NIH.[52] In 2018 Immel *et al.* used a floating chirality restrained distance geometry and distance bound driven dynamics (fc-rDG/DDD) protocol to generate structural models and optimize them according to RDC restraints in configurational and conformational architect (ConArch^{+}).[53] Furthermore, tensorial restraints are employed in the MD protocol published as computer simulation of molecular structures (COSMOS) by Sternberg and Luy.[54-56] These algorithms have in common that the optimization of the structures is performed on the difference of user defined experimental NMR observables and the back-calculated values to define or extend a (pseudo) force field. In addition, multiple alignment media are treated as individual sources of information for the refinement of structures and not globally as is proposed here.

We present a new five alignment media MFA, which has to the best of our knowledge not been established for organic compounds. It is implemented in the new C++ program TITANIA (TITANIA performs iterative analysis of independent alignments), which interprets RDCs by *directly calculating individual RDC vector orientations and their dynamics*. For the given sets of RDC data and an arbitrary starting geometry, this enables the combined investigation and refinement of conformation, relative configuration and internal dynamics from five of more RDC sets, which are interpreted as one global source of information on the 3D structure and the dynamical averaging of small molecules. We demonstrate the MFA-based RDC analysis with TITANIA on several small to medium-sized organic compounds with well-known stereochemistry and varying degrees of molecular complexity.

Theory. RDCs are anisotropic interactions described by the relation of inter-nuclear vector orientations with respect to the external magnetic field B_0:

$$D_{ij} = \frac{\kappa_{ij}}{\langle r_{ij}^3 \rangle} \frac{\langle 3\cos^2\Theta_{ij} - 1 \rangle}{2} \qquad (1)$$

where $\kappa_{ij} = -\frac{\gamma_i \gamma_j \mu_0 \hbar}{8\pi^2}$ groups physical constants for two nuclei i and j, r_{ij} is the distance between the nuclei and Θ_{ij} is the angle enclosed by the RDC vector and B_0. The $\langle\ \rangle$ brackets denote time and ensemble averaging of the respective parameters. A common approximation neglects an explicit time average of the distances r and instead uses their equilibrium distance.

Assuming a rigid geometry, the orientational order imposed onto the solute by the alignment medium is expressed by the Saupe order tensor $\mathbf{S}$[57-58] or its scaled analogue, the alignment tensor $\mathbf{A}$.[17] The alignment tensor $\mathbf{A}$ is a traceless symmetric second-rank tensor, often expressed in terms of the Euler rotations $\boldsymbol{R}(\alpha,\beta,\gamma)$ necessary to rotate its principle axis system onto the arbitrary molecular frame and its axial (A_a) and rhombic components (A_r, or more generally, the rhombicity R) denoting its shape. This common property defined relative to an external reference is the reason for the global structure information contained in RDCs. Internal dynamics lead to deviations from this simple alignment model and have to be modeled appropriately (see below). In the classically used cross validation of structures with RDCs these dynamical aspects are described by multiple conformers.[10, 19-20, 59-62]

When dealing with rotations of tensors and inter nuclear vectors, as well as the overall molecular tumbling in the alignment medium, it is convenient to express equation 1 in terms of spherical harmonics:[63]

$$\langle D_k \rangle = A_a D_{max,k} \sqrt{\frac{4\pi}{5}} \left[\begin{array}{c} \langle Y_{2,0}(\theta_k, \phi_k) \rangle + \\ \sqrt{\frac{3}{8}} R\left(\langle Y_{2,2}(\theta_k, \phi_k) \rangle + \langle Y_{2,2}^*(\theta_k, \phi_k) \rangle \right) \end{array} \right] \qquad (2)$$

Here $D_{max,k}$ is the maximum possible dipolar coupling of the spin pair k (short for the nuclei i and j), and Y are the spherical harmonics of the spherical coordinates θ and ϕ (in the principle axis system (PAS) of $\mathbf{A}$). Equivalent expressions can be formulated using Cartesian coordinates resulting in direction cosines.[17-18] The time and ensemble averages in equation 2 may be resolved by utilizing Wigner rotations for the spherical harmonics, thus giving a mathematical separation of the overall molecular tumbling (alignment parameters) from the individual vector orientation (internal dynamics).[59-61]

$$\boldsymbol{R}(\alpha,\beta,\gamma) Y_{2,m}^{(2)}(\theta,\phi) = \sum_{M=-2}^{2} e^{-i\alpha M} d_{M,m}^{(2)}(\beta) e^{-i\gamma m} Y_{2,M}^{(2)}(\theta,\phi) \qquad (3)$$

Where $\boldsymbol{R}$ is a rotation applied to spherical harmonics, represented by the reduced Wigner elements $d_{M,m}^{(2)}$ using the Euler angles α, β and γ. This formalism simplifies the transformation into any arbitrary reference system. Common reference systems (see Figure 2) are the alignment frame (AF), the vector frame (VF) and arbitrary molecular frames (MF). The AF is the principle axis system of

the alignment tensor where all non-diagonal elements become zero. In this frame, equation 2 is valid and no rotation has to be applied to describe the alignment. A more convenient frame when discussing molecular structure is the MF, which – barring any symmetry-related arguments[64] – can be chosen arbitrarily. By default, TITANIA uses the PAS of the inertia tensor of the input structure. The transformation between the MF and the AF is defined by the Euler angles α, β and γ (see equation 3) obtained from the eigenvectors of **A**. The additional VF, which is essential in the approach described herein, is unique for every RDC vector and describes the PAS of the individual vectors where $Y_{2,m} = 0$ for $m \neq 0$. The respective transformation between the VF and the MF is defined by the spherical coordinates θ and ϕ. In principle a third rotation angle φ can be defined, which describes the direction of the anisotropic RDC vector motion, i.e. the angle needed to align the major semi-axis with the y-axis of the anisotropic RDC vector cone (see red cone in Figure 2). This angle may be neglected if only RDC vector orientations are of interest (*vide infra*).

Starting from the individual VF of the respective RDC vectors a sequence of the described rotations (VF → MF → AF) can be used to obtain the general matrix equation 4. The derivation of equation 4 is conducted as in the literature[23-24] (see supporting information).

$$\mathbf{D}(M,K) = \langle \mathbf{F} \rangle (M,5) \cdot \langle \mathbf{Y} \rangle (5,M) \qquad (4)$$

Here **D** contains K RDCs in M alignment conditions and is normalized to A_a (row wise) and D_{max} (column wise). **F** combines the M Wigner rotations and rhombicity R of the respective alignment tensor and **Y** the spherical harmonics of the K RDC vectors. This denotes the previously mentioned separation of internal (local) and external (global) motion(al averaging). The normalization of **D** fully removes external, alignment media dependent averaging and allows for a model free extraction of structural parameters, defined by the rotations between the MF and the VF, and internal dynamics, encoded in the magnitude of $Y_{2,m}$.

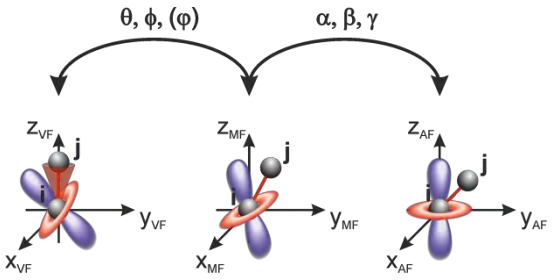

Figure 2. Reference frames used in the MFA for the determination of RDC vector orientations of the spin pair i and j. The arbitrary molecular frame (MF, middle) can be transformed into either the vector frame (VF, left-hand side) or the alignment frame (AF, right hand side). The AF is defined as the PAS of ***A*** (represented by the surface plot of $Y_{2,0}$ with color encoding the sign) where all non-diagonal elements vanish. The respective rotation is defined by the Euler angles α, β and γ. In the VF the RDC vector is parallel to the z-axis and all spherical harmonics $Y_{2,m}$ become zero for $m \neq 0$. The spherical coordinates θ and ϕ define the rotation between the VF and the MF. Dynamics of the RDC vector is represented by the red cone in the VF. The third angle φ, expressing the orientation of the anisotropic RDC motion, can be neglected when just describing the vector orientation.

With data from at least five independent alignment conditions, the spherical harmonics **Y** can be refined by SVD of **F**. If additional alignment media are used for the optimization, the accuracy and precision can be improved, but no further structure information can be obtained.[21] To extract the mean vector orientation from the respective spherical harmonics the transformation between MF and the respective VF has to be found (e.g. by the Levenberg-Marquardt algorithm).

While there are recent approaches to simulate interactions of small molecules with alignment media and predict RDCs based on a combination of molecular dynamics simulations and potential based methods[65-66] the individual alignment conditions of equation 4 are usually *a priori* unknown and have to be estimated before employing the MFA.[23-24] To increase robustness of the MFA, Lakomek *et al.* proposed the self-consistent residual dipolar coupling based model-free analysis (SCRM), which essentially is the iterative implementation of the MFA to reduce a possible bias induced by the initial alignment tensor (and thereby the initial structure model).[27] In this protocol, the initial MFA step estimates the starting alignment based on an initial model (e.g. a rigid X-ray structure, but as shown here any arbitrary set of coordinates is possible). The resulting θ and ϕ are used to start the iterative cycle, in which the refined spherical coordinates are used to recalculate the alignment tensors *via* SVD. The Wigner rotations are updated to refine the spherical harmonics and to finally update the spherical coordinates.

In addition to the structure parameters θ and ϕ, the parameters S^2_{RDC} and η describing RDC dynamics, are calculated from the spherical harmonics, where S^2_{RDC} is the order parameter for RDCs, following the definition of the Lipari-Szabo parameter S^2_{LS}.[25-26] S^2_{RDC} can be interpreted as the axial component of a local RDC tensor. The same is true for the anisotropy parameter η, which is directly linked to the third rotation angle φ (see Figure 2).

For biomacromolecules, the challenge is often the large conformational space and distribution of internal dynamics sampled by RDCs. Small organic compounds on the other hand usually have fewer intrinsic degrees of freedom but the analysis of relative vector orientation from RDCs is complicated by the smaller number of RDCs available and the unknown relative configuration of stereogenic centers. The use of long-range RDCs needed for the MFA in combination with comparatively large structural changes of small organic compounds associated to these internal degrees of freedom may lead to instabilities of the optimization algorithm when updating the Wigner rotations. Thus TITANIA not only uses the refined spherical coordinates to recalculate the Wigner rotations but also performs a full structure optimization on every step for a superior estimation of the corresponding D_{max} values. The algorithm to update the structure and the interpretation of the dynamic information is discussed in the following sections.

RESULTS AND DISCUSSION

Interpretation of structural parameters. The spherical coordinates θ and φ are the two parameters needed to define the directional vector of the respective spin pairs. One problem in RDC analysis is the indistinguishability of this vector and its inverse.

A simple algorithm for updating structures would be to string the updated $^{1}D_{ij}$ RDC vectors together, while keeping vectors constant that are not defined by RDCs (for more information on how this vector addition algorithm is implemented and on which flag needs to be used to activate it, see SI section 1.3.5). This approach has the downside that small errors in individual vector orientations can lead to major distortions in the overall structure due to propagation of errors. The differentiation of the two degenerate RDC vector directions, when updating the position of an atom i, is performed by assessing the agreement of long range RDC direction vectors ($\vec{r}_{li,RDC}$) and the respective vectors in the updated structure model ($\vec{r}_{li,struc}$) for the two possible vectors $\vec{r}_{ij,RDC}$ and $-\vec{r}_{ij,RDC}$. This assessment only affects the sign of the direction vector as determined by MFA and not the individual Cartesian coefficients.

A more advanced algorithm, implemented in the TITANIA workflow, uses redundant internal coordinates known from quantum chemical computing protocols.[67-68] In this approach standard internal coordinates[69], namely bond lengths, bond angles or dihedral angles of more atom tuples than needed to unambiguously define a structure are combined to form an overdetermined representation of a structure model. The holonomic terms (used synonymously for internal coordinates in the following) may easily be extended by additional parameters and subjected to optimization algorithms when calculating Cartesian coordinates. Obviously RDC direction vectors are a good choice in this context, with additional parameters like exclusion distances[70] or chiral volumes (especially for planar centers and moieties).[71]

With the Cartesian coordinates of a starting geometry and a set of redundant internal coordinates (including RDC-based restraints) as input, the Cartesian displacement associated to the (small) internal coordinate displacement is evaluated following the iterative protocol by Peng *et al.*[67] (see supporting information for implementation details). The iterative implementation allows for the full utilization of long-range couplings (see **Figure 3**) to discriminate the two possible vectors $\vec{r}_{ij,RDC}$ (for green position) and $-\vec{r}_{ij,RDC}$ (for red position). This global treatment not only discriminates the previously indistinguishable vector orientations but also leads to the best-fit solution of all RDCs for one nucleus and may also optimize the Cartesian coefficients in the process.

As shown in Figure 3 the best-fit position of all holonomic terms (bond lengths and angles; these were not marked to keep the figure simple) and all RDC information (solid arrows: $^{1}D_{CH}$ and dotted arrows: $^{n}D_{HH}$) is calculated using redundant internal coordinates. To achieve lower inversion barriers (i.e. to more easily sample the full conformational and configurational space), dihedral angle restraints were not included in the implemented algorithm.

Redundant internal coordinates in combination with sufficient experimental data should thus enable determination of the conformation and relative configuration of small organic compounds. As with all other approaches, absolute configurations cannot be derived by this algorithm.[72] The two major downsides of this algorithm are the poor robustness of the algorithm towards large changes in internal coordinates and the lack of scalability towards larger compounds with increased degrees of freedom. The first point can lead to instabilities if large changes occur (e.g. due to large errors). This can be bypassed by downscaling the changes (see supporting information for more details) or by choosing the non-default vector addition algorithm. The second point is due to the SVD applied in this algorithm, which slows down drastically when optimizing large molecules. Improvements to the underlying algorithm to boost performance are currently under investigation.

Treatment of dynamics. As described by Meiler *et al.*[23] dynamics interpretation is conducted analogous to the Lipari-Szabo interpretation of nOe data:[25-26]

$$S^2_{RDC,k} = \frac{4\pi}{5}\sum_{M=-2}^{2}\langle Y_{2,M}(\theta_k,\phi_k)\rangle \cdot \langle Y^*_{2,M}(\theta_k,\phi_k)\rangle \qquad (5)$$

S^2_{RDC} is the local order parameter describing the dynamics of each individual RDC. In biomacromolecular NMR this parameter is crucial for the assessment of conformational changes and the target of all multi alignment approaches.[21, 23-24, 27-29, 73] Here we are primarily interested in obtaining the correct conformation and configuration, but nevertheless need to correctly account for dynamics. In MFA analysis the alignment is derived from a rigid structural model while experimental RDCs are additionally scaled by internal motion. This reduces the effective alignment magnitude. Therefore the refined spherical harmonics obtained from equation 4 and S^2_{RDC} are both equally scaled by the same factor.

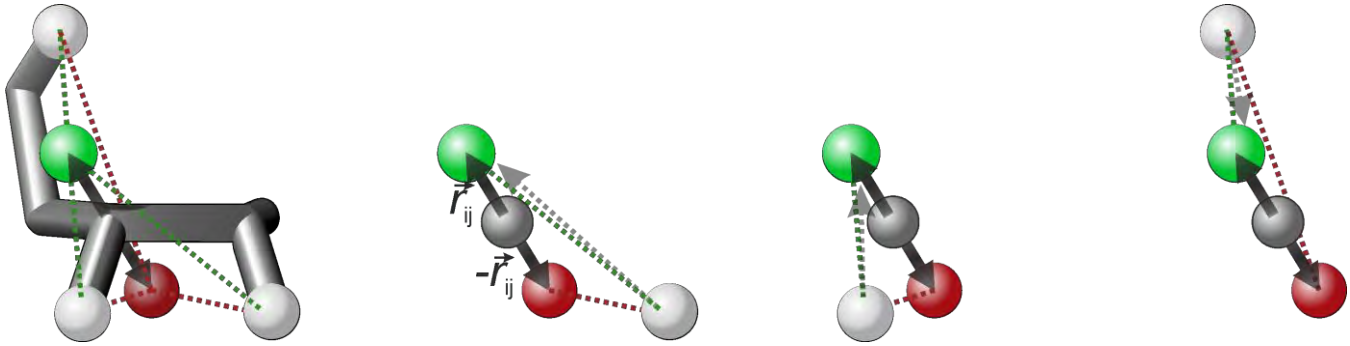

Figure 3. Representation of degenerate RDC vector orientations in the case of a $^{1}D_{CH}$ coupling (black vectors) resulting in two mathematically indistinguishable solutions (green and red atoms). When adding three additional $^{n}D_{HH}$ couplings (grey vectors in right hand part) the solution with the least mean error squares (green vs. red vectors) can be determined. Thereby the correct atom position can be determined.

To remove this effect and extract the correct order parameter the scaling parameter $S_{overall}$ reflecting this reduction has to be estimated[23] (see SI on how this is done within TITANIA).

Use of SECONDA to investigate linear independence. As described earlier the linear independence of the alignment media is crucial for a successful optimization by RDCs, especially when experimental errors are present. The simplest method to compare two alignments in the generalized angle β as defined by Sass *et al.*[74] This measure is useful for the pairwise comparison of two alignment conditions, e.g. when assessing enantiodifferentiation in chiral alignment media.[75] When extending this to a large number of RDC sets the interpretation becomes difficult and is only possible qualitatively (see SI Figure S-3). Ideally one would want to analyze a data matrix containing all RDC sets (or information on those) at once. Tolman used the condition number of the RDC matrix obtained by SVD.[21] A related but more adaptable[76] method as proposed here is the principle component analysis (PCA)[77-78] of the covariance matrix **C**. The goal is to find a low dimensional pattern in a data matrix of *K* RDCs measured in *M* alignment media, to assess an underlying model – in our case five linearly independent alignment conditions. The PCA of **C** was implemented by Hus *et al.* in the SECONDA protocol to investigate the influence of structural noise (computed using a MD trajectory) on RDCs.[50] The normalized covariance matrix of the RDCs (equation 6) is calculated and diagonalized to obtain its principle variances (eigenvalues λ_q) and eigenmodes (eigenvectors $|q\rangle$). Here, the principle variances indicate the amount of data variance that is captured by the respective dimension. In addition, the eigenmodes form the reference frame that captures the principle variances along their axes.

$$C_{ij} = \frac{1}{M-1}\sum_{m}^{M} w_m (D_i^m - \langle D_i \rangle)\left(D_j^m - \langle D_j \rangle\right) \tag{6}$$

The weighting w_m of the individual RDC sets can be defined in different ways. TITANIA's standard implementation is reported in the SI (see equation 1). Closer inspection of the principle variances and their corresponding eigenmodes is required to disentangle the individual contributions to the overall RDC dataset. The distribution of the first five eigenvalues is a measure of the individual sampling of the dimensions. If five non-zero eigenvalues are obtained and these have similar contributions to the cumulative sum (see equation 7) this confirms linear independence of the five data sets. Additional eigenvalues will occur (dimensionality > 5) if the RDCs contain heterogeneous behavior, like experimental error or structural noise.

The corresponding eigenvalues are evaluated either by the λ_5/λ_6 ratio (defined as $\rho_{5/6}$ gap by Hus and Brüschweiler) or their percentage of the total variance. The contribution of the RDC pairs to the individual principle variances, can be assessed in a local fashion, using the eigenvector components, or by using the global collectivity κ_q (see equation 8), which quantifies the contribution of the RDC pairs to the corresponding principle variance in percent (with the range $\kappa_q = [100/K, 100]\%$).[50, 79]

$$S_c(\lambda_k) = \frac{\sum_{i=1}^{k}\lambda_i}{\sum_{i=1}^{K}\lambda_i}\cdot 100\% \tag{7}$$

$$\kappa_q = \frac{1}{K}\exp\left[-\sum_{k=1}^{K}|\langle q|k\rangle|^2 \log(|\langle q|k\rangle|^2)\right]\cdot 100\% \tag{8}$$

This allows the representation of an eigenvalue and eigenvector pair by the two values λ_q and κ_q. The overall heterogeneity of individual RDC pairs can be expressed by the cumulative sum of the heterogeneous modes a^2:[51]

$$a_k^2 = \sum_{q=6}^{K}\lambda_q |\langle q|k\rangle|^2 \tag{9}$$

To the best of our knowledge there is no comprehensive application of SECONDA to the often limited RDC datasets available for organic compounds. Some examples for SECONDA analyses are given below, while a more extensive discussion on the interpretation of SECONDA runs is given in the supporting information.

The TITANIA protocol. The mathematical framework described herein is combined and extended in the TITANIA C++ software. A general flow scheme representing the major blocks of TITANIA is shown Figure 4.

TITANIA is a command line program that is started with a user defined input file containing RDCs, an initial structure model (coordinates and connectivity) and keywords to adapt the behavior of the optimization scheme. Examples for input files can be found in the supplementary material.

For a proper run a parametrization is performed, in which scaled and normalized RDC matrices are calculated, the structure parameters (holonomic terms) and redundant internal coordinates are set up. Additionally a molecular frame is defined by transforming the initial structure to the PAS of the inertia tensor. Using the in-house implementation of the SECONDA protocol the (normalized) RDC data matrix is assessed.

From there on the iterative refinement of the RDC and structure parameters starts. The orientation parameters of all RDC sets are calculated simultaneously using the SVD of the normalized cosine matrix **B** (see SI equations 2a/c).[18, 21] The alignment tensors obtained are used to build the Wigner rotations and update the spherical harmonics *via* SVD of the **F** matrix in equations 4. It is important to note that the spherical coordinates, and thereby the RDC direction vectors, are derived from the entirety of RDCs (see SI equation 17) and not by consideration of single datasets as individual sources of information. The spherical coordinates are used to construct the Cartesian coordinates based on redundant internal coordinates (see SI section 1.3.4). To estimate the uncertainty of the calculated parameters and check for convergence of the procedure, the refined structure models are used for a Monte-Carlo bootstrap based on the user estimated experimental errors.

Application on Isopinocampheol. We have chosen Isopinocampheol (IPC) **1** as a test case as it is a bicyclic compound with a highly rigid scaffold, containing four chiral centers (C1, C2, C3, C5, with C1 and C5 being interdependent) and three pro-chiral centers (C4, C6 and C7). The rigidity allows for a separation of the configurational analysis from any conformational investigations. Furthermore plenty of RDC data are available, thus we assume that enough independent orientations are available (see below).

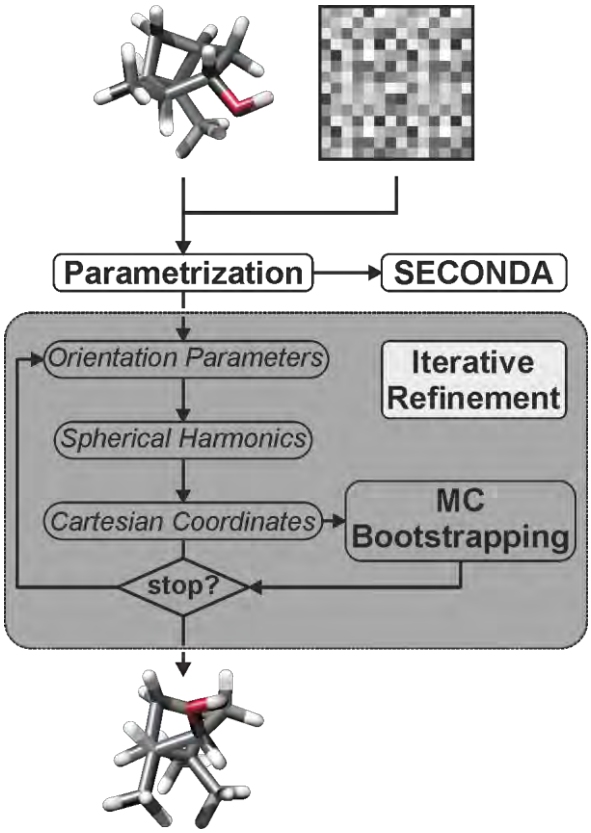

Figure 4. Schematic flowchart of the TITANIA protocol. The user has to define an initial input structure and RDCs from at least five alignment media (indicated as heatmap). TITANIA starts a parametrization of these data and performs SECONDA. The iterative refinement of the structure starts by updating the orientational parameters and calculating the refined spherical harmonics from this. Using redundant internal coordinates the updated Cartesian coordinates are calculated and a Monte-Carlo bootstrap is performed to check for convergence. The final output contains the updated mean structure and additional RDC information like S^2_{RDC}, the SECONDA results and statistical information on the RDC vectors.

Several scenarios will be investigated: 20 artificial orientations for maximum sampling of the orientational space (setup **1-A**), real orientation which are expected to be largely independent (setup **1-B**) and real orientations, which are chosen in a way to maximize linear dependence (setup **1-C**). Additionally error was added to these data sets (setups **1-D** to **1-F**, see experimental section for more details). The amount of data is varied for the setups resulting in different runs with the number indicating the number of RDCs used (for a table which RDCs were used in which run, see SI Table S-81).

First we will discuss the optimization runs **1-A** which employ 20 artificial RDC sets. Since linear independence is crucial for reliable optimizations, this will be investigated first by applying SECONDA to each RDC run (see Figure 5). Only the runs with 11, 23 and 39 RDCs per set are shown here. The respective data for all runs can be found in the supporting information (see section 2.2.1).

All plots show a similar trend. In the absence of heterogeneities like structural noise or experimental error on the RDCs, no more than five eigenvalues ($\lambda_{1\text{-}5}$) differ from zero. In the presence of heterogeneities additional non-zero eigenvalues (λ_n with $n \geq 6$) would be expected. As data sets are artificial no experimental error is present and a rigid compound is investigated there are no heterogeneities. The ratio of the largest (λ_1) and the lowest eigenvalue (λ_5) gives a direct assessment of the sampling of independent orientations. In all runs for **1-A** excellent ratios λ_1/λ_5 of < 10 are found, indicating sufficient sampling of orientations.

When evaluating the cumulative sum S_c (see equation 7), the **1-A** examples all show a contribution of the smallest variance (λ_5) to the overall variance of at least 6%. This indicates that the five alignment media are independent. If linear dependence would be present, the contribution of the last eigenvalues to the overall variance would be much smaller (see run **1-C**).

The associated collectivities κ_q quantify if the variation of the K RDCs occurs in a more local or rather global fashion. When analyzing the κ_q values of Figure 5 it becomes clear, that the distribution of the collectivities becomes wider when adding $^nD_{HH}$ RDCs (**1-A23**, see SI for further SECONDA plots: **1-A17** to **1-A39**), while the overall pattern remains similar.

Based on the SECONDA analysis the 20 RDC sets of setup 1-A should form a solid basis for the iterative optimization using TITANIA which is conducted next. As a first test the C3-epimer was chosen. The chiral volumes are monitored to visualize the course of the optimization (see Figure 6). It is expected that the correct stereochemistry is reliably achieved for all centers, if sufficient data is used. If this condition is not met (see **1-A11** which uses only $^1D_{CH}$ RDC) the inverse RDC vector can be a possible result (see Figure 3). Adding even a few $^nD_{HH}$ RDCs improves the situation significantly, such that the correct relative configuration is obtained straight away (shown here for 23 RDCs, **1-A23**). It works already with 17 RDCs (see **1-A17**, Figure S-12 in the SI).

All runs show an inversion in the sign of the chiral volume of C3 in the course of the optimization (blue lines in Figure 6). In the case of **1-A11** (only $^1D_{CH}$ data) this inversion occurs instantaneously but remains correct only for the first 10 steps. The final structure contains the wrong configuration at C3. Still the correct orientation information on the RDC vector C3-H3 is obtained (for a similar finding in tubocurarine, see Figure 12). This is a direct consequence of the mathematically indistinguishable solutions discussed above and can be improved by inclusion of long-range RDCs. A hint on the inverse vector orientation is the distortion of the respective tetrahedral geometry. After the initial steps, a nearly planar arrangement of the C3-C2, C3-O3 and C3-C4 vectors is obtained. Without additional restraints, the redundant internal coordinates retain the optimization (in this case) in the wrong minimum / configuration. This becomes even clearer when no redundant coordinates are used for the optimization (see SI section 1.3.5). To assess geometry violations of the resulting structures, TITANIA calculates the magnitude of the chiral volumes for all possible permutations of the bond vectors and determines the respective *rmsd* between those values.[80]

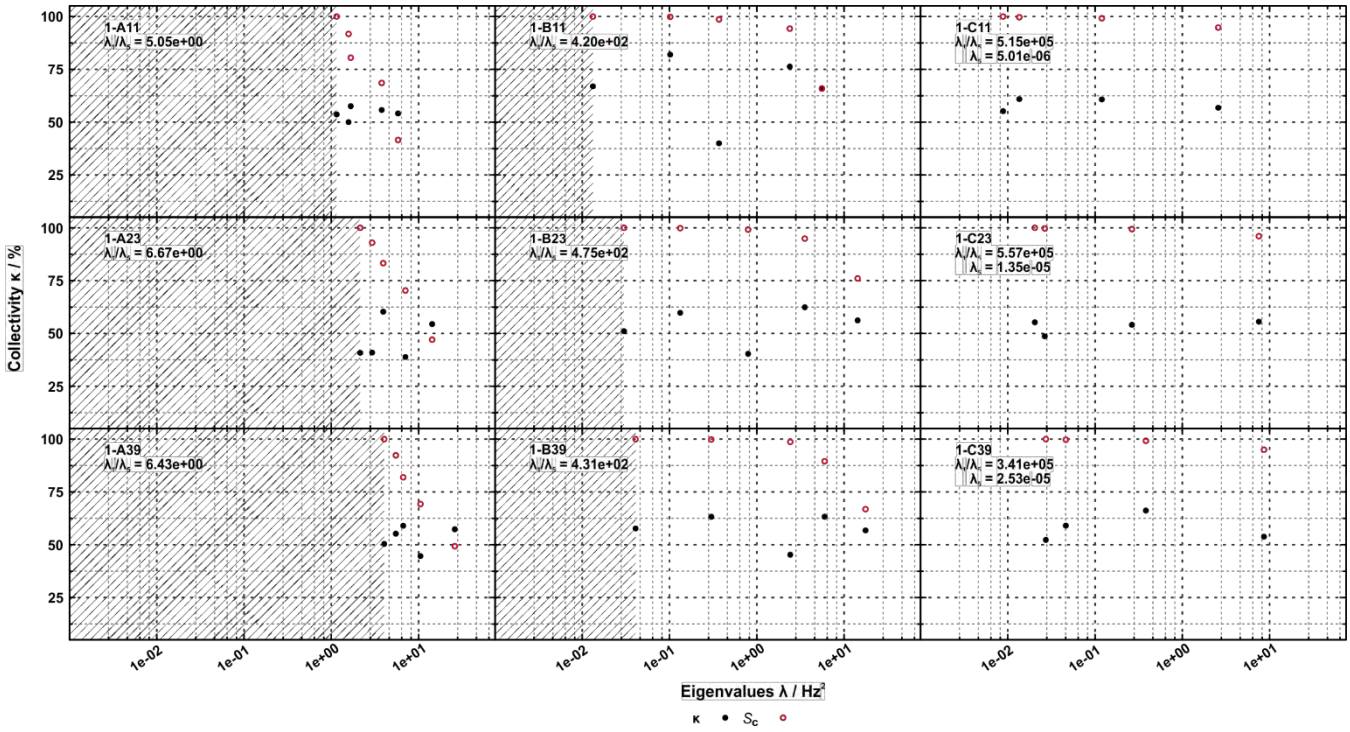

Figure 5. SECONDA plots for three runs of **1-A** to **1-C** using 11, 23 and 39 RDCs. The collectivities κ (●) are plotted with respect to the eigenvalues λ of the RDC covariance matrix. All eigenvalues λn < 1e-3 are not plotted to retain the same scaling for all SECONDA plots. In addition the cumulative sum S_c (○) of the eigenvalues are plotted to estimate the contribution of the principle variances to the overall variance of the RDC matrix. In run 1-B11, the points of κ(λ1) and S_c(λ1) overlap coincidentally.

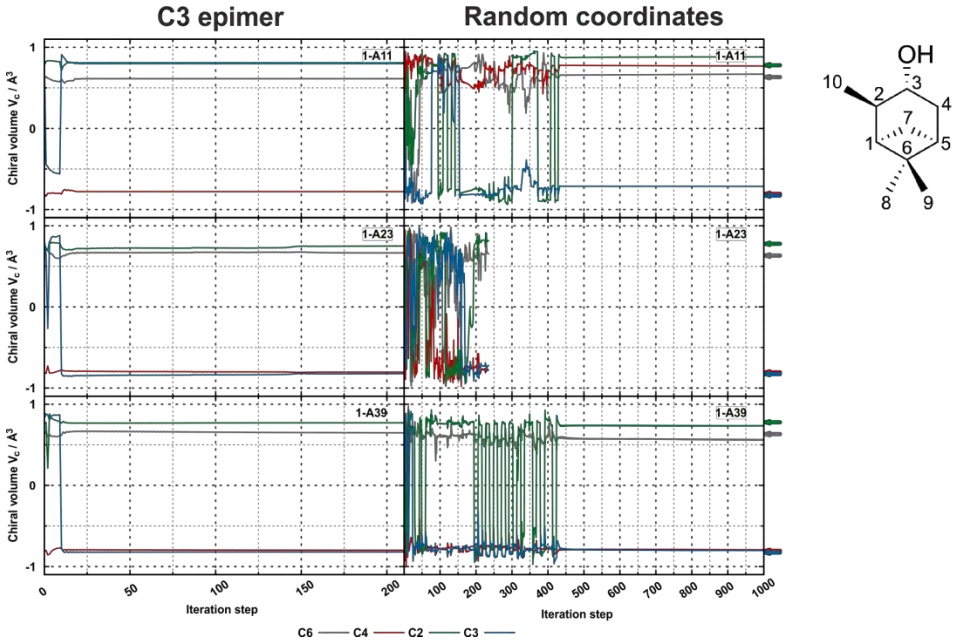

Figure 6. Trajectories of the chiral volumes of interest for setup **1-A**. All plots on the left hand side monitor optimization starting with the deliberately inverted structure at C3. Additionally the two attached carbons (C2 and C4) and the quaternary carbon C6 (only two $^1D_{CC}$ in all runs) are shown. The correct chiral volumes are indicated by an arrow at the right hand side. Note that the results for starting from random coordinates are shown on the left hand side.

Centers with strongly distorted tetrahedral geometry will result in larger deviations and therefore are less likely to represent a proper result. For **1-A11** the *rmsd* of C3 is 0.20 Å^3 while well-defined centers like C4 in the same run have an *rmsd* of 0.05 Å^3.The runs utilizing $^nD_{HH}$ RDCs (**1-A17** to **39**, see SI Figure S-12 for **1-A23** and **1-A31**) all show their final inversion in iteration step 10. All

following iterations confirm the correct stereochemistry with low values on the *rmsd*s of chiral volumes.

The progression of the optimization trajectory can be monitored closely by the Monte-Carlo bootstrapping (see SI Figure S-10 for the corresponding plots for all runs). For all runs of **1-A**, the orientation and structure parameters quickly achieve convergence even though there are some fluctuations in the initial iterations. In addition to the stop criteria the $S_{overall}$ parameter converges towards its theoretically expected limit of 1.0 (since the RDCs were predicted by using a single rigid structure in the absence of heterogeneities) with deviations due to counteractions of the RDC information and the holonomic terms in the redundant internal coordinates. This constantly leads to small fluctuations in the coordinates and subsequently a slight underestimation of the $S_{overall}$ parameter.

Notably, the above optimization results are only marginally affected by the starting geometry. When starting from a set of random coordinates (or a flat geometry without any stereochemical information), the calculations may take several hundred iteration steps to achieve similar thresholds of convergence. However, the runs arrive at the same geometries and orientation conditions as the corresponding runs starting from the C3 epimer. The 1-A11 run starting from a random geometry again results in the wrong configuration, while all runs involving $^{n}D_{HH}$ RDCs produce the correct configuration (see Figure 6). The resulting geometries and orientation parameters coincide very closely with the results from the previous runs (see SI section 2.3), highlighting the robustness of the algorithm.

From the setup 1-A with artificial data it can be clearly concluded that the correct stereochemical configuration is obtained from sufficiently large and well-sampled RDC data result in the correct stereochemical configuration, while poor data may either not converge at all or lead to a distorted geometry as in the C3 case.

Application on IPC: realistic data. The applicability to a more realistic number and choice of RDC sets is investigated in setups **1-B** and **1-C**. Both underlying data sets are based on synthetic data with tensor orientations from real samples. Setup **1-B** represents RDC data with linearly independent orientations using six alignment conditions. Setup **1-C** on the other side showcases high linear dependency by using similar alignment conditions. For **1-B**, the SECONDA plots (see Figure 5) show large differences to the respective **1-A** runs in the magnitude of the eigenvalues λ_1 to λ_5. The collectivities show no extraordinary values for the runs containing $^{n}D_{HH}$ RDCs. As expected for data without experimental error and structural noise no more than five non-zero eigenvalues are found. In **1-A** the λ_1/λ_5 gap was lower than ten for all runs. This was interpreted as excellent linear independence. Setup **1-B** on the other hand shows λ_1/λ_5 gaps larger than 400, indicating that the experimental data used in the synthetic setups **1-B** (and **1-C**) exhibit a lower degree of linear independence than the corresponding artificial runs (**1-A**). This is mainly apparent in the magnitudes of the eigenvalues λ_2-λ_5, while λ_1 is of comparable size for the individual runs of **1-A** and **1-B**. The question for a suitable measure for linear independence arises, thus we have chosen a threshold of 1% contribution of the individual eigenvalues in the overall variance in order to be considered. In setup **1-A** the fifth (smallest) eigenvalue contributes at least 6%, which we consider significant. In setup **1-B** the 1% threshold is already reached with eigenvalue λ_3 for most runs, thus λ_4 and λ_5 have little contribution to the overall variance. The apparent reduction to only three notable eigenvalues (roughly equating to only three significantly contributing independent alignment conditions) should still be sufficient for a TITANIA optimization as noted previously be Ruan *et al.*[30] For setup **1-C** the fifth eigenvalue is more than five orders of magnitude smaller than the first one leading to extraordinarily large λ_1/λ_5 gaps. The eigenvalue with a contribution of more than 1% is λ_2 in all cases.

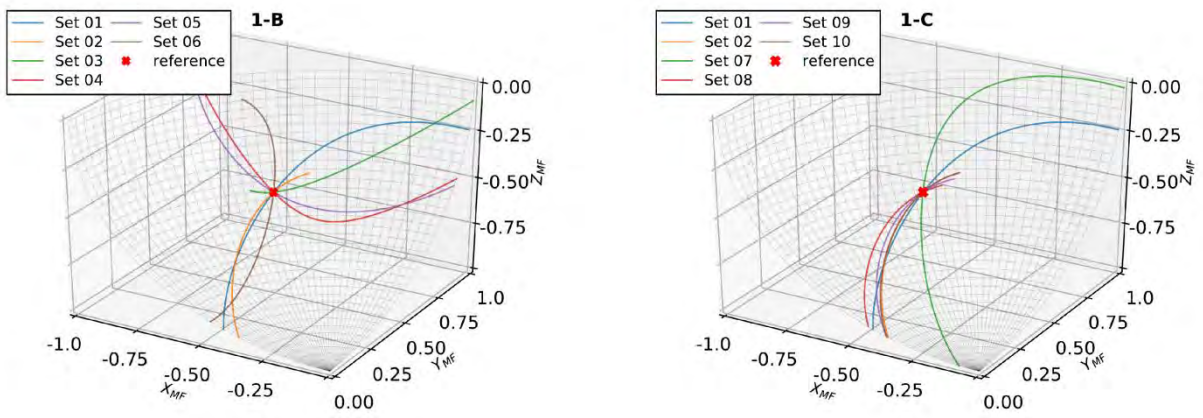

Figure 7. Threedimensional plot of possible directions for the C3H3 RDC vector based on synthetic data from experimental orientations (see SI equation 6a). The intersection of the cones represent the mean vector orientation obtained by RDC data. The exact same intersection is found for 1-B and 1-C as encountered in the artificial RDC data (**1-A**), which perfectly matches the orientation of the C3H3 RDC vector in the reference structure. The orientation data used to generate the plot were all obtained from the reference structure.

This indicates that only two independent (based on our deliberate threshold) orientations are present; thus structure elucidation is expected to fail using TITANIA. Thus it needs to be investigated whether the optimizations in TITANIA confirm our expectations from the SECONDA analysis.

Surprisingly, the chiral volume trajectories of **1-B** and **1-C** for the C3-epimer as starting geometry (see SI Figure S-12) show nearly the exact same progression as **1-A** did. The differences are rather small (except **1-B39** vs. **1-C39**) and can only be revealed by examination of the exact chiral volumes (for example C3 iteration 1: V_c[**1-B11**] = -0.44438 Å^3, V_c[**1-C11**] = -0.44500 Å^3). The final structures of **1-B11** and **1-C11** show the same distorted tetrahedron with incorrect configuration at C3 (as shown in Figure 12 for tubocurarine).

The similarity of results is, furthermore, illustrated by the intersection cones generated by all possible θ, ϕ combinations obtained when solving equation 2 for the respective RDCs of C3-H3. When plotting all possible orientations of this RDC vector calculated in the setups **1-B** and **1-C** on a unit sphere, two unique intersections are found, coinciding with the reference vector orientation in the molecular frame (see Figure 7).[81-82] These are the two degenerate solutions of the RDC vector (correct orientation and its inverse).

Interestingly, one intercept is found for the individual runs despite the rather dramatic dependence in **1-C**. This illustrates, that as long as homogeneous RDC data (i.e. free of heterogeneous behavior (in this case error)) are available, even small differences in the alignment conditions (like in **1-C**) are sufficient for the optimization with TITANIA. The impact of heterogeneities in the form of data uncertainty on the intersection and thereby on the optimization using TITANIA will be discussed below on the runs **1-E** and **1-F**. The counter acting of the linear dependence and heterogeneities in the RDCs on the ability to superiorly define the RDC vectors is observed in the trajectory plot (see SI Figure S-11). Here changes in the mean vector length (*rmsd*(R)) as well as the fluctuations in the change of the spherical coordinates (*rmsd*(p)) increase with linear dependence. No perfect intersection of the individual cones (defined by the respective alignment media) will be obtained since the Monte-Carlo bootstrap adds errors to the RDCs. This originates from the fact that **1-A** will still define the orientation with high accuracy due to an expected error cancelation by the 20 RDC sets. When reducing the number of sets this error cancelation will not be as efficient as in **1-A**. This reduction of the error cancelation is even stronger when the degree of linear dependence grows (**1-C**). This can be observed when calculating the average of the Monte-Carlo mean vector lengths for all RDCs vectors in one setup ($\langle R_{\mathbf{1-A}} \rangle$=0.965, $\langle R_{\mathbf{1-B}} \rangle$=0.906, $\langle R_{\mathbf{1-C}} \rangle$=0.862).

As before for setup **1-A**, all runs were also performed with random starting coordinates (see SI figure S-14 and S-15). The optimization trajectories are much rougher for **1-B** and for **1-C**, and generally show even more inversion steps before reaching convergence. Interestingly, some **1-B** runs arrive at the enantiomeric form, while converging towards the correct relative configuration. This is not unexpected due to the nature of the *random* start and because RDCs are inherently unable to determine the absolute configuration without enantiospecific interactions with the alignment medium being used to drive the optimization towards the correct absolute configuration.[72] For **1-B11** again the incorrect (relative) configuration at C3 is observed. The deliberately chosen poor linear independence of runs **1-C** has a stronger impact for the optimization, than observed for **1-B**. **1-C11** shows two incorrect configurations and **1-C23** shows one. The other **1-C** runs converge to the correct configurations and show that even relying on such a limited set of contributing alignment media still allows for a successful structure optimization with TITANIA. The results, however, must carefully be evaluated and the optimization trajectory may depend strongly on the RDC data set and choice of starting geometry.

The analyses detailed above demonstrate the ability of TITANIA to optimize the structure of IPC resulting in the correct configuration when using a sufficient amount of error-free data.

Inducing experimental error. The next step is now to investigate whether and how experimental error together with varying degrees of linear dependence impacts the optimizations. Therefore Gaussian random noise is added as synthetic error to the RDCs in setups **1-A** to **1-C** generating the setups **1-D** to **1-F**, respectively. It is expected that **1-F** (**1-C** with error) will not converge to the correct solution since data were deliberately chosen to be linearly dependent. It is reported that the propagation of errors strongly depends on the linear (in-)dependence of the RDC data sets.[24] Since the contribution of the linear independence in alignment conditions is known and SECONDA is capable of detecting heterogeneities in **1-E** to **1-F**, the impact of errors can directly be analyzed.

The SECONDA plots of the RDC data in the presence of error are shown in the SI (section 2.2.1). While the eigenvalues λ_1 to λ_5 of **1-D** only show minor changes compared to **1-A** the collectivities change significantly. As expected the λ_5/λ_6-gaps now become observable due to the RDC errors in **1-D**. It shrinks in magnitude with increasing set sizes. As the κ_q values associated with the latter eigenvalues drop in magnitude with increasing set sizes, we assume heterogeneities of a localized nature to be present.

The SECONDA data for **1-E** unexpectedly show barely any change in magnitude or the respective κ_q value of the first three eigenvalues when compared to **1-B**. The eigenvalues λ_4 and λ_5 on the other side increase while κ_q drops when adding more RDCs and the sixth eigenvalue remains smaller than the cutoff of 1e-9. The latter is also true for the runs **1-F**. Most likely, the low degree of linear independence in the RDC data leads to heterogeneities being observed in the first eigenvalues and not generating additional eigenvalues. This behavior was not observed by Hus *et al.*, who reported that heterogeneities will result in additional eigenvalues but λ_1 to λ_5 remain nearly unchanged for linear independent data (i.e. see 1-D).[50]

The data containing errors on the RDCs show huge differences to the error-free data. The trajectories of setup **1-F** did not show convergence or ended in highly distorted geometries. Thus linearly dependent data with experimental error will not lead to a valid solution as expected. The respective trajectories are not plotted but are shown in the supporting information. Instead the vector addition algorithm, only optimizing the orientation of the RDC vectors, is shown for setup **1-E** (explanation see SI section 1.3.5).

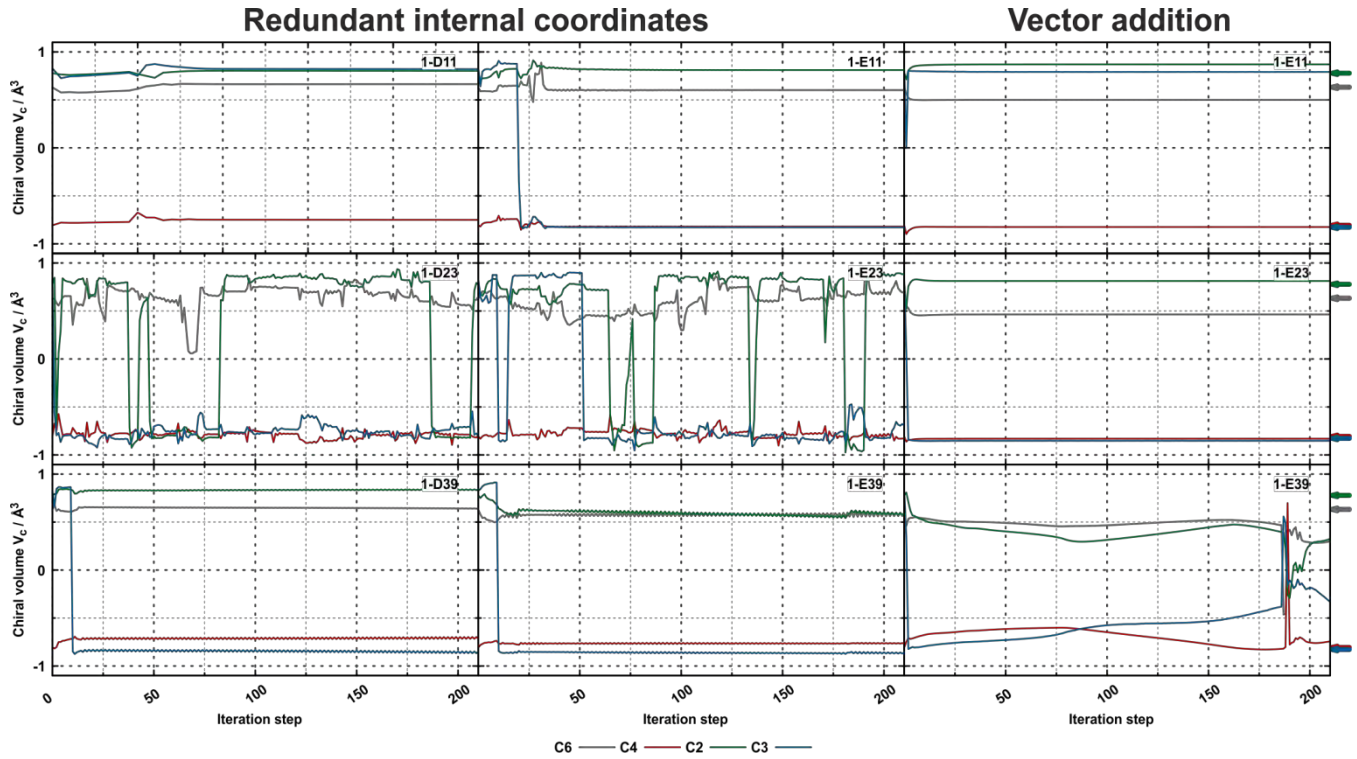

Figure 8. Trajectories of the chiral volumes of interest for the runs **1-D** and **1-E** using 11, 23 and 39 RDCs. All plots monitor optimization starting with the deliberately inverted structure at C3, the two attached carbons (C2 and C4) and the quaternary carbon C6 (only two $^1D_{CC}$ in all runs). In addition to the standard algorithm to generate Cartesian coordinates (redundant internal coordinates, left and middle panel) the vector addition algorithm was also used (right panel). The vector addition shows a much smoother trajectory. The correct chiral volumes are indicated by an arrow at the right hand side.

The trajectories are now more distinct for individual runs with the same set sizes. In the runs utilizing 11 RDCs the previous behavior is observed again; with the curious exception that **1-E11** in the redundant coordinate algorithm (middle panel) now achieves the inversion to the correct stereochemistry, while the center is obtained in the wrong configuration in the vector addition algorithm. The runs with 23 RDCs undergo several flips of methyl group RDC vectors (C2/C6) for the **1-D** and **1-E** sub run in the redundant coordinates algorithm. While the interchange of the methyl groups at C6 is of no consequence for structure determination here, the inversion at C2 leads to a wrong configuration (see structures in supplementary material). Thus it is essential to check the final structure for inconsistencies (distorted geometries or wrong bond length), but also an inspection of the chiral volume trajectories is recommended to detect such problems. This - admittedly problematic - behavior of the optimization when using redundant coordinates is resolved when using the vector addition algorithm (see Figure 8 right hand side). The correct relative configuration is obtained quickly. The downside of this algorithm is that only a subset of coordinates (those for which RDC data is available) is optimized. This can lead to distortions in the overall structure (see inset of **1-E39**), while retaining the proper orientations between the RDC vectors. The problems in properly defining methyl group orientations are not encountered when extending the set sizes (see **1-D39** and **1-E39**). This shows that a structure optimization resulting in the correct final configuration is possible not only with ideal and error-free data but also with more realistic data of moderate linear independence.

As mentioned before the **1-F** runs did not converge or lead to proper structures. These differences between the runs (**1-D**/**1-E** vs. **1-F**) are also observed when looking at the intersection of the possible orientation cones (see Figure 9). In the case of **1-E** five of the six alignment media intersect very close to the reference orientation. In contrast, in setup **1-F** no common unique intersection is found anymore due to the added errors (compare Figure 7 to Figure 9). An extended discussion of the stop criteria and the respective trajectories are presented in the supporting information (see section 2.2.3). The data in this chapter leads to the conclusion that the quality of data as chosen in **1-E** (experimental orientations with moderate dependency with (artificial) experimental error) are already sufficient to obtain the correct structure, whereas linearly dependent data (**1-F** with artificial experimental error) do not allow to converge to the correct structure. Thus already a limited set of different orientations may be adequate for structure optimization of small organic compounds if enough RDCs are available and the sampled alignment conditions are sufficiently independent. Larger set sizes increase the accuracy of the refined structure when experimental heterogeneities are present. In the absence of experimental errors the need for linear independence is reduced to an extent, while the presence of such sources of heterogeneity exacerbates this requirement.

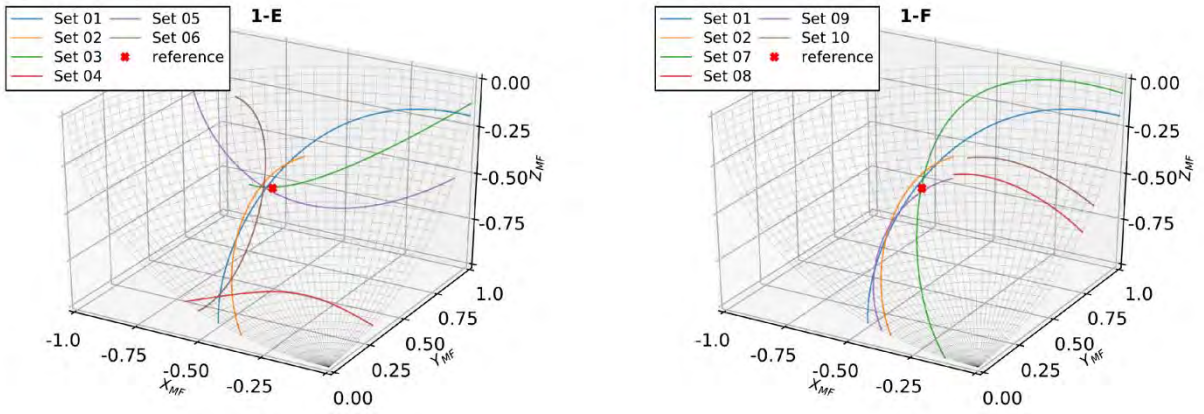

Figure 9. Three-dimensionall plot of possible directions for the C3H3 RDC vector based on the synthetic data utilizing 11 RDCs each with varying degrees of linear dependency (see SI equation 6a). The intersection of the cones represent the mean vector orientation obtained by RDC data. Using RDC data containing heterogeneities the optimized solution stronly depends on the difference of the alignment conditions. Therefore the intersection found for **1-E** (the linearly less dependent data set) is similar to the correct one (see Figure 7), with only one alignment set (set 04) showing a large deviation. 1-F (the data set that is linearly dependent on purpose) on the other hand has no well defined array fitting the data. Again the orientation of the C3H3 RDC vector in the reference structure is plotted as red cross. The orientation data used to generate the plot were all obtained from the reference structure.

Application on Tubocurarine. Tubocurarine **2** is a cyclic neurotoxin that consists of four cyclic subunits containing aromatic rings and piperidinium ions. The crystal structure was solved 1975 by Reynold and Palmer[83] and in 2019 tubocurarine was used for a proof of concept by Immel *et al.* for a configurational and conformational analysis using fc-rDG/DDD with special interest on the orientation of the rings **C** and **F** with respect to **A**/**B** and **D**/**E**. It was shown that at least three linearly independent RDC sets have to be used (successively) to properly assign the correct relative configuration.[53]

Tubocurarine is capable of undergoing large conformational changes, emphasizing the need to jointly determine the conformation and relative configuration. The compound features two separated, rigid RDC subunits (rings **A**/**B** and **E**/**D**), which are connected by flexible linkers (bridging methylene groups 18 and 36 and rings **C** and **F**). Lastly, the introduction of heteronuclear couplings to nitrogen is accompanied by large relative errors.

Eight alignment conditions were used to generate artificial RDCs which were directly used (**2-A**) and extended to model experimental errors as described above (**2-B**). Each set contained a total of 30 RDCs using $^{1}D_{CH}$, $^{1}D_{NH}$, $^{1}D_{CN}$ and all $^{n}D_{HH}$ couplings within a cutoff radius of 3.0 Å. Notably, the methylene groups 18 and 36 were only defined by $^{1}D_{CH}$ RDCs (see SI for the exact assignment). The RDCs were calculated from a single rigid structure and the respective errors were explicitly generated to not mimic any conformational noise, i.e. no additional down-scaling of RDCs in flexible groups was added. The effect of the large relative error is immediately observed in the difference of the SECONDA plots for **2-A** and **2-B**. The **2-A** plot shows a λ_1/λ_5 ratio which lies in-between the ratios of **1-A** (around 5) and **1-B** (above 400). All eigenvalues contribute with more than 1%, with the fourth eigenvalue having a contribution of 5.9% to the overall variance, and all collectivities κ are larger than 50%. This suggests a high degree of linear independence for **2-A**. Interestingly, the pattern of the eigenvalue-collectivity pairs changes drastically when random noise is added in **2-B**. As expected more than five non-zero eigenvalues are observed, revealing heterogeneities in the RDC sets used for the run **2-B**. The eigenvalue λ_1 drops in collectivity while λ_2 remains nearly unchanged. λ_3 increases in size but the collectivity is reduced by a factor of ~3. In addition, the fourth eigenvalue $\lambda_{4,2\text{-B}}$ has no correspondent in run **2-A**, while $\lambda_{4,2\text{-A}}$ is represented in $\lambda_{5,2\text{-B}}$. Similarly, $\lambda_{5,2\text{-A}}$ ends up close to the values of $\lambda_{7,2\text{-B}}$. This means, that $\lambda_{4,2\text{-B}}$ and $\lambda_{6,2\text{-B}}$ reflect the random noise and $\kappa_{3,2\text{-B}}$ is strongly reduced due to the error. To support this interpretation, the respective squared eigenmodes are plotted in the supporting information. Both the SECONDA and eigenmodes plots reflect the strong influence of the large $^{1}D_{CN}$ relative errors.

The chiral volumes also show the expected behavior. No fast inversions of all stereogenic centers can be observed anymore and multiple inversions occur on N1. For **2-A** the chiral volume of the nitrogen centers remain stable after the final configuration was reached. In **2-B** small fluctuations are observed throughout the whole optimization.

All chiral centers end up in the correct configuration. Only the *pro*-chiral center C18 does not converge to the correct assignment of the diastereotopic protons. This behavior was already observed for C3 of IPC. After a stable configuration is achieved on C18 the chiral volume is extraordinarily high for an unstrained sp^3 carbon. Figure 12 shows the respective centers for **2-A** and **2-B** (solid structures) and the reference structure used to derive the RDCs (transparent). The planar geometry, resulting in a chiral volume close to 1.0 $Å^3$, shows that the correct vector orientations are found

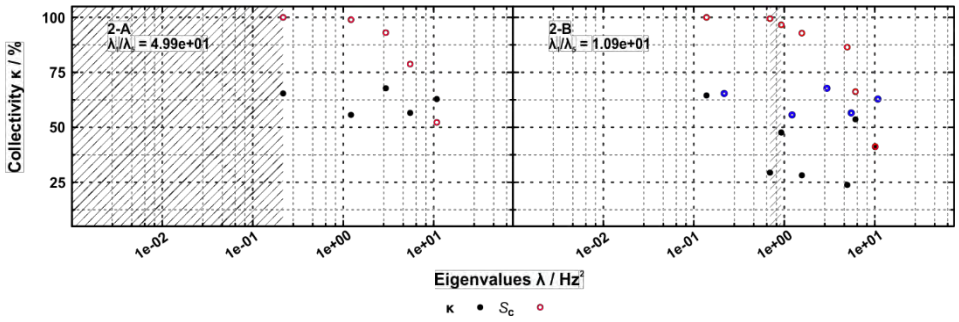

Figure 10. SECONDA plots for the two runs **2-A** (without noise) and **2-B** (with Gaussian random noise) of tubocurarine 2. Plotted are the collectivities κ (●) with respect to the eigenvalues λ of the RDC covariance matrix (blue eigenvalues in the right hand side plot are from **2-A**). In addition the cumulative sum (○) of the eigenvalues were plotted to measure the participation of the principle variances to the overall variance of the RDC matrix.

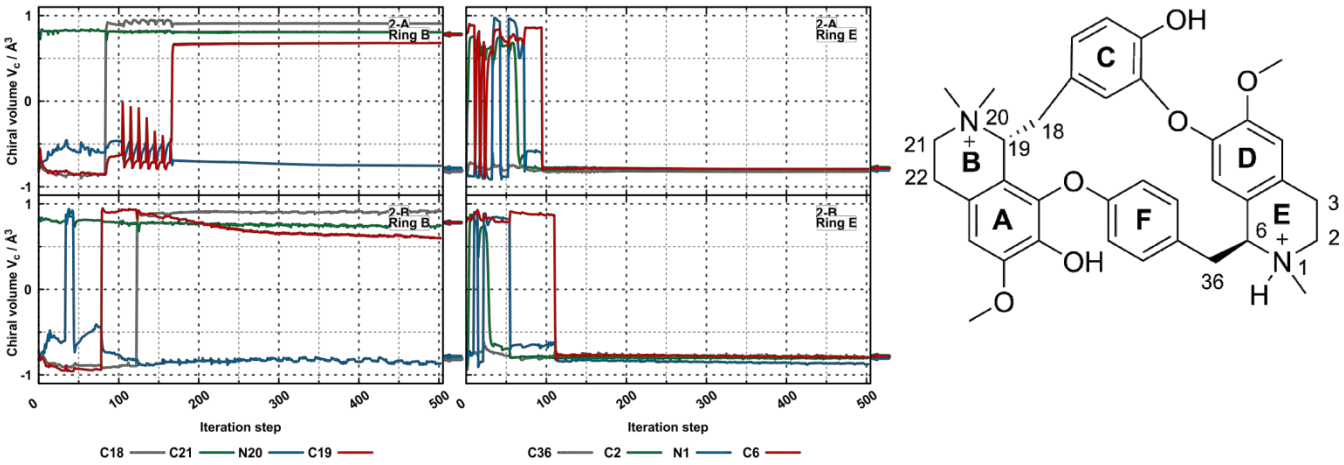

Figure 11. Trajectories of the chiral volumes of interest (rings **B** and **E**) for the runs **2-A** (top side) and **2-B** (bottom side). Additionally the respective methylene groups C18 and C36 are plotted.

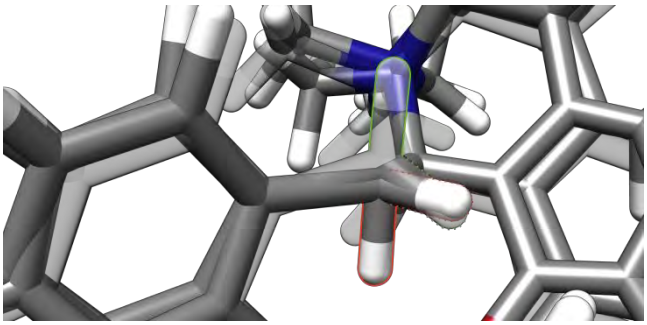

Figure 12. Zoom on the *pro*-chiral center C18 of the final structures of **2-A** and **2-B** (both solid) and the reference structure (transparent) used for the RDC prediction.

but not translated to the stereochemically correct configuration. Additionally, the inverse vector solution (marked red) shows an excellent agreement with the reference structure (marked green). The correct assignment of the two degenerate solutions should be possible if long-range couplings were added. In the background of Figure 12 the nitrogen center N20 (blue) can be seen. Deviations on the methyl vector orientation are observed. This again is the consequence of the high relative errors. Additional plots showing the reorientation of the aromatic rings **C** and **D** as well as the corresponding full trajectories and Monte-Carlo *rmsd*s are given in the supporting information.

Application on Strychnine. The final example is strychnine 3 which contains six chiral and six *pro*-chiral centers. In contrast to IPC 1, in which inversions of stereogenic centers will not lead to large distortions of the overall geometry, this example showcases a compound with chiral centers bridging two or more rings. Inversions on centers like C16 in strychnine 3 will lead to major distortions of the whole scaffold's geometry. The effect of the resulting large rearrangements on the overall optimization in combination with the full use of the stop criteria, set to a feasible limit to demonstrate the capability to detect convergence, will be discussed here. Eleven artificial RDC sets with 43 RDCs were used for the TITANIA run (called **3-A** here for consistency with the other examples). The 43 RDCs were again generated by using $^{1}D_{CH}$ couplings and long range $^{n}D_{HH}$ couplings limited to those with internuclear distances of not more than 3 Å. As in the previous examples the SECONDA plot was used to confirm the linear independence in combination to the absence of errors in the RDC sets (see SI Figure S-22).

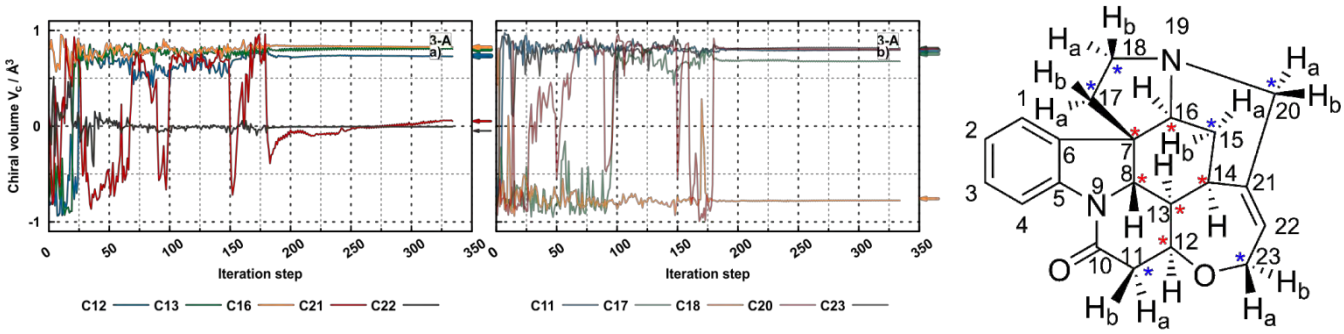

Figure 13. Trajectories of the chiral volumes of interest for strychnine (run **3-A**). The subplot a) shows the chiral volumes of the tertiary and quaternary carbons (C21 and C22 are sp^2 carbons and therefore should have a chiral volume V_c = 0 Å^3). The second subplot b) shows the chiral volumes of the *pro*-chiral centers.

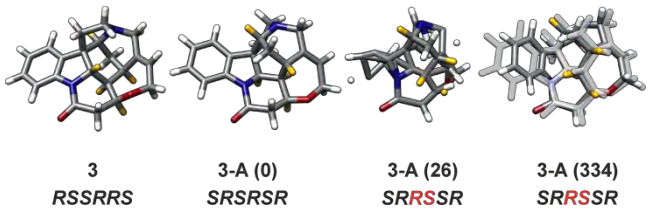

Figure 14. Comparison of different strychnine structures, with hydrogens of the chiral centers marked in gold. The first structure is the reference structure taken from literature. The other structures are encountered at different points of the iterations (denoted in brackets) in run **3-A** with the second structure depicting the deliberately "inverted" scaffold of the starting geometry. As the resulting final structure is the enantiomer, it was superimposed with the enantiomer of **3** (transparent) generated from the literature coordinates. For a better assessment of the structures the stereo descriptors of the chiral centers, which are ordered according to the atom numbering, are reported. The red descriptors are the inverted ones.

The eigenvalues of **3-A** show excellent linear independence, comparable to the IPC runs 1-A. All eigenvalues contribute to the overall variance and do not show extraordinarily low collectivities. This implies that a fast convergence should be possible.

As starting geometry for this test (see Figure 14, **3-A(0)**), four stereogenic centers of the scaffold were deliberately inverted (for more information see experimental section). The optimization of **3-A** shows much more complex trajectories than the previous runs. The majority of the chiral centers invert in the first part of the optimization (see Figure 13 subplot **a**). This can also be seen in the 3D structure of **3-A** at iteration 26 in Figure 14, where the chiral centers have been rearranged into the correct configuration by TITANIA. In contrast, the sp^2 carbon C21 shows large fluctuations and loses the expected planar geometry. This is likely elicited by the late convergence into the correct diastereotopic assignment and tetrahedral geometry of the neighboring *pro*-chiral center C20. Figure 14 illustrates an example for the large distortions of the 3D structure accompanied. The structure first loses its molecular shape. This is impressively observed at the aryl ring of iteration step 26 in Figure 14. In the following steps TITANIA reassembles strychnine achieving the correct vector orientations and relative configuration. As observed before for runs of **1-B** using random start coordinates, the enantiomer of **3** is obtained in this run. The relatively late inversion of the pro-chiral C20, however, would be of little consequence for structure elucidation if it was overlooked.

Strychnine shows how TITANIA is able to perform optimizations on rather complex compounds. In the course of the optimization the molecular shape is lost and rebuild to a proper structure based on the RDCs.

CONCLUSION

We demonstrate the use of multiple alignment media to determine the vector orientations solely from RDC data and use them to optimize the structure of small organic compounds with the newly developed software TITANIA on three representative examples. It was expected that such an approach is only feasible if enough linearly independent data sets are available. We could show here, that in an error-free scenario the linear independence is not as crucial in the structure refinement of IPC (setup **1-C**). Interestingly, above a certain threshold an increase in the number of alignment media does not affect the result in the absence of error. The set size, however, does: especially the inclusion of long-range couplings has a significant beneficial effect on the optimization (see **1-X11** runs with **X** equals **A** to **C**). More importantly, the process is not only possible using reasonable starting geometries, but also is successful when using random coordinates. This shows the enormous potential of the multiple alignment approach proposed here as this allows structure determination even in the absence of any prior information on stereogenic relations.

These very encouraging findings change when more realistic data with (artificial) experimental error are used. Here linearly dependent data may not lead to a reliable result (see **1-F**). Random inversions may occur in the optimization due to the incomplete sampling of possible alignments. RDC data with better linear independence (see **1-D** and **1-E**) converge to the correct solution when using long-range couplings. Even few long-range couplings, which are indeed available from modern experiments,[48] will improve accuracy in the vector orientations. The few examples which converged to the wrong configuration showed strong distortions of the tetrahedral geometries indicating the correct structure by showing the inverse RDC vector solution at the respective stereogenic center thus allowing an easy identification by the operator.

The assessment of the linear independence within the TITANIA protocol is based on the SECONDA approach. Here the linear (in-)dependence is analyzed simultaneously to possible heterogeneities. While initially developed to asses internal motions leading to heterogeneities captured in the RDCs, we use the combination of the eigenvalues and eigenmodes to identify linear (in)dependence of the alignment media used. Here the eigenvalues can be assessed by the distribution of the eigenvector elements. A global character (uniform distribution) shows eigenvalues that are caused by a change in orientation, thus showing a new linear independent orientation. Localized characters (few elements with large magnitude) are more likely to be related to heterogeneities in terms of structural or RDC noise.

Additionally to the small, rigid geometry like IPC (**1**) larger compounds with separated stereogenic domains and flexibility like tubocurarine (**2**) or complex and dependent scaffold geometries like strychnine (**3**) can be optimized using TITANIA. The trajectories become more complex and show more inversions until the final configuration is reached. Future work aims at using real experimental datasets. Modern alignment media, especially stimuli responsive media, in combination with the development of new pulse sequences, allowing the measurement of a large variety of long-range homo- and heteronuclear RDCs, build a toolbox to test TITANIA in the limits of modern NMR spectroscopy and structure elucidation. Additionally TITANIA reveals not only relative configurations and conformations of small organic compounds, but also allows for the determination of local order parameters, which will certainly be a very valuable source of information on dynamics in the future. All of the above features make TITANIA an optimal tool for the interpretation of RDC data in the context of a full structure elucidation.

EXPERIMENTAL SECTION

For the structure optimizations using TITANIA different kinds of RDC data are used. One is referred to as synthetic RDC set, where a set is a collection of RDCs under the same alignment condition. These synthetic values are predicted by utilizing a reference structure and alignment parameters derived from RDC sets reported in literature. The second kind of RDCs is referred to as artificial. The respective RDC sets are predicted by randomly generated orientation parameters (Azz < 10-2, R = [0, 2/3], α = [0°, 180°], β = [-180°, 180°], γ = [-180°, 180°] with ZYZ Euler convention for the AF to MF rotation). Unless stated otherwise, the optimizations were performed without proper stop criteria (only maximum number of iterations) for a better demonstration of the trajectories. The implemented stop criteria will be discussed in the results section.

The first example to demonstrate the concepts of TITANIA is isopinocampheol 1 which is well studied with RDCs. The input structure for this task was generated by inverting the chiral center C3 of a structure published earlier.[75] 20 artificial RDC sets were predicted using the literature structure and used directly in the setup called 1-A (information on how RDCs were chosen, see below). Additional data sets were generated from literature data,[37, 75, 84] resulting in one setup with the goal to achieve linear independence (**1-B**) and another one expected to show linear dependence (**1-C**) by utilizing only six RDC sets each. The assignments of the sets to the respective references can be found in the supporting information (see Table S-1). Additionally, the RDC setups 1-A to 1-C were also optimized starting from random coordinates with x, y, z = [0.0, 1.0] Å to show the ability of TITANIA to optimize structures without any prior stereochemical information.

To simulate experimental error of the RDCs Gaussian distributed random numbers (σ = 0.5 Hz) was added to the setups **1-A** to **1-C** resulting in **1-D** (**1-A** with errors), **1-E** (**1-B** with errors) and **1-F** (**1-C** with errors). The error for the homonuclear RDCs were downscaled due to their lower D_{max} compared to $^1D_{CH}$ couplings (common scaling factor for $^1D_{CC}$ 25% and $^nD_{HH}$ 50%).

All setups were optimized in five individual runs utilizing different set sizes (run **1-A11**, **A17**, **A23**, **A31** and **A39** and analogous for setups **B** to **F**) where the respective identifier encodes the number of RDCs per set of alignment conditions. The basis for all sets consists of all $^1D_{CH}$ (and derived methyl $^1D_{CC}$) couplings (**1-A11**). Additional six $^3D_{HH}$ couplings wrapping the structure once (**1-A17**), all $^2D_{HH}$ and $^3D_{HH}$ couplings (**1-A23**), an experimental set defined by 31 RDCs reported in literature[48] (**1-A31**) and all possible $^nD_{HH}$ couplings (**1-A39**) were chosen as meaningful set sizes. The RDC nuclei of the individual runs are listed in the supporting information (see Table S-81).

Tubocurarine **2** was optimized using eight artificial RDC sets with 37 RDCs each (see Table S-87). The RDCs were predicted using the published, modified solid state structure[53] with the original labels.[83] The chiral centers C6 and C19 were inverted and the resulting structure was minimized using the MMFF94 force field. The RDC sets contain the $^1D_{CH}$ and additional nine $^nD_{HH}$ couplings of the piperidinium protons. As for IPC, artificial error was added to the underlying RDC sets of run **2-A** to generate **2-B**. The added errors (Gaussian distributed with σ = 0.5 Hz) were not scaled for $^1D_{NC}$ and $^1D_{NH}$ to discuss the impact of the larger and more localized relative errors (especially $^1D_{CN}$) and we only rejected random numbers exceeding 1.5 Hz to prevent unrealistic high errors.

Strychnine **3** was optimized using eleven artificial RDC sets with 43 RDCs each in run **3-A** (see Table S-91). The RDCs were predicted using a structure from literature.[7] The RDC sets were generated using all $^1D_{CH}$ couplings and the $^{2/3}D_{HH}$ couplings of the protons with distances lower than 3 Å. The input structure was generated by inverting the chiral centers C7, C8, C14 and C16 of the ring scaffold. The resulting structure was minimized using the MMFF94 force field.

All input and output files containing the presented data (RDCs, structures, alignment conditions and SECONDA) are available as supplementary material. More details on the TITANIA protocol, the keywords to choose, further SECONDA analyses and all (further) trajectories can be found in the supporting information. As supplementary material we provide a zip archive, that contains all input and output files used here.

The source code for the TITANIA program as well as precompiled binaries are available from the authors upon request.

ASSOCIATED CONTENT

Supporting Information. This material is available free of charge via the Internet at http://pubs.acs.org.

Detailed description of the TITANIA protocol (chapter 1), experimental orientations in **1-B**/**1-C** (table S-1), SECONDA data of IPC **1** (section 2.2.1), all orientations associated to IPC using the C3-epimer as starting structure (section 2.2.2 – 2.2.5), data and discussion when starting from random coordinates (section 2.3), data and discussion when using non-default vector addition algorithm (section 2.4), detailed list of RDCs used for IPC (table S-81), final IPC structures (section 2.6), SECONDA eigenmodes for tubocurarine **2** (figure S-20), all orientations associated to tubocurarine (section 3.2), list of RDCs used for tubocurarine (table S-87), SECONDA plot for strychnine **3** (figure S-22), all orientations associated to strychnine (section 4.2), list of RDCs used for strychnine (table S-91), content of supplementary material zip-archive (chapter 5).

AUTHOR INFORMATION

Corresponding Author

Prof. Dr. Christina. M. Thiele
Clemens-Schöpf-Institut für Organische Chemie und Biochemie
Technical University of Darmstadt, Alarich-Weiss-Str. 16, 64287 Darmstadt (Germany); http://orcid.org/0000-0001-7876-536X; E-mail: cthiele@thielelab.de

Authors

Felix A. Roth
Clemens-Schöpf-Institut für Organische Chemie und Biochemie
Technical University of Darmstadt, Alarich-Weiss-Str. 16, 64287 Darmstadt (Germany)

Dr. Volker Schmidts
Clemens-Schöpf-Institut für Organische Chemie und Biochemie
Technical University of Darmstadt, Alarich-Weiss-Str. 16, 64287 Darmstadt (Germany); https://orcid.org/0000-0002-7195-312X

Author Contributions

The manuscript was written through contributions of all authors.

ACKNOWLEDGMENT

The authors thank Rafael Brüschweiler for helpful discussions on SECONDA.

ABBREVIATIONS

RDC residual dipolar couplings, MFA model-free approach, TITANIA TITANIA performs iterative analysis of independent alignments, SECONDA self-consistency of dipolar couplings analysis, AF alignment frame, VF vector frame, MF molecular frame.

REFERENCES

1. Levitt, M. H., *Spin Dynamics: basics of nuclear magnetic resonance*. 2 ed.; Wiley VCH: 2008.
2. Neuhaus, D.; Williamson, M. P., *The Nuclear Overhauser Effect in Structural and Conformational Analysis*. 2000.
3. Karplus, M., Contact Electron - Spin Coupling of Nuclear Magnetic Moments. *J. Chem. Phys.* **1959,** *30*, 11-15.
4. Bifulco, G.; Dambruoso, P.; Gomez-Paloma, L.; Riccio, R., Determination of relative configuration in organic compounds by NMR spectroscopy and computational methods. *Chem. Rev.* **2007,** *107* (9), 3744-3779.
5. Tolman, J. R.; Flanagan, J. M.; Kennedy, M. A.; Prestegard, J. H., NMR evidence for slow collective motions in cyanometmyoglobin. *Nature Structural Biology* **1997,** *4* (4), 292-297.
6. Tjandra, N.; Bax, A., Direct measurement of distances and angles in biomolecules by NMR in a dilute liquid crystalline medium. *Science* **1997,** *278* (5340), 1111-4.
7. Thiele, C. M.; Berger, S., Probing the Diastereotopicity of Methylene Protons in Strychnine Using Residual Dipolar Couplings. *Org. Lett.* **2003,** *5* (5), 705-708.
8. Verdier, L.; Sakhaii, P.; Zweckstetter, M.; Griesinger, C., Measurement of long range H,C couplings in natural products in orienting media: a tool for structure elucidation of natural products. *J. Magn. Reson.* **2003,** *163* (2), 353-9.
9. Aroulanda, C.; Boucard, V.; Guibé, F.; Courtieu, J.; Merlet, D., Weakly oriented liquid-crystal NMR solvents as a general tool to determine relative configurations. *Chem. Eur. J.* **2003,** *9* (18), 4536-9.
10. Böttcher, B.; Thiele, C. M., Determining the Stereochemistry of Molecules from Residual Dipolar Couplings (RDCs). *Encyclopedia of Magnetic Resonance* **2012.**
11. Chen, K.; Tjandra, N., The Use of Residual Dipolar Coupling in Studying Proteins by NMR. In *NMR of Proteins and Small Biomolecules. Topics in Current Chemistry*, G., Z., Ed. SpringerBerlin: Berlin, Heidelberg, 2001; Vol. 326.
12. Ban, D.; Sabo, T. M.; Griesinger, C.; Lee, D., Measuring dynamic and kinetic information in the previously inaccessible supra-tau(c) window of nanoseconds to microseconds by solution NMR spectroscopy. *Molecules* **2013,** *18* (10), 11904-37.
13. Huben, K.; Jewgiński, M.; Pabis, A.; Paluch, P.; Luy, B.; Jankowski, S., The structure of cyclolinopeptide A in chloroform refined by RDC measurements. *J. Pept. Sci.* **2014,** *20* (11), 901-907.
14. Salmon, L.; Blackledge, M., Investigating protein conformational energy landscapes and atomic resolution dynamics from NMR dipolar couplings: a review. *Rep Prog Phys* **2015,** *78* (12), 126601.
15. Fredersdorf, M.; Göstl, R.; Kolmer, A.; Schmidts, V.; Monecke, P.; Hecht, S.; Thiele, C. M., Exploring the conformational space of bridge-substituted dithienylcyclopentenes. *Chem. Eur. J.* **2015,** *21* (41), 14545-54.
16. Saupe, A., Recent Results in the Field of Liquid Crystals. *Angew. Chem. Int. Ed.* **1968,** *7* (2), 97-112.
17. Kramer, F.; Deshmukh, M. V.; Kessler, H.; Glaser, S. J., Residual dipolar coupling constants: An elementary derivation of key equations. *Conc. Magn. Reson. A* **2004,** *21A* (1), 10-21.
18. Losonczi, J. A.; Andrec, M.; Fischer, M. W. F.; Prestegard, J. H., Order Matrix Analysis of Residual Dipolar Couplings Using Singular Value Decomposition. *J. Magn. Reson.* **1999,** *138* (2), 334-342.
19. Thiele, C. M.; Schmidts, V.; Böttcher, B.; Louzao, I.; Berger, R.; Maliniak, A.; Stevensson, B., On the Treatment of Conformational Flexibility when Using Residual Dipolar Couplings for Structure Determination. *Angew. Chem. Int. Ed.* **2009,** *48* (36), 6708-6712.
20. Sun, H.; Reinscheid, U. M.; Whitson, E. L.; d'Auvergne, E. J.; Ireland, C. M.; Navarro-Vázquez, A.; Griesinger, C., Challenge of Large-Scale Motion for Residual Dipolar Coupling Based Analysis of Configuration: The Case of Fibrosterol Sulfate A. *J. Am. Chem. Soc.* **2011,** *133* (37), 14629-14636.
21. Tolman, J. R., A Novel Approach to the Retrieval of Structural and Dynamic Information from Residual Dipolar Couplings Using Several Oriented Media in Biomolecular NMR Spectroscopy. *J. Am. Chem. Soc.* **2002,** *124* (40), 12020-12030.
22. Briggman, K. B.; Tolman, J. R., De Novo Determination of Bond Orientations and Order Parameters from Residual Dipolar Couplings with High Accuracy. *J. Am. Chem. Soc.* **2003,** *125* (34), 10164-10165.
23. Meiler, J.; Prompers, J. J.; Peti, W.; Griesinger, C.; Brüschweiler, R., Model-Free Approach to the Dynamic Interpretation of Residual Dipolar Couplings in Globular Proteins. *J. Am. Chem. Soc.* **2001,** *123* (25), 6098-6107.
24. Peti, W.; Meiler, J.; Brüschweiler, R.; Griesinger, C., Model-Free Analysis of Protein Backbone Motion from Residual Dipolar Couplings. *J. Am. Chem. Soc.* **2002,** *124* (20), 5822-5833.

25. Lipari, G.; Szabo, A., Model-free approach to the interpretation of nuclear magnetic resonance relaxation in macromolecules. 1. Theory and range of validity. *J. Am. Chem. Soc.* **1982,** *104* (17), 4546-4559.
26. Lipari, G.; Szabo, A., Model-free approach to the interpretation of nuclear magnetic resonance relaxation in macromolecules. 2. Analysis of experimental results. *J. Am. Chem. Soc.* **1982,** *104* (17), 4559-4570.
27. Lakomek, N.-A.; Walter, K. F. A.; Farès, C.; Lange, O. F.; de Groot, B. L.; Grubmüller, H.; Brüschweiler, R.; Munk, A.; Becker, S.; Meiler, J.; Griesinger, C., Self-consistent residual dipolar coupling based model-free analysis for the robust determination of nanosecond to microsecond protein dynamics. *J. Biomol. NMR* **2008,** *41* (3), 139.
28. Sabo, T. M.; Smith, C. A.; Ban, D.; Mazur, A.; Lee, D.; Griesinger, C., ORIUM: Optimized RDC-based Iterative and Unified Model-free analysis. *J. Biomol. NMR* **2014,** *58* (4), 287-301.
29. Yao, L.; Vögeli, B.; Torchia, D. A.; Bax, A., Simultaneous NMR Study of Protein Structure and Dynamics Using Conservative Mutagenesis. *J. Phys. Chem. B* **2008,** *112* (19), 6045-6056.
30. Ruan, K.; Briggman, K. B.; Tolman, J. R., De novo determination of internuclear vector orientations from residual dipolar couplings measured in three independent alignment media. *J. Biomol. NMR* **2008,** *41* (2), 61-76.
31. Marx, A.; Böttcher, B.; Thiele, C. M., Enhancing the orienting properties of poly(gamma-benzyl-L-glutamate) by means of additives. *Chem. Eur. J.* **2010,** *16* (5), 1656-63.
32. Meyer, N.-C.; Krupp, A.; Schmidts, V.; Thiele, C. M.; Reggelin, M., Polyacetylenes as Enantiodifferentiating Alignment Media. *Angew. Chem. Int. Ed.* **2012,** *51* (33), 8334-8338.
33. Merle, C.; Kummerlöwe, G.; Freudenberger, J. C.; Halbach, F.; Stöwer, W.; Gostomski, C. L. v.; Höpfner, J.; Beskers, T.; Wilhelm, M.; Luy, B., Crosslinked Poly(ethylene oxide) as a Versatile Alignment Medium for the Measurement of Residual Anisotropic NMR Parameters. *Angew. Chem. Int. Ed.* **2013,** *52* (39), 10309-10312.
34. Lei, X.; Xu, Z.; Sun, H.; Wang, S.; Griesinger, C.; Peng, L.; Gao, C.; Tan, R. X., Graphene Oxide Liquid Crystals as a Versatile and Tunable Alignment Medium for the Measurement of Residual Dipolar Couplings in Organic Solvents. *J. Am. Chem. Soc.* **2014,** *136* (32), 11280-11283.
35. Jeziorowski, S.; Thiele, C. M., Poly-γ-p-Biphenylmethyl-Glutamate as Enantiodifferentiating Alignment Medium for NMR Spectroscopy with Temperature-Tunable Properties. *Chem. Eur. J.* **2018,** *24* (58), 15631-15637.
36. Schwab, M.; Schmidts, V.; Thiele, C. M., Thermoresponsive Alignment Media in NMR Spectroscopy: Helix Reversal of a Copolyaspartate at Ambient Temperatures. *Chem. Eur. J.* **2018,** *24* (54), 14373-14377.
37. Schwab, M.; Herold, D.; Thiele, C. M., Polyaspartates as Thermoresponsive Enantiodifferentiating Helically Chiral Alignment Media for Anisotropic NMR Spectroscopy. *Chem. Eur. J.* **2017,** *23* (58), 14576-14584.
38. Gil-Silva, L. F.; Santamaría-Fernández, R.; Navarro-Vázquez, A.; Gil, R. R., Collection of NMR Scalar and Residual Dipolar Couplings Using a Single Experiment. *Chem. Eur. J.* **2016,** *22* (2), 472-476.
39. Reller, M.; Wesp, S.; Koos, M. R. M.; Reggelin, M.; Luy, B., Biphasic Liquid Crystal and the Simultaneous Measurement of Isotropic and Anisotropic Parameters by Spatially Resolved NMR Spectroscopy. *Chem. Eur. J.* **2017,** *23* (54), 13351-13359.
40. Kurz, M.; Schmieder, P.; Kessler, H., HETLOC, an Efficient Method for Determining Heteronuclear Long-Range Couplings with Heteronuclei in Natural Abundance. *Angew. Chem. Int. Ed.* **1991,** *30* (10), 1329-1331.
41. Uhrín, D.; Batta, G.; Hruby, V. J.; Barlow, P. N.; Kövér, K. E., Sensitivity- and Gradient-Enhanced Hetero (ω1) Half-Filtered TOCSY Experiment for Measuring Long-Range Heteronuclear Coupling Constants. *J. Magn. Reson.* **1998,** *130* (2), 155-161.
42. Meissner, A.; Sørensen, O. W., Measurement of J(H,H) and long-range J(X,H) coupling constants in small molecules. Broadband XLOC and J-HMBC. *Magn. Reson. Chem.* **2001,** *39* (1), 49-52.
43. Fehér, K.; Berger, S.; Kövér, K. E., Accurate determination of small one-bond heteronuclear residual dipolar couplings by F1 coupled HSQC modified with a G-BIRD(r) module. *J. Magn. Reson.* **2003,** *163* (2), 340-346.
44. Kövér, K. E.; Fehér, K., Measurement of one-bond heteronuclear dipolar coupling contributions for amine and diastereotopic methylene protons. *J. Magn. Reson.* **2004,** *168* (2), 307-313.
45. Enthart, A.; Freudenberger, J. C.; Furrer, J.; Kessler, H.; Luy, B., The CLIP/CLAP-HSQC: pure absorptive spectra for the measurement of one-bond couplings. *J. Magn. Reson.* **2008,** *192* (2), 314-22.
46. Thiele, C. M.; Bermel, W., Speeding up the measurement of one-bond scalar (1J) and residual dipolar couplings (1D) by using non-uniform sampling (NUS). *J. Magn. Reson.* **2012,** *216*, 134-143.
47. Castañar, L.; Sauri, J.; Williamson, R. T.; Virgili, A.; Parella, T., Pure in-phase heteronuclear correlation NMR experiments. *Angew. Chem. Int. Ed.* **2014,** *53* (32), 8379-82.
48. Sinnaeve, D.; Ilgen, J.; Di Pietro, M. E.; Primozic, J. J.; Schmidts, V.; Thiele, C. M.; Luy, B., Probing Long-Range Anisotropic Interactions: a General and Sign-Sensitive Strategy to Measure (1) H-(1) H Residual Dipolar Couplings as a Key Advance for Organic Structure Determination. *Angew. Chem. Int. Ed.* **2020,** *59* (13), 5316-5320.
49. Koźmiński, W.; Nanz, D., Sensitivity Improvement and New Acquisition Scheme of Heteronuclear Active-Coupling-Pattern-Tilting Spectroscopy. *J. Magn. Reson.* **2000,** *142* (2), 294-299.
50. Hus, J.-C.; Brüschweiler, R., Principal component method for assessing structural heterogeneity across multiple alignment media. *J. Biomol. NMR* **2002,** *24* (2), 123-132.
51. Hus, J.-C.; Peti, W.; Griesinger, C.; Brüschweiler, R., Self-Consistency Analysis of Dipolar Couplings in Multiple Alignments of Ubiquitin. *J. Am. Chem. Soc.* **2003,** *125* (19), 5596-5597.
52. Cornilescu, G.; Ramos Alvarenga, R. F.; Wyche, T. P.; Bugni, T. S.; Gil, R. R.; Cornilescu, C. C.; Westler, W. M.; Markley, J. L.; Schwieters, C. D., Progressive Stereo Locking (PSL): A Residual Dipolar Coupling Based Force Field Method for Determining the Relative Configuration of Natural Products and Other Small Molecules. *ACS Chem. Biol.* **2017,** *12* (8), 2157-2163.
53. Immel, S.; Köck, M.; Reggelin, M., Configurational Analysis by Residual Dipolar Coupling Driven Floating Chirality Distance Geometry Calculations. *Chem. Eur. J.* **2018,** *24* (52), 13918-13930.
54. Tzvetkova, P.; Sternberg, U.; Gloge, T.; Navarro-Vázquez, A.; Luy, B., Configuration determination by residual dipolar couplings: accessing the full conformational space by molecular dynamics with tensorial constraints. *Chem. Sci.* **2019,** *10* (38), 8774-8791.
55. Fares, C.; Lingnau, J. B.; Wirtz, C.; Sternberg, U., Conformational Investigations in Flexible Molecules Using Orientational NMR Constraints in Combination with (3)J-Couplings and NOE Distances. *Molecules* **2019,** *24* (23).
56. Di Pietro, M. E.; Sternberg, U.; Luy, B., Molecular Dynamics with Orientational Tensorial Constraints: A New Approach to Probe the Torsional Angle Distributions of Small Rotationally Flexible Molecules. *J. Phys. Chem. B* **2019,** *123* (40), 8480-8491.
57. Saupe, A.; Englert, G., High-Resolution Nuclear Magnetic Resonance Spectra of Orientated Molecules. *Phys. Rev. Lett.* **1963,** *11* (10), 462-464.
58. Saupe, A., Kernresonanzen in kristallinen Flüssigkeiten und in kristallinflüssigen Lösungen. Teil I. In *Zeitschrift für Naturforschung A,* 1964; Vol. 19, p 161.
59. Burnell, E. E., Effects of Interaction between Molecular Internal Motion and Reorientation on Nmr of Anisotropic Liquids. *J. Magn. Reson.* **1980,** *39* (3), 461-480.
60. Emsley, J. W.; Luckhurst, G. R., The effect of internal motion on the orientational order parameters for liquid crystalline systems. *Mol. Phys.* **1980,** *41* (1), 19-29.
61. Burnell, E. E.; de Lange, C. A.; Mouritsen, O. G., Effects of intramolecular motion on the magnetic resonance of anisotropic liquids: The equivalence of kinetic and equilibrium statistical mechanical approaches. *J. Mag. Reson.* **1982,** *50* (2), 188-196.
62. Thiele, C. M.; Marx, A.; Berger, R.; Fischer, J.; Biel, M.; Giannis, A., Determination of the Relative Configuration of a Five-Membered Lactone from Residual Dipolar Couplings. *Angew. Chem. Int. Ed.* **2006,** *45* (27), 4455-4460.
63. Skrynnikov, N. R.; Goto, N. K.; Yang, D.; Choy, W.-Y.; Tolman, J. R.; Mueller, G. A.; Kay, L. E., Orienting domains in proteins using dipolar

couplings measured by liquid-state NMR: differences in solution and crystal forms of maltodextrin binding protein loaded with β-cyclodextrin11Edited by P. E. Wright. *J. Mol. Biol.* **2000,** *295* (5), 1265-1273.
64. Merlet, D.; Emsley, J. W.; Lesot, P.; Courtieu, J., The relationship between molecular symmetry and second-rank orientational order parameters for molecules in chiral liquid crystalline solvents. *J. Chem. Phys.* **1999,** *111* (15), 6890-6896.
65. Zweckstetter, M.; Bax, A., Prediction of Sterically Induced Alignment in a Dilute Liquid Crystalline Phase: Aid to Protein Structure Determination by NMR. *J. Am. Chem. Soc.* **2000,** *122* (15), 3791-3792.
66. Ibáñez de Opakua, A.; Klama, F.; Ndukwe, I. E.; Martin, G. E.; Williamson, R. T.; Zweckstetter, M., Determination of Complex Small-Molecule Structures Using Molecular Alignment Simulation. *Angew. Chem. Int. Ed.* **2020,** *59* (15), 6172-6176.
67. Peng, C.; Ayala, P. Y.; Schlegel, H. B.; Frisch, M. J., Using redundant internal coordinates to optimize equilibrium geometries and transition states. *J. Comput. Chem.* **1996,** *17* (1), 49-56.
68. Bakken, V.; Helgaker, T., The efficient optimization of molecular geometries using redundant internal coordinates. *J. Chem. Phys.* **2002,** *117* (20), 9160-9174.
69. Eyring, H., The resultant electric moment of complex molecules. *Phys. Rev.* **1932,** *39* (4), 746--748.
70. Exclusion distances are implemented as a linear term equivalent to bond lengths, when interatomic distances fall below a predefined threshold (on average ~70% of standard 1-3 distances).
71. Havel, T. F.; Kuntz, I. D.; Crippen, G. M., The theory and practice of distance geometry. *Bull. Math. Biol.* **1983,** *45* (5), 665-720.
72. Berger, R.; Courtieu, J.; Gil, R. R.; Griesinger, C.; Köck, M.; Lesot, P.; Luy, B.; Merlet, D.; Navarro-Vázquez, A.; Reggelin, M.; Reinscheid, U. M.; Thiele, C. M.; Zweckstetter, M., Is Enantiomer Assignment Possible by NMR Spectroscopy Using Residual Dipolar Couplings from Chiral Nonracemic Alignment Media?—A Critical Assessment. *Angew. Chem. Int. Ed.* **2012,** *51* (33), 8388-8391.
73. Lakomek, N. A.; Carlomagno, T.; Becker, S.; Griesinger, C.; Meiler, J., A Thorough Dynamic Interpretation of Residual Dipolar Couplings in Ubiquitin. *J. Biomol. NMR* **2006,** *34* (2), 101-115.
74. Sass, J.; Cordier, F.; Hoffmann, A.; Rogowski, M.; Cousin, A.; Omichinski, J. G.; Löwen, H.; Grzesiek, S., Purple Membrane Induced Alignment of Biological Macromolecules in the Magnetic Field. *J. Am. Chem. Soc.* **1999,** *121* (10), 2047-2055.
75. Marx, A.; Schmidts, V.; Thiele, C. M., How different are diastereomorphous orientations of enantiomers in the liquid crystalline phases of PBLG and PBDG: a case study. *Magn. Reson. Chem.* **2009,** *47* (9), 734-740.
76. F.A. Roth, V. Schmidts, J. Rettig, C.M. Thiele, Manuscript in preparation.
77. Pearson, K., LIII. On lines and planes of closest fit to systems of points in space. *The London, Edinburgh, and Dublin Philosophical Magazine and Journal of Science* **1901,** *2* (11), 559-572.
78. Hotelling, H., Analysis of a complex of statistical variables into principal components. *Journal of Educational Psychology* **1933,** *24* (6), 417-441.
79. Brüschweiler, R., Collective protein dynamics and nuclear spin relaxation. *J. Chem. Phys.* **1995,** *102* (8), 3396-3403.
80. The magnitude of the chiral Volume $|Vc| = |a * (b \times c)|$ is calculated for all possible permutations of the bondvectors. The rmsd of all |Vc| is calculated to assess the geometry of the respective center. If the geometry is well defined the rmsd will result in a low value.
81. Ulmer, T. S.; Ramirez, B. E.; Delaglio, F.; Bax, A., Evaluation of Backbone Proton Positions and Dynamics in a Small Protein by Liquid Crystal NMR Spectroscopy. *J. Am. Chem. Soc.* **2003,** *125* (30), 9179-9191.
82. Tolman, J. R.; Ruan, K., NMR Residual Dipolar Couplings as Probes of Biomolecular Dynamics. *Chem. Rev.* **2006,** *106* (5), 1720-1736.
83. Reynolds, C. D.; Palmer, R. A., The crystal structure, absolute configuration and stereochemistry of (+)-tubocurarine dibromide methanol solvate: a potent neuromuscular blocking agent. *Acta Cryst. B* **1976,** *32* (5), 1431-1439.
84. Hansmann, S.; Larem née Montag, T.; Thiele, C. M., Enantiodifferentiating Properties of the Alignment Media PELG and PBLG - A Comparison. *Eur. J. Org. Chem.* **2016,** *2016* (7), 1324-1329.

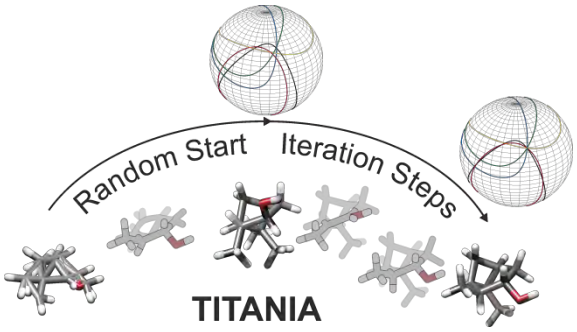
Random Start
Iteration Steps
TITANIA

Supporting information TITANIA

Felix A. Roth, Volker Schmidts, Christina M. Thiele

Contents

1 TITANIA protocol

1.1 Flowchart

TITANIA performs three major steps (parametrization, iterative refinement and Monte-Carlo bootstrap. See figure 4 in main text) which can be further extended as shown in fig. S-1.

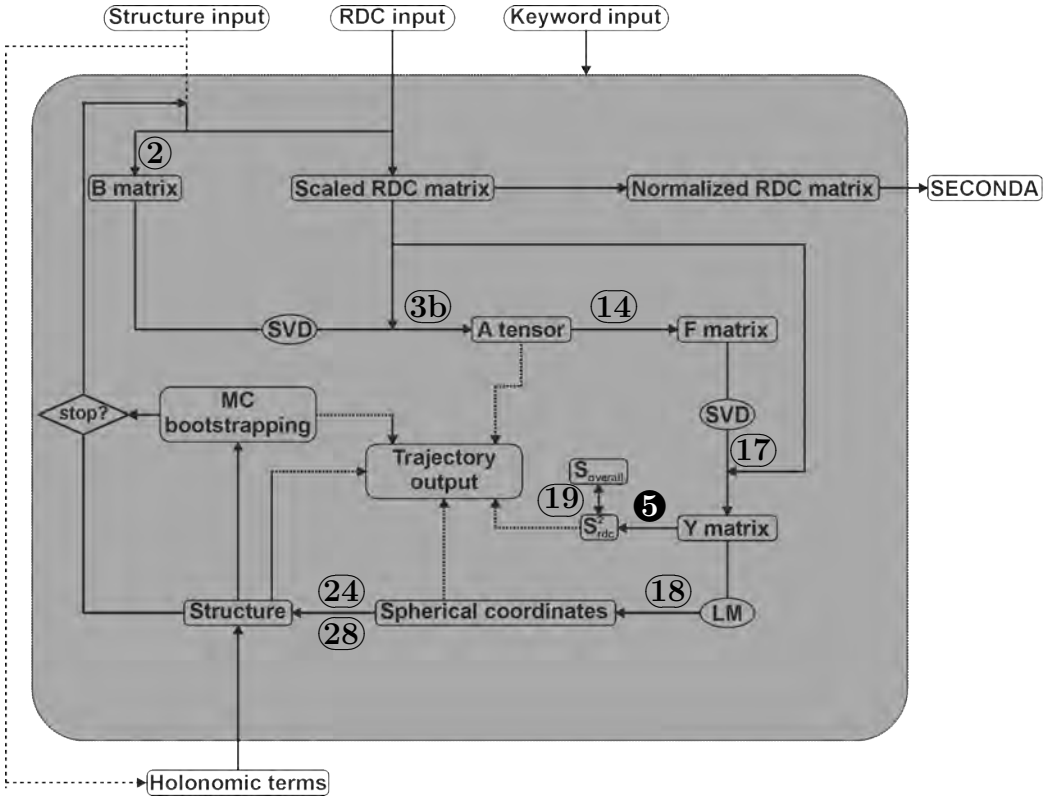

Figure S-1: Extended flowchart for TITANIA. The numbers shown in the scheme refer to the respective equation in the SI (gray) and main text (black).

The user has to define an initial structure (default: Cartesian coordinates and connectivity, see section 1.2.1) and the RDC data. In addition keywords can be used to adapt nearly every step of the TITANIA run to the current optimization. The first step is the parametrization of the structure, for which the holonomic terms (standard bond lengths, bond angles) are extracted from the initial input structure or the MMFF94[1] force field, the **B**-matrix is defined[2] and initial parameters are calculated (e.g. bond lengths and

$D_{\max}$). These initial parameters are used with the user defined RDCs to build a scaled and normalized RDC matrix, which is needed for the SECONDA analysis, the calculation of orientations and refined spherical harmonics $\mathbf{Y}$.

The alignment tensor $\mathbf{A}$ is calculated using the scaled RDC matrix $\mathbf{D}$ (for more information on the RDC matrix see section 1.3.2) and the normalized cosine matrix $\mathbf{B}$ and is analyzed *via* eigenvalue decomposition (describing the alignment frame AF). Using the resulting eigenvectors and rhombicity R the $\mathbf{F}$-matrix is constructed and utilized to determine the refined spherical harmonics $\mathbf{Y}$ by SVD of $\mathbf{F}$. To extract the spherical coordinates θ and ϕ from $\mathbf{Y}$ the Levenberg-Marquardt (LM) algorithm is used to find the Wigner rotation between the vector frame (VF) and molecular frame (MF). The structure can directly be derived from these angles using different algorithms, which can be chosen by the user by keywords. The default algorithm are the redundant internal coordinates (see section 1.3.4). An additional algorithm uses vector addition (see section 1.3.5) which leaves the carbon scaffold untouched. Thus no large changes required to correct wrong ring junctions (as in the strychnine example, see **3-A** in the main text) are possible.

To check for convergence in the optimization and to estimate uncertainties of the previously calculated orientation and structure parameters a Monte-Carlo bootstrap is performed. Some uncertainties can be determined directly (e.g. the uncertainty of the alignment tensor elements ΔA_{ij}). Others have to be estimated using Gaussian propagation of errors (e.g. the uncertainty of the spherical coordinates Δp). If convergence is reached, the iterative cylce is stopped (after n additional user defined cycles), an additional SECONDA analysis is performed (since the normalization factors depend on the structure) and the output files are finalized. In the course of the optimization the calculated parameters of all individual iteration steps are written to a trajectory file.

1.2 Input and output files

All input and output files of the individual runs reported in the main text are part of the supplementary material. The information content is described in the following.

1.2.1 Input file

TITANIA uses three types of inputs:

- **Structure input**: contains Cartesian coordinates of an initial structure. The structure contains labels for the individual atoms and follows a simple syntax:

```
xyzcoordinates[<molecule_name>] =
number_of_atoms
<structure_name>
C1      −0.073   2.395   0.114   #C1
C2      −0.750   1.046   0.423   #C2
...
```

Additionally a connectivity matrix is defined.

```
connectivity[<molecule_name>] =
number_of_atoms
<structure_name>
C1      H1      C2      C6      C7
C2      H2      C3      C10     C1
...
```

- **RDC input**: defines the RDCs, their uncertainty and weighting. The respective spin pair is defined by the identifier defined in the structure.

```
C1;H1;14.6;0.5;1.0
C2;H2;−11.0;0.5;1.0
...
```

- **Keyword input**: controls the behavior of TITANIA. Important (case insensitive) keywords are:

  - **MaxTITANIAiterations:** defines the number of iterations TITANIA performes before it is stopped (independent of convergence).
  - **overoptimizationSteps:** defines the number of iterations TITANIA performes after the maximum number of iterations or convergence is reached.
  - **QfactorConvergence:** defines convergence threshold for the *rmsd*(Q-factors) of two consecutive iteration steps.
  - **MeanAlignmentConvergence:** defines convergence threshold for the $rmsd(\mathbf{S}_{\mathrm{MC}})$ (*rmsd* of the Saupe tensor elements) of two consecutive iteration steps.
  - **SigmaAlignmentConvergence:** defines convergence threshold for the $rmsd(\sigma[\mathbf{S}_{\mathrm{MC}}])$ (*rmsd* of the Saupe tensor element uncertainties) of two consecutive iteration steps.
  - **MeanAngleConvergence:** defines convergence threshold for the $rmsd(\mathbf{p}_{\mathrm{MC}})$ (*rmsd* of the spherical coordinates) of two consecutive iteration steps.

- **SigmaAngleConvergence:** defines convergence threshold for the $rmsd(\sigma[\mathbf{p}_{\mathrm{MC}}])$ ($rmsd$ of the spherical coordinate uncertainties) of two consecutive iteration steps.
- **SpreadAngleConvergence:** defines convergence threshold for the $rmsd(R_{\mathrm{s}})$ ($rmsd$ of the mean RDC vector lengths) of two consecutive iteration steps.
- **useRedundantsOnlyAfter** defines the number of iterations after which TITANIA only perform redundant internal coordinates structure optimization and skips a prior vector addition step (section 1.3.5).
- **useDistances**: defines if lower distance bounds are considered in the optimization:
  - **0**: lower distance bounds are ignored.
  - **1**: lower distance bounds are fully considered (combination of **2** and **3**).
  - **2**: lower distance bounds are used in redundant internal coordinates as additional internal coordinate type.
  - **3**: lower distance bounds are used to force an inversion on atom (groups) if violations are present for consecutive steps.
- **redundantsDamping:** defines the damping factor δ (see eq. (26)) for the redundant internal coordinates.
- **StaticBondWeighting:** defines the static weighting (w_{bond}) for bond lengths of redundant internal coordinates (see eq. (25)).
- **StaticAngleWeighting:** defines the static weighting (w_{angle}) for bond angles of redundant internal coordinates (see eq. (25)).
- **StaticRDCWeighting:** defines the static weighting (w_{RDC}) for RDC orientations of redundant internal coordinates (see eq. (25)).
- **StaticChiralVolumeWeighting:** defines the static weighting ($w_{\mathrm{V_c}}$) for chiral volumes of redundant internal coordinates (see eq. (25)).
- **StaticDistanceWeighting:** defines the static weighting ($w_{\mathrm{dist.}}$) for lower distances of redundant internal coordinates (see eq. (25)).
- **floatingRDCangles:** defines if an angle enclosed by an RDC defined and undefined bond is weighted.
- **CalculateFullMatrix:** defines how eq. (3b) and eq. (17) are solved:
  - **0**: solved as a set of vector equations. Enables the use of individual RDC weighting (and even neglecting RDCs).
  - **1**: solved as full matrix equations.

- **errorWeightInSVD:** weights RDCs using their user defined errors. `CalculateFullMatrix=0` has to be set.
- **MonteCarloBootstrapping:** defines if a Monte-Carlo bootstrap is performed on every iteration step.

This inputs are gathered in the main input (.tna) file which is used as argument when starting TITANIA. The output file is generated by extending the input file with the respective suffixes (*vide infra*).

1.2.2 Output files

TIANIA has four output files:

- `.out` contains general informations on the optimization, the input file and keywords. Additionally it contains information on the structure, RDC sampling and final results. Besides this the trajectory of the Q-factors and chiral volumes are reported.
- `.out.<setLabel>.ali` is a output for the individual RDC sets.
- `.out.trj` contains the full SECONDA analysis (since it is performed on the initial and final structure). In addition it gives information on transformations (initial reference frame and PAS of intertia tensor, change of frames between the iteration steps). The main content are all relevant results obtained from the individual steps:
  - Polar angles (with Monte-Carlo results).
  - Levenberg-Marquardt parameters.
  - Redundant internal coordinate information (including individual damping factors).
  - Cartesian coordinates and transformation information.
  - Cosine matrix.
  - Q-Factors.
  - Alignment information (with Monte-Carlo results).
  - Dynamics information.
  - Stop criteria and the corresponding parameters monitored.
- `.out.xyz` contains the Cartesian coordinates of the individual iteration steps in the standard xyz-convention.

1.3 Mathematics

1.3.1 SECONDA weighting scheme

The covariance matrix used for the SECONDA analysis (see equation 6 in the main text) uses the mean of an individual RDC vector in all media (eq. (1a)) and the weighting factor w_m (eq. (1c)) which uses the mean of all RDCs in one medium (eq. (1b)).

$$\langle D_\mathrm{k} \rangle = \frac{1}{M} \sum_{m}^{M} D_\mathrm{k}^\mathrm{m} \tag{1a}$$

$$\langle D^\mathrm{m} \rangle = \frac{1}{K} \sum_{k}^{K} D_\mathrm{k}^\mathrm{m} \tag{1b}$$

$$w_\mathrm{m} = \frac{1}{\sigma_\mathrm{m}^2} = \frac{1}{\frac{1}{K-1} \sum_\mathrm{k}^\mathrm{K} \left(D_\mathrm{k}^\mathrm{m} - \langle D^\mathrm{m} \rangle \right)^2} \tag{1c}$$

The weighting can in principle be chosen in other ways, but eq. (1c) is the hard coded implementation of TITANIA.
For a proper analysis of the eigenvalues a cutoff of 1e-9 is implemented as numerical threshold.

1.3.2 RDC theory

RDCs are defined *via* the normalized cosine matrix $\boldsymbol{B}$ and alignment matrix $\boldsymbol{A}$, which contain the independent elements of the second-rank alignment tensor $\mathbf{A}$ and the structure related cosine tensor $\mathbf{B}$. These independent elements of a second rank tensor $\mathbf{T}$ are expressed in $\boldsymbol{T}^{(2)}$ by the corresponding normalized elements T_ij.[2]

$$\boldsymbol{T}^{(2)} = \left[T_\mathrm{zz}, \frac{1}{\sqrt{3}} \left(T_\mathrm{xx} - T_\mathrm{yy} \right), \frac{2}{\sqrt{3}} T_\mathrm{xy}, \frac{2}{\sqrt{3}} T_\mathrm{xz}, \frac{2}{\sqrt{3}} T_\mathrm{yz} \right] \tag{2a}$$

$$A_\mathrm{ij} = \left\langle \frac{1}{2} \left(3 \cos \alpha_\mathrm{i} \cos \alpha_\mathrm{j} - \delta_\mathrm{ij} \right) \right\rangle \tag{2b}$$

$$B_\mathrm{ij} = \left\langle \frac{1}{2} \left(3 \cos \beta_\mathrm{i} \cos \beta_\mathrm{j} - \delta_\mathrm{ij} \right) \right\rangle \tag{2c}$$

Here α_i is the angles enclosed by the magnetic field vector and the reference axes ($\mathrm{i} = \{x, y, z\}$) of the molecular frame, β_u is the angle enclosed by the RDC vector and the reference axes and δ_ij is the Kronecker symbol.

$$\mathbf{D_A} = diag\left[D_{\max}\right]\boldsymbol{BA} \tag{3a}$$
$$\left(\boldsymbol{B^+B}\right)\boldsymbol{A} = \boldsymbol{B^+}diag\left[D^{-1}_{\max}\right]\mathbf{D_A} \tag{3b}$$

Note that $\mathbf{D_A}$ is the non-normalized RDC matrix, which is the transpose of $\mathbf{D}$ used in equation 4 of the main text. Transposing is not needed but allows for an easier recognition of the orthogonal projector ($\boldsymbol{B^+B}$) (and later the respective operator $\boldsymbol{F^+F}$).[2] $diag\left[D_{\max}\right]$ is a matrix containing the maximum possible dipolar coupling for the individual spin pairs on its diagonal. By performing an eigenvalue decomposition on $\mathbf{A}$ the eigenvalue A_{zz}, the rhombicity R as well as the Euler angles α, β and γ can be calculated. Utilizing the second-rank spherical harmonics $Y_{2,\mathrm{m}}\left(\theta,\phi\right)$, with the spherical coordinates θ and ϕ, the general rotations $\mathbf{R}$, using the Wigner elements $D^{(2)}_{\mathrm{M,m}}$, can be formulated:

$$Y^{(2)}_{2,0}\left(\theta,\phi\right) = \sqrt{\frac{5}{16\pi}}\left(3\cos^2\left(\theta\right)-1\right) \tag{4a}$$
$$Y^{(2)}_{2,1}\left(\theta,\phi\right) = -\sqrt{\frac{15}{8\pi}}\cos\left(\theta\right)\sin\left(\theta\right)\exp^{2\mathrm{i}\phi} \tag{4b}$$
$$Y^{(2)}_{2,\text{-}1}\left(\theta,\phi\right) = -Y^{*(2)}_{2,1}\left(\theta,\phi\right) \tag{4c}$$
$$Y^{(2)}_{2,2}\left(\theta,\phi\right) = \sqrt{\frac{15}{32\pi}}\sin^2\left(\theta\right)\exp^{-2\mathrm{i}\phi} \tag{4d}$$
$$Y^{(2)}_{2,\text{-}2}\left(\theta,\phi\right) = Y^{*(2)}_{2,2}\left(\theta,\phi\right) \tag{4e}$$

$$\mathbf{R}\left(\alpha,\beta,\gamma\right)Y^{(2)}_{2,\mathrm{m}}\left(\theta,\phi\right) = \sum_{\mathrm{M=}\text{-}2}^{2}\exp^{-\mathrm{i}\alpha\mathrm{M}}d^{(2)}_{\mathrm{M,m}}\left(\beta\right)\exp^{-\mathrm{i}\gamma\mathrm{m}}Y^{(2)}_{2,\mathrm{M}}\left(\theta,\phi\right) \tag{5a}$$
$$= \sum_{\mathrm{M=}\text{-}2}^{2}D^{(2)}_{\mathrm{M,m}}\left(\alpha,\beta,\gamma\right)Y^{(2)}_{2,\mathrm{M}}\left(\theta,\phi\right) \tag{5b}$$

This allows for the definition of eq. (6b) (which is the static formulation

of equation 2 in the main text) in any arbitrary reference frame:

$$D = A_{\mathrm{a}} D_{\max} \left[3\cos^2\theta^{\mathrm{AF}} - 1 + \frac{3}{2} R \sin^2\theta^{\mathrm{AF}} \cos 2\phi^{\mathrm{AF}} \right] \tag{6a}$$

$$D = A_{\mathrm{a}} D_{\max} \sqrt{\frac{4}{5\pi}} \left[Y_{2,0}^{(2)} + \sqrt{\frac{3}{8}} R \left(Y_{2,2}^{(2)} + Y_{2,2}^{*(2)} \right) \right] \tag{6b}$$

The full rotation sequence from the VF to the MF and finally to the AF (eqs. (7) to (11)) for the individual spherical harmonics used in eq. (6b) can be formulated by:

$$\mathbf{R}_{\mathrm{VF}\to\mathrm{MF}}(\alpha,\beta,\gamma)\mathbf{R}_{\mathrm{MF}\to\mathrm{AF}}(0,\theta,\phi)\, Y_{2,0}^{(2)}(0,0) \tag{7a}$$

$$= \mathbf{R}_{\mathrm{VF}\to\mathrm{MF}}(\alpha,\beta,\gamma) \sum_{\mathrm{M=-2}}^{2} D_{\mathrm{M},0}^{(2)}(0,\theta,\phi)\, Y_{2,\mathrm{M}}^{(2)}(0,0) \tag{7b}$$

$$= \mathbf{R}_{\mathrm{VF}\to\mathrm{MF}}(\alpha,\beta,\gamma)\, D_{0,0}^{(2)}(0,\theta,\phi) \tag{7c}$$

$$= \sum_{\mathrm{M=-2}}^{2} D_{\mathrm{M},0}^{(2)}(\alpha,\beta,\gamma)\, Y_{2,\mathrm{M}}^{(2)}(\theta,\phi) \tag{7d}$$

$$D_{0,0}^{(2)}(0,\theta,\phi) = Y_{2,0}^{(2)}(\theta,\phi) \tag{8}$$

$$\mathbf{R}_{\mathrm{VF}\to\mathrm{MF}}(\alpha,\beta,\gamma)\mathbf{R}_{\mathrm{MF}\to\mathrm{AF}}(0,\theta,\phi)\, Y_{2,2}^{(2)}(0,0) \tag{9a}$$

$$= \mathbf{R}_{\mathrm{VF}\to\mathrm{MF}}(\alpha,\beta,\gamma) \sum_{\mathrm{M=-2}}^{2} D_{\mathrm{M},2}^{(2)}(0,\theta,\phi)\, Y_{2,\mathrm{M}}^{(2)}(0,0) \tag{9b}$$

$$= \mathbf{R}_{\mathrm{VF}\to\mathrm{MF}}(\alpha,\beta,\gamma)\, D_{0,2}^{(2)}(0,\theta,\phi) \tag{9c}$$

$$= \sum_{\mathrm{M=-2}}^{2} D_{\mathrm{M},2}^{(2)}(\alpha,\beta,\gamma)\, Y_{2,\mathrm{M}}^{(2)}(\theta,\phi) \tag{9d}$$

$$D_{0,2}^{(2)}(0,\theta,\phi) = Y_{2,2}^{(2)}(\theta,\phi) \tag{10}$$

$$\mathbf{R}_{\mathrm{VF}\to\mathrm{MF}}(\alpha,\beta,\gamma)\mathbf{R}_{\mathrm{MF}\to\mathrm{AF}}(0,\theta,\phi)\,Y^{(2)}_{2,\text{-}2}(0,0) \tag{11a}$$

$$= \mathbf{R}_{\mathrm{VF}\to\mathrm{MF}}(\alpha,\beta,\gamma)\sum_{\mathrm{M}=\text{-}2}^{2} D^{(2)}_{\mathrm{M},\text{-}2}(0,\theta,\phi)\,Y^{(2)}_{2,\mathrm{M}}(0,0) \tag{11b}$$

$$= \mathbf{R}_{\mathrm{VF}\to\mathrm{MF}}(\alpha,\beta,\gamma)\,D^{(2)}_{0,\text{-}2}(0,\theta,\phi) \tag{11c}$$

$$= \sum_{\mathrm{M}=\text{-}2}^{2} D^{(2)}_{\mathrm{M},\text{-}2}(\alpha,\beta,\gamma)\,Y^{(2)}_{2,\mathrm{M}}(\theta,\phi) \tag{11d}$$

$$D^{(2)}_{0,\text{-}2}(0,\theta,\phi) = Y^{(2)}_{2,\text{-}2}(\theta,\phi) \tag{12}$$

Using these rotations the final expression for an RDC in an arbitrary reference frame is obtained:

$$D = A_{\mathrm{a}} D_{\max}\sqrt{\frac{4}{5\pi}}\left[\sum_{\mathrm{M}=\text{-}2}^{2}\left\langle D^{(2)}_{\mathrm{M},0}\right\rangle\left\langle Y^{(2)}_{2,\mathrm{M}}\right\rangle + \sqrt{\frac{3}{8}}R\left(\sum_{\mathrm{M}=\text{-}2}^{2}\left\langle D^{(2)}_{\mathrm{M},2}\right\rangle\left\langle Y^{(2)}_{2,\mathrm{M}}\right\rangle + \sum_{\mathrm{M}=\text{-}2}^{2}\left\langle D^{(2)}_{\mathrm{M},\text{-}2}\right\rangle\left\langle Y^{(2)}_{2,\mathrm{M}}\right\rangle\right)\right] \tag{13a}$$

$$\begin{aligned} D = A_{\mathrm{a}} D_{\max}\sqrt{\frac{4}{5\pi}} \\ \Big[\left\langle D^{(2)}_{\text{-}2,0}\right\rangle\left\langle Y^{(2)}_{2,\text{-}2}\right\rangle + \left\langle D^{(2)}_{\text{-}1,0}\right\rangle\left\langle Y^{(2)}_{2,\text{-}1}\right\rangle + \left\langle D^{(2)}_{0,0}\right\rangle\left\langle Y^{(2)}_{2,0}\right\rangle + \\ \left\langle D^{(2)}_{1,0}\right\rangle\left\langle Y^{(2)}_{2,1}\right\rangle + \left\langle D^{(2)}_{2,0}\right\rangle\left\langle Y^{(2)}_{2,2}\right\rangle + \sqrt{\frac{3}{8}}R \\ \Big[\left\langle D^{(2)}_{\text{-}2,2}\right\rangle\left\langle Y^{(2)}_{2,\text{-}2}\right\rangle + \left\langle D^{(2)}_{\text{-}1,2}\right\rangle\left\langle Y^{(2)}_{2,\text{-}1}\right\rangle + \left\langle D^{(2)}_{0,2}\right\rangle\left\langle Y^{(2)}_{2,0}\right\rangle + \\ \left\langle D^{(2)}_{1,2}\right\rangle\left\langle Y^{(2)}_{2,1}\right\rangle + \left\langle D^{(2)}_{2,2}\right\rangle\left\langle Y^{(2)}_{2,2}\right\rangle + \\ \left\langle D^{(2)}_{\text{-}2,\text{-}2}\right\rangle\left\langle Y^{(2)}_{2,\text{-}2}\right\rangle + \left\langle D^{(2)}_{\text{-}1,\text{-}2}\right\rangle\left\langle Y^{(2)}_{2,\text{-}1}\right\rangle + \left\langle D^{(2)}_{0,\text{-}2}\right\rangle\left\langle Y^{(2)}_{2,0}\right\rangle + \\ \left\langle D^{(2)}_{1,\text{-}2}\right\rangle\left\langle Y^{(2)}_{2,1}\right\rangle + \left\langle D^{(2)}_{2,\text{-}2}\right\rangle\left\langle Y^{(2)}_{2,2}\right\rangle\Big]\Big] \end{aligned} \tag{13b}$$

$$D = A_{\mathrm{a}} D_{\max}\vec{\mathbf{F}}\vec{\mathbf{Y}} \tag{13c}$$

where the Wigner rotation elements are combined in $\vec{\mathbf{F}}$ and the spherical harmonics in $\vec{\mathbf{Y}}$, respectively.

$$\vec{\mathbf{F}} = \begin{bmatrix} F_{\text{-}2} & F_{\text{-}1} & F_0 & F_1 & F_2 \end{bmatrix} \tag{14a}$$

$$F_{\text{i}} = D^{(2)}_{\text{i},0} + \sqrt{\frac{3}{8}} R \left(D^{(2)}_{\text{i},2} + D^{(2)}_{\text{i},\text{-}2} \right) \tag{14b}$$

$$\mathbf{Y}_{\text{ij}} = \begin{bmatrix} Y_{\text{-}2,0,\text{ ij}} \\ Y_{\text{-}1,0,\text{ ij}} \\ Y_{0,0,\text{ ij}} \\ Y_{1,0,\text{ ij}} \\ Y_{2,0,\text{ ij}} \end{bmatrix} \tag{15}$$

By normalizing D on the axial component of $\mathbf{A}$ and D_{max} and extending the dimensions of D the final matrix equation (equation 4 in the main text) is obtained. Note that the resulting matrix $\mathbf{D_Y}$ has the transposed shape of $\mathbf{D_A}$ used in eq. (3). This is not necessary for mathematical correctness but the use of orthogonal projectors[2] ($\mathbf{F}^{+}\mathbf{F}$) can be seen easier.

$$\mathbf{D_Y} = \mathbf{F} \left\langle \mathbf{Y} \right\rangle \tag{16}$$

By SVD of $\mathbf{F}$ refined spherical harmonics $\mathbf{Y}_{\text{ref}}$ are calculated.

$$\left(\mathbf{F}^{+}\mathbf{F} \right) \left\langle \mathbf{Y}_{\text{ref}} \right\rangle = \mathbf{F}^{+}\mathbf{D_Y} \tag{17}$$

1.3.3 Information content of Y

To extract the spherical coordinates θ_{av} and ϕ_{av} the Wigner rotations are used to maximize $Y^{(2)}_{2,0}$ in its vector frame (compare figure 2 in main text):

$$\max \left(Y^{(2)}_{2,0} \left(\theta^{\text{VF}}, \phi^{\text{VF}} \right) \right) = \sum_{\text{M=-2}}^{2} D^{(2)}_{\text{M},0} \left(\phi^{\text{MF}}_{\text{av}}, \theta^{\text{MF}}_{\text{av}}, 0 \right) \left\langle Y^{(2)}_{2,\text{M}} \left(\theta^{\text{MF}}, \phi^{\text{MF}} \right) \right\rangle \tag{18}$$

This maximization is performed by using an in-house implementation of the Levenberg-Marquardt algorithm. Additionally the local order parameter of the individual RDCs (see equation 5 in main text), S_{overall}, the asymmetry parameter η (see eq. (20)) and the direction of the asymmetry axis φ (see eq. (21)) can be calculated from the spherical harmonics.

$$S_{\text{overall}} = \sqrt{\frac{1}{S^2_{\text{rdc,MFA,max}}}} \tag{19}$$

$$\eta = \sqrt{\frac{\sum_{M=-2,2} \langle Y_{2,\text{M}}\left(\Theta^{\text{VF}}\right)\rangle \langle Y_{2,\text{-M}}\left(\Theta^{\text{VF}}\right)\rangle}{\sum^{2}_{M=-2} \langle Y_{2,\text{M}}\left(\Theta^{\text{VF}}\right)\rangle \langle Y_{2,\text{-M}}\left(\Theta^{\text{VF}}\right)\rangle}} \tag{20}$$

$$\varphi = \frac{1}{2}\,\text{atan}\,\frac{\left\langle Y_{2,2}\left(\Theta^{\text{VF}}\right)\right\rangle - \left\langle Y_{2,\text{-}2}\left(\Theta^{\text{VF}}\right)\right\rangle}{\text{i}\left(\langle Y_{2,2}\left(\Theta^{\text{VF}}\right)\rangle + \langle Y_{2,\text{-}2}\left(\Theta^{\text{VF}}\right)\rangle\right)} \tag{21a}$$

$$= \frac{1}{2}\,\text{atan}\,\frac{\text{Im}(\left\langle Y_{2,2}\left(\Theta^{\text{VF}}\right)\right\rangle)}{\text{Re}(\langle Y_{2,2}\left(\Theta^{\text{VF}}\right)\rangle)} \tag{21b}$$

Here $S^2_{\text{rdc,MFA,max}}$ is the largest $S^2_{\text{rdc,MFA}}$ directly obtained from the MFA utilizing eq. (17). The spherical coordinates θ and ϕ are combined as tuple in Θ.

1.3.4 Use of Redundant internal coordinates in TITANIA

A proper way to represent structures of N atoms is by using a set of 3N−6 internal coordinates (which herein are also called holonomic terms). In this case the conversion to Cartesian coordinates can be performed by simple geometric considerations. A more advanced algorithm, implemented in the TITANIA workflow, uses redundant internal coordinates known from quantum chemical computation protocols. In this approach standard internal coordinates, namely bond lengths, bond angles or dihedral angles of more atom tuples than needed to unambiguously define a structure are combined to form an overdetermined representation (more than 3N-6 internal coordinates) of a structure model. As reported in literature,[3,4] the conversion of redundant internal coordinates q, containing standard structure parameters (like bond lengths and angles), into Cartesian coordinates is done by the Wilson matrix $\mathbf{B}_{\text{w}}$:

$$B_{\text{w}}\left(q_i, x_j\right) = \frac{\partial q_i}{\partial x_j} \tag{22}$$

The change $\Delta\vec{X}$ in Cartesian coordinates x_{j} (with j = {x, y, z}) can be calculated utilizing the Moore-Penrose inverse of $\mathbf{B}_{\text{w}}$. For this the deviation between the current and optimal internal coordinates ($\Delta q = q_{\text{opt}} - q_{\text{cur}}$) are summarized in the vector $\Delta\vec{\mathbf{q}}$. This is also called the *internal displacement vector*.

$$\Delta\vec{\mathbf{X}} = \mathbf{B}_{\mathbf{w}}^{+}\Delta\vec{\mathbf{q}} \tag{23}$$

Therefore the iterative optimization of the Cartesian coordinates can be formulated according to:

$$\vec{\mathbf{X}}_{\mathbf{i+1}} = \vec{\mathbf{X}}_{\mathbf{i}} + \mathbf{B}_{\mathbf{w}}^{+}\Delta\vec{\mathbf{q}}_{\mathbf{i}} \tag{24}$$

Since the algorithm is designed to handle small changes (see eq. (22)) its stability can be increased by damping of the individual structure updates (see eq. (24)).

$$\Delta\vec{\mathbf{q}} = D \cdot diag\left[w_{\mathrm{i}}\right]\Delta\vec{\tilde{\mathbf{q}}} \tag{25}$$

Where w_{i} is the static weighting for the type of q_{i}, $\Delta\vec{\tilde{\mathbf{q}}}$ is the undamped internal displacement vector and D is the global damping factor, which is updated in every step:

$$D = \frac{\exp\left(3.5\frac{iter}{maxiter}\right)^2}{\delta + \exp\left(3.5\frac{iter}{maxiter}\right)^2}\frac{\delta + \exp\left(3.5\right)^2}{\exp\left(3.5\right)^2} \tag{26}$$

The course of the function for the damping factors is shown in fig. S-2 for different (user defined) damping constants δ. The factor 3.5 was determined empirically and results in a rather smooth curve of the global damping factor D, while allowing for flexible adjustments of it by the user.

Orthogonal projectors $\mathbf{P}$ of the type $\mathbf{P} = \mathbf{B}_{\mathrm{w}}\mathbf{B}_{\mathrm{w}}^{+}$ are also used to achieve higher stablity of the algorithm, by projecting the internal displacement vector $\Delta\vec{\mathbf{q}}$ on the range of $\mathbf{B}_{\mathrm{w}}$. This results in the overall equation for one redundant internal coordinate iteration step:

$$\vec{\mathbf{X}}_{\mathbf{i+1}} = \vec{\mathbf{X}}_{\mathbf{i}} + \mathbf{B}_{\mathbf{w}}^{+}D \cdot diag\left[w_{\mathrm{i}}\right]\left(\mathbf{B}_{\mathbf{w}}\mathbf{B}_{\mathbf{w}}^{+}\Delta\vec{\tilde{\mathbf{q}}}_{\mathrm{i}}\right) \tag{27}$$

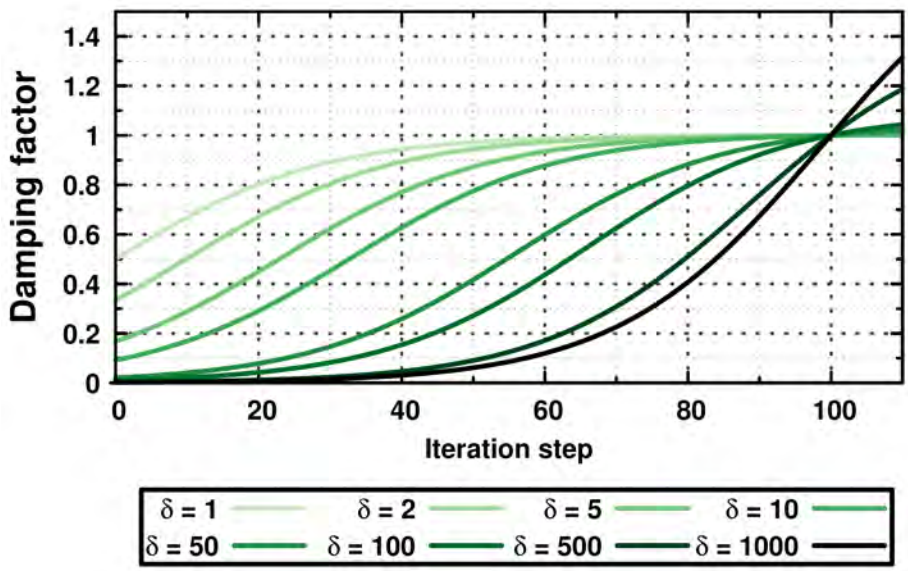

Figure S-2: Damping factors D for a set of damping constants δ. For the calculations a maximum of 100 iterations was assumed.

Care has to be taken when defining the damping constant δ for an optimization run. Eq (26) is designed to achieve a weighting of 1.0 in the last iteration step. Very large damping constants (approximatly larger than 100) will lead to stronger weighting when defining additional steps (see keyword `overoptimizationSteps` in section 1.2.1) that can lead to instabilities in the redundant internal coordinates within these additional steps. Another result can be convergence to a local minimum, that cannot be escaped using redundant internal coordinates due to too high damping in the first steps of the TITANIA optimization.

Additionally to the ability to optimize a structure based on an overdetermined set of internal coordinates the algorithm allows for the definition of further terms as restraints. These can (in this context) be RDC-vector orientations or chiral volumes of planar centers to combine the holonomic terms with experimental data. The implementation of RDCs in TITANIA is done by the angle enclosed by $\vec{r}_{ij}\,(\theta,\phi)$ (determined by the MFA) and the vector $\vec{r}_{ij,cur}$ calculated from the current structure model. This angle defines a new internal coordinate q_{cur} which has to be minimized, resulting in $q_{\mathrm{opt}} = 0$ and hence $\Delta q = -q_{\mathrm{cur}}$, which is added to the internal displacement vector $\Delta\vec{q}$

described above.

1.3.5 Structures from vector addition

Alternatively to the default use of redundant internal coordinates TITANIA can use a vector addition algorithm to update structures. It can be very helpful to start an optimization with low maximum iteration steps using this algorithm if redundant internal coordinates do not converge. In this algorithm the non-RDC defined bond vectors (mainly the carbon scaffold) are retained in the initial geometry and only RDC defined bond vectors are updated. This can additionally be combined with the redundant internal coordinate optimization (see keyword `useRedundantsOnlyAfter` in section 1.2.1), where the following algorithm is performed prior to the redundant internal coordinates step.

$$\vec{\mathbf{r}}_{\mathrm{RDC,i}} = ||\vec{\mathbf{r}}_{\mathrm{i\text{-}1}}||\mathrm{sgn}\left(\frac{\vec{\mathbf{r}}\left(\theta_{\mathrm{i}},\phi_{\mathrm{i}}\right)^{\mathrm{t}}\cdot\vec{\mathbf{r}}_{\mathrm{i\text{-}1}}}{||\vec{\mathbf{r}}_{\mathrm{i\text{-}1}}||}\right)\vec{\mathbf{r}}\left(\theta_{\mathrm{i}},\phi_{\mathrm{i}}\right) \tag{28a}$$

$$\vec{\mathbf{r}}\left(\theta_{\mathrm{i}},\phi_{\mathrm{i}}\right) = \begin{pmatrix}\sin\left(\theta\right)\cos\left(\phi\right)\\ \sin\left(\theta\right)\sin\left(\phi\right)\\ \cos\left(\theta\right)\end{pmatrix} \tag{28b}$$

The resulting vectors are used to update the structure. As first estimation for the correct vector orientation ($\vec{\mathbf{r}}_{\mathrm{RDC}}$ vs. $-\vec{\mathbf{r}}_{\mathrm{RDC}}$) the smaller deviation to the previous orientation is used (see sign function in eq. (28)). The bond vectors can be validated and inverted by assessing the mean vector deviation of long range RDCs ${}^{\mathrm{n}}D_{\mathrm{HH}}$.

$$\langle\Delta\vec{\mathbf{r}}\rangle = \frac{1}{N}\sum_{i}^{N}\left|\left|\frac{\vec{\mathbf{r}}_{\mathrm{i}}}{||\vec{\mathbf{r}}_{\mathrm{i}}||} - \vec{\mathbf{r}}_{\mathrm{RDC,i}}\right|\right| \tag{29}$$

By this measure the vector orientation is reevaluated. This vector addition algorithm is deactivated by default. The user can activate this algorithm prior to redundant internal coordinates for N iterations if needed (see above). Positions of atoms which do not contribute to RDC vectors (e.g. hydroxy groups or methyl protons) are updated by a MMFF94 minimization in the course of this algorithm to retain chemically meaningful functional groups / structure moieties.

1.3.6 Statistics of directional data

To estimate $\Delta\theta$ and $\Delta\phi$ (and other uncertainties) a Monte-Carlo bootstrap (with normal distributed sampling in the range of ΔD) is used in combination with Gaussian propagation of errors.

$$\mathbf{D}_{\mathrm{MC}} = \mathbf{D} + \mathbf{rand}_{\mathrm{norm}}\left[-1.0, 1.0\right] \boldsymbol{\Delta}\mathbf{D} \tag{30}$$

For the resulting $\mathbf{D}_{\mathrm{MC}}$ matrix equations (3b) and (17) are solved. The uncertainties, which cannot be accessed directly (e.g. spherical coordinates or Euler angles) the Gaussian propagation of errors is employed. For this the general form to estimate the uncertainty for a value Y (not to be confused with the spherical harmonics $Y_{\mathrm{l,m}}$) with respect to the dependent measurements x_{i} is used:

$$\Delta Y = \sqrt{\sum_{\mathrm{i}}^{\mathrm{m}} \left(\frac{\partial Y}{\partial x_{\mathrm{i}}}\sigma\left(x_{\mathrm{i}}\right)\right)^2 + 2\sum_{\mathrm{i}}^{\mathrm{m\text{-}1}}\sum_{\mathrm{j=i+1}}^{\mathrm{m}} \left(\frac{\partial Y}{\partial x_{\mathrm{i}}}\frac{\partial Y}{\partial x_{\mathrm{j}}}\mathrm{cov}\left(x_{\mathrm{i}}, x_{\mathrm{j}}\right)\right)} \tag{31a}$$

$$= \sqrt{\sum_{\mathrm{i}}^{\mathrm{m}}\sum_{\mathrm{j}}^{\mathrm{m}} \left(\frac{\partial Y}{\partial x_{\mathrm{i}}}\frac{\partial Y}{\partial x_{\mathrm{j}}}\mathrm{cov}\left(x_{\mathrm{i}}, x_{\mathrm{j}}\right)\right)} \tag{31b}$$

With the covariance cov:

$$\mathrm{cov}\left(x_i, x_j\right) = \frac{1}{n}\sum_{k}^{n}\left[\left(\bar{x}_i - x_{i,k}\right)\left(\bar{x}_j - x_{j,k}\right)\right] \tag{32}$$

For the Euler angles the numerical gradient is estimated. For the spherical coordinates the analytical gradient is used. Therefore Cartesian vectors representing the orientation of the individual steps are averaged to obtain the mean coordinates:

$$\bar{X}_o = \frac{1}{n}\sum_{i}^{n}\sin\left(\theta_i\right)\cos\left(\phi_i\right) \tag{33a}$$

$$\bar{Y}_o = \frac{1}{n}\sum_{i}^{n}\sin\left(\theta_i\right)\sin\left(\phi_i\right) \tag{33b}$$

$$\bar{Z}_o = \frac{1}{n}\sum_{i}^{n}\cos\left(\theta_i\right) \tag{33c}$$

The spherical coordinates of the mean vector and its length are accessible by eqs. (34) to (35).

$$\bar{R}_s = \sqrt{\bar{X}_o^2 + \bar{Y}_o^2 + \bar{Z}_o^2} \tag{34}$$

$$\bar{\theta}_{\bar{X},\bar{Y},\bar{Z}} = \operatorname{acos}\left(\bar{Z}_o \bar{R}_s^{-1}\right) \tag{35a}$$

$$\bar{\phi}_{\bar{X},\bar{Y},\bar{Z}} = \operatorname{atan2}\left(\bar{Y}_o \bar{R}_s^{-1}, \bar{X}_o \bar{R}_s^{-1}\right) \tag{35b}$$

The Gaussian propagation of errors for the spherical coordinates $\Delta\theta$ and $\Delta\phi$ can be expressed by:

$$\Delta\theta = \sqrt{\sum_i^n \sum_j^n \left(\frac{\partial\theta}{\partial x_i}\frac{\partial\theta}{\partial x_j}\operatorname{cov}\left(x_i, x_j\right)\right)} \tag{36a}$$

$$\Delta\phi = \sqrt{\sum_i^n \sum_j^n \left(\frac{\partial\phi}{\partial x_i}\frac{\partial\phi}{\partial x_j}\operatorname{cov}\left(x_i, x_j\right)\right)} \tag{36b}$$

The derivatives in eq. (36) (where $x_i = \{x, y, z\}$) are:

$$\frac{\partial \bar{R}_s}{\partial x_i} = \frac{x_i}{\bar{R}_s} \tag{37a}$$

$$\frac{\partial\theta}{\partial x_i} = -\left(\frac{1}{\sqrt{1 - \left(\frac{\bar{Z}_o}{\bar{R}_s}\right)^2}}\right)\left(\frac{\frac{\partial \bar{Z}_o}{\partial x_i}\bar{R}_s - \frac{\partial \bar{R}_s}{\partial x_i}\hat{Z}_o}{\bar{R}_s^2}\right) \tag{37b}$$

$$\begin{aligned}\frac{\partial\phi}{\partial x_i} = &\left(\frac{\frac{\bar{X}_o}{\bar{R}_s}}{\left(\frac{\bar{X}_o}{\bar{R}_s}\right)^2 + \left(\frac{\bar{Y}_o}{\bar{R}_s}\right)^2}\right)\left(\frac{\frac{\partial \bar{Y}_o}{\partial x_i}\bar{R}_s - \frac{\partial \bar{R}_s}{\partial x_i}\bar{Y}_o}{\bar{R}_s^2}\right) \\ &- \left(\frac{\frac{\bar{Y}_o}{\bar{R}_s}}{\left(\frac{\bar{X}_o}{\bar{R}_s}\right)^2 + \left(\frac{\bar{Y}_o}{\bar{R}_s}\right)^2}\right)\left(\frac{\frac{\partial \bar{X}_o}{\partial x_i}\bar{R}_s - \frac{\partial \bar{R}_s}{\partial x_i}\bar{X}_o}{\bar{R}_s^2}\right)\end{aligned} \tag{37c}$$

The spherical variance (eq. (38a)) and spherical standard deviation (eq. (38b)) are calculated as:[5]

$$\bar{\sigma}_o^2 = 1 - \bar{R}_s \tag{38a}$$

$$\bar{\sigma}_o = \sqrt{-2\ln\bar{R}_s} \tag{38b}$$

2 Isopinocampheol (1)

Isopinocampheol (IPC) was optimized in six setups, the preparation of which will be briefly explained here. The setup **1-A** was generated from 20 randomly generated alignment tensors (refered to as artificial data), to achieve an optimum sampling of the orientations. Two additional setups, to represent experimentally achievable data (**1-B**) and highly linear dependent data (**1-C**). The orientations are taken from literature, but the number of RDCs was increased. This was done by back-calculation of the full RDC set (referred to as synthetic data). These setups were all calculated from a single rigid structure and alignment tensors, leading to RDCs completly free of errors. Normal distributed random values ($\sigma\left({}^{1}D_{\mathrm{CH}}\right) = 0.5$ Hz, $\sigma\left({}^{1}D_{\mathrm{CC}}\right) = 0.125$ Hz, $\sigma\left({}^{n}D_{\mathrm{HH}}\right) = 0.25$ Hz, $\mu = 0.0$) were added to the RDCs of the setups **1-A** to **1-C** to generate the setups **1-D** to **1-F**. By this the impact of experimental error on the optimization is investigated.

2.1 Orientations

RDC sets

The alignment parameters of the IPC setups **1-B** and **1-C** were derived from RDCs reported in literature.[6–8] These were used to determine the orientation *via* SVD. This was done using the in-house RDC module (`RDC@hotFCHT`) of the `hotFCHT` software.[9] The recalculation of the orientations might result in different orientations than reported previously due to different weighting of the cosine matrix (to match the TITANIA implementation) and the use of the all-positive Euler angle permutation.

Table S-1: RDC sets and alignment parameters used for the synthetic RDC sets of run **1-B** and **1-C**.

Set	Medium	Solvent	Analyte	T / K	Ref.
set 1	PELG	$CDCl_3$	(+)-IPC	300	[6]
set 2	PBDG	$CDCl_3$	(+)-IPC	300	[8]
set 3	PPLA	TCE-d_2	(+)-IPC	300	[7]
set 4	PPLA	TCE-d_2	(+)-IPC	383	[7]
set 5	PPDA	TCE-d_2	(+)-IPC	383	[7]
set 6	PPDA	TCE-d_2	(+)-IPC	300	[7]
set 7	PELG	$CDCl_3$	(−)-IPC	300	[6]
set 8	PBDG	$CDCl_3$	(−)-IPC	300	[8]
set 9	PBLG	$CDCl_3$	(+)-IPC	300	[8]
set 10	PBLG	$CDCl_3$	(−)-IPC	300	[8]

The linear (in)dependence of the respective sets used for the setups **1-B** and **1-C** were assessed using the generalized angle β:

$$\cos\beta = \frac{\langle \mathbf{A_1}|\mathbf{A_2}\rangle}{\sqrt{\langle \mathbf{A_1}|\mathbf{A_1}\rangle}\sqrt{\langle \mathbf{A_2}|\mathbf{A_2}\rangle}} \tag{39a}$$

$$\langle \mathbf{A_1}|\mathbf{A_2}\rangle = tr\left(\mathbf{A_1^t}\cdot\mathbf{A_2}\right) \tag{39b}$$

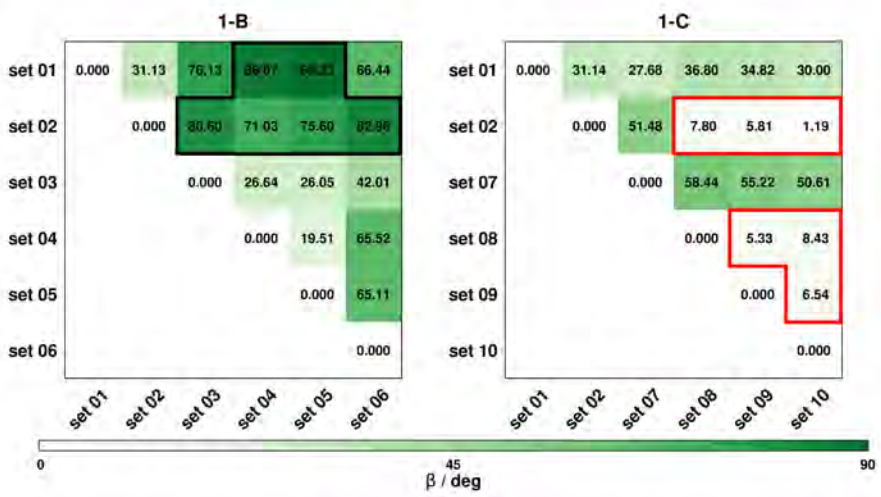

Figure S-3: Pairwise β angles of the sets used for setup **1-B** and **1-C**. The marked fields (black) on the left side show extraordinary large β angles. The marks (red) on the right side show the purposefully low angles to ensure linear dependency of the setup.

2.2 *epi*-C3 start structure

The standard runs were performed with a C3-inverted structure. For runs starting from random coordinates see below (section 2.3) These runs are used to plot the SECONDA data (discussion of **1-A** can be found in the main text) and the change of orientations induced by error. SECONDA is performed on the normalized RDC matrix. The change induced by error is discussed for the *epi*-C3 structure only, since the random coordinates were used for the error free data only. The setups **1-D** to **1-F** were additionally optimized using vector addition. The change induced by error (see section 2.2.5) is not discussed for the vector addition algorithm as a bias would be added due to the change of the structure generation algorithm.

2.2.1 SECONDA plots

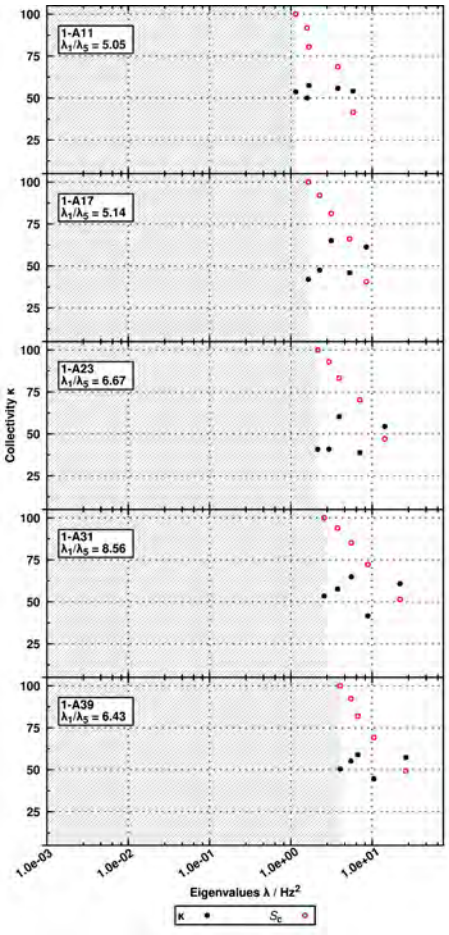

Figure S-4: SECONDA plot of the individual runs in setup **1-A**.

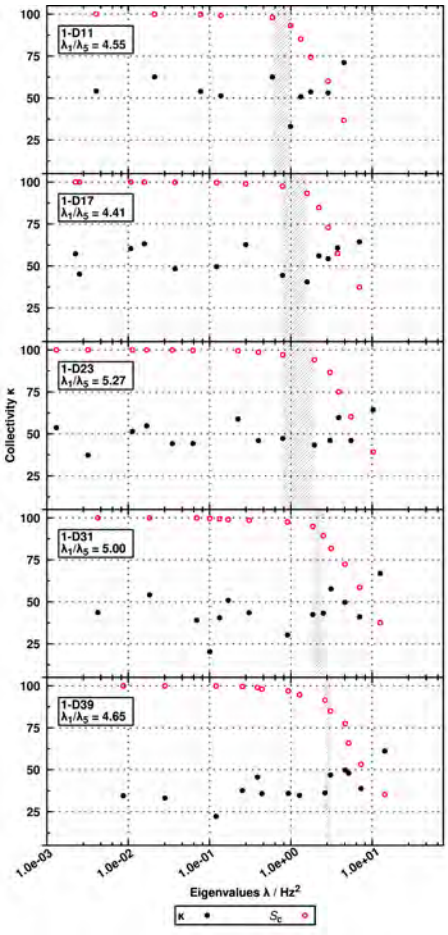

Figure S-5: SECONDA plot of the individual runs in setup **1-D**.

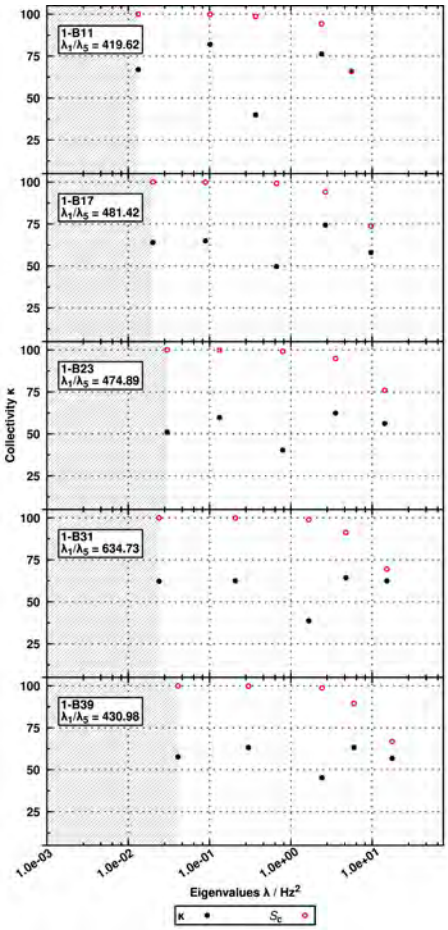

Figure S-6: SECONDA plot of the individual runs in setup **1-B**.

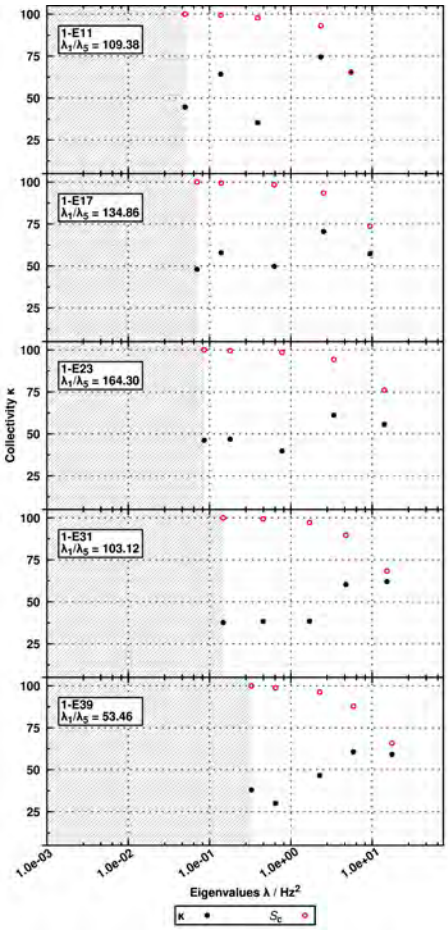

Figure S-7: SECONDA plot of the individual runs in setup **1-E**.

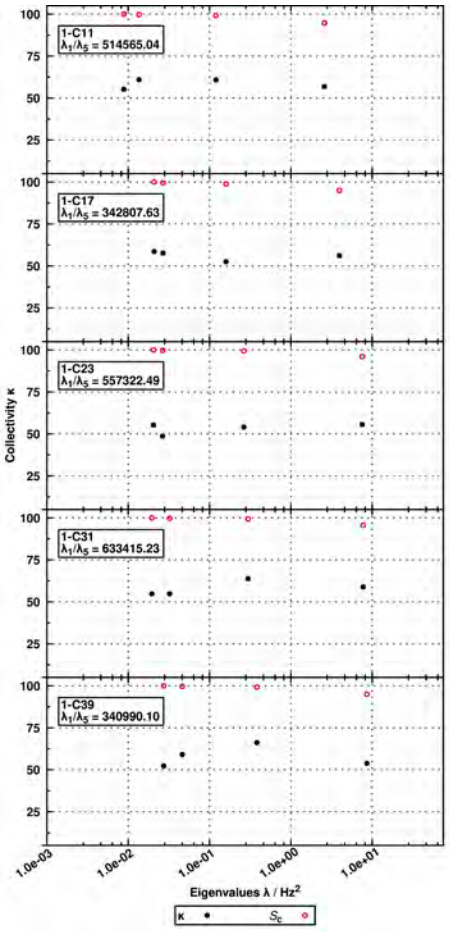

Figure S-8: SECONDA plot of the individual runs in setup **1-C**.

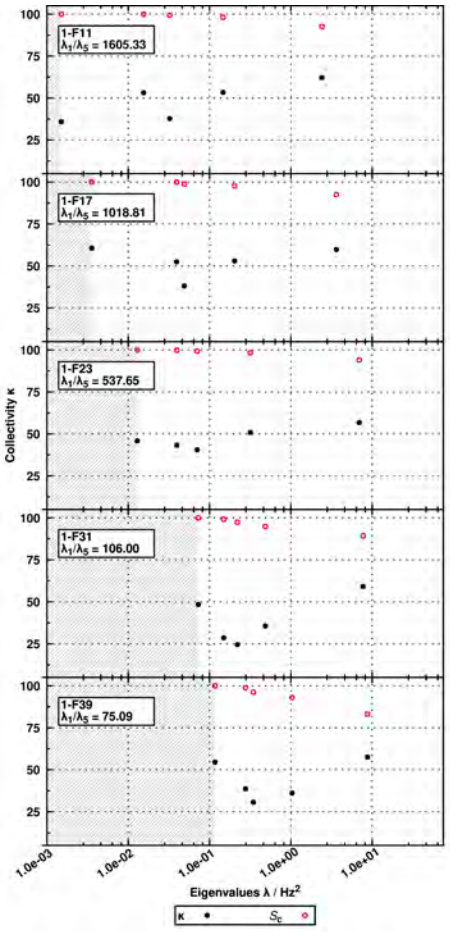

Figure S-9: SECONDA plot of the individual runs in setup **1-F**.

The SECONDA plots give insight into the RDC information content of the setups **1-A** to **1-F**. In the main text we focused on the assessment of the linear independence of the setups. Here we investigate the impact of synthetic heterogeneity (in this case error, added *via* normal distributed random numbers) on the error free setups **1-A** to **1-C**, by comparing these to the respective setups **1-D** to **1-F**. Hus and Brüschweiler have shown earlier that the addition of heterogeneity to a back-calculated RDC matrix of full rank has little impact on the principle variances λ_1 to λ_5.[10]

This result can as well be found in the comparison of fig. S-4 and S-5 (comparison of **1-A** and **1-D**). Here the eigenvalues λ_1 to λ_5 are nearly unchanged by the Gaussian random numbers. As expected for **1-D** additional eigenvalues λ_n ($n > 5$) become non-zero. This is typical for RDC matrices with heterogeneity. The high number of additional eigenvalues can be explained by the large relative errors (see table S-41).

The setups **1-B** and **1-E** show the above behavior for the first three principle variances. The eigenvalues λ_4 and λ_5 in contrast already show a slight dependence on the heterogeneity. These are the same eigenvalues which had a contribution of less than 1.0 % to the overall variance for these setups (see threshold discussed in main text).

This, in combination with the rather large λ_1/λ_5 ratio, implies that no complete linear independence of five orientations is achieved for the setup. In contrast to **1-D** no additional non-zero eigenvalues ($\lambda_6 < 1e-9$ for all runs of **1-E**) are found. To the best of our knowledge no (published) investigation of synthetic RDC data containing only 6 sets, to which synthetic errors were added, exists. In the setup **1-B**, **1-C**, **1-E** and **1-F** we used the minimum number of RDC sets needed to allow for a detection of heterogeneity (The rank of an $n \times m$ matrix cannot exceed n if $n < m$ or m if $m < n$, respectively. Therefore an RDC matrix of 5 media can only achieve a maximum rank of 5.). It is thus assumed that the minimum number of RDC sets in combination with the mediocre sampling of the orientations was not sufficient to detect the heterogeneity.

This behavior is even more pronounced for the setups **1-C** and **1-F**. Additionally to not showing a non-zero eigenvalue λ_6 when adding synthetic error, **1-C** does not show λ_5 within the scale used in the plot ($\lambda_5 < 1e-3$). For the sets with 11 to 23 RDCs the principle variances λ_1 and λ_2 only show slight dependence on the heterogeneity. For the last two setups **1-C31** and **1-C39** this is only true for λ_1. This behavior coincides with the high linear dependence desired for the setup **1-C**. Again the values dependent on the heterogeneity have less than 1.0 % contribution to the overall variance as discussed in the main text.

2.2.2 Orientations

1-A

Input orientations

The RDCs of setup **1-A** were calculated by the orientations summarized in table S-2.

Table S-2: Orientational data used for the synthetic RDC sets of setup **1-A** and **1-D**.

Set	$\boldsymbol{A}_{zz}$	$\boldsymbol{R}$	$\boldsymbol{\alpha}/^\circ$	$\boldsymbol{\beta}/^\circ$	$\boldsymbol{\gamma}/^\circ$
set 1	6.502e-04	2.810e-01	8.144	141.340	82.889
set 2	8.426e-05	2.222e-01	145.757	110.718	24.512
set 3	8.788e-05	3.201e-01	7.168	99.611	155.036
set 4	4.350e-04	5.409e-01	100.047	51.633	116.928
set 5	3.411e-04	3.893e-01	140.036	73.152	84.947
set 6	8.659e-04	4.858e-01	165.509	48.826	27.761
set 7	8.074e-04	7.404e-03	44.055	123.341	119.405
set 8	4.177e-04	2.348e-01	87.834	54.652	157.368
set 9	4.881e-05	2.929e-01	111.992	33.749	60.348
set 10	7.993e-04	5.760e-01	12.000	148.761	72.686
set 11	3.255e-04	1.066e-01	90.282	22.718	122.776
set 12	4.468e-04	4.043e-01	9.639	62.911	98.912
set 13	3.196e-04	1.107e-01	82.100	168.690	6.311
set 14	6.600e-05	2.687e-01	107.921	153.048	77.132
set 15	7.857e-04	2.918e-02	69.136	138.490	101.059
set 16	4.146e-04	4.251e-01	30.733	107.546	178.566
set 17	6.562e-04	5.205e-01	89.664	38.741	107.788
set 18	5.977e-04	4.170e-01	54.711	118.926	144.841
set 19	8.809e-04	1.118e-01	63.241	75.212	163.185
set 20	6.492e-04	6.360e-01	117.915	146.575	88.796

Output orientations

All orientiations of setup **1-A** (**11-39**) obtained from the full TITANIA optimization runs are listed in the following section. Changes of the Euler angles compared to the data listed in table S-2 are due to the change of the reference frames (TITANIA used the principle axis system of the molecule) and changes in the structure. The comparison of the input and output data is summarized in table S-35 (section 2.2.4).

Table S-3: Orientational data of IPC **1** obtained by TITANIA on the last optimization iteration for the run **1-A11**.

Set	$\boldsymbol{A}_{zz}$	$\boldsymbol{R}$	$\boldsymbol{\alpha}/^\circ$	$\boldsymbol{\beta}/^\circ$	$\boldsymbol{\gamma}/^\circ$
set 1	6.987e-04	2.391e-01	173.230	35.413	98.063
set 2	8.006e-05	3.196e-01	148.225	72.877	149.183
set 3	8.250e-05	3.865e-01	9.152	78.483	19.577
set 4	4.395e-04	5.370e-01	91.183	122.082	58.114
set 5	3.324e-04	2.391e-01	121.320	105.117	85.795
set 6	8.935e-04	5.056e-01	170.915	126.443	142.591
set 7	8.092e-04	1.625e-01	158.125	52.441	55.599
set 8	4.153e-04	2.421e-01	83.303	121.542	21.879
set 9	4.413e-05	2.669e-01	120.063	140.779	114.967
set 10	8.821e-04	5.122e-01	2.805	31.745	110.056
set 11	2.943e-04	2.059e-01	100.496	153.250	47.404
set 12	4.430e-04	3.750e-01	15.503	110.386	71.077
set 13	3.267e-04	1.696e-01	96.550	16.491	168.600
set 14	7.347e-05	2.476e-01	101.082	25.566	111.816
set 15	8.259e-04	8.799e-02	135.239	36.597	79.886
set 16	4.041e-04	3.886e-01	144.814	111.189	171.088
set 17	5.990e-04	6.274e-01	90.037	135.426	69.611
set 18	5.901e-04	3.496e-01	51.474	57.966	30.026
set 19	8.517e-04	2.136e-01	53.130	101.840	13.466
set 20	7.067e-04	6.281e-01	108.920	28.612	100.249

Table S-4: Orientational data of IPC **1** obtained by TITANIA on the last optimization iteration of run **1-A17**.

Set	$\boldsymbol{A}_{zz}$	$\boldsymbol{R}$	$\boldsymbol{\alpha}/^\circ$	$\boldsymbol{\beta}/^\circ$	$\boldsymbol{\gamma}/^\circ$
set 1	5.996e-04	2.893e-01	4.063	33.244	89.880
set 2	8.144e-05	2.329e-01	143.398	65.458	150.476
set 3	8.304e-05	3.081e-01	10.468	78.033	18.078
set 4	3.899e-04	5.990e-01	104.113	125.515	58.970
set 5	3.217e-04	4.017e-01	139.266	101.826	89.719
set 6	8.305e-04	4.677e-01	159.538	127.394	142.928
set 7	7.815e-04	3.050e-02	18.681	54.198	51.713
set 8	3.877e-04	2.212e-01	93.107	125.785	17.000
set 9	4.655e-05	3.118e-01	110.950	140.973	113.043
set 10	7.367e-04	5.681e-01	8.403	25.069	102.677
set 11	3.118e-04	1.368e-01	93.194	154.583	57.714
set 12	4.167e-04	3.884e-01	13.190	112.505	75.969
set 13	3.121e-04	8.711e-02	129.026	169.064	13.957
set 14	6.307e-05	2.912e-01	109.675	21.197	97.510
set 15	7.344e-04	2.431e-02	163.417	37.521	69.041
set 16	3.938e-04	3.937e-01	143.396	107.184	173.467
set 17	6.030e-04	5.700e-01	94.811	137.993	69.793
set 18	5.850e-04	4.410e-01	59.823	59.975	27.285
set 19	8.042e-04	7.467e-02	72.594	104.486	10.478
set 20	6.241e-04	6.500e-01	121.371	28.026	83.300

Table S-5: Orientational data of IPC **1** obtained by TITANIA on the last optimization iteration of run **1-A23**.

Set	$\boldsymbol{A}_{zz}$	$\boldsymbol{R}$	$\boldsymbol{\alpha}/^\circ$	$\boldsymbol{\beta}/^\circ$	$\boldsymbol{\gamma}/^\circ$
set 1	6.169e-04	2.594e-01	10.075	29.966	89.231
set 2	8.209e-05	2.349e-01	138.138	62.814	154.005
set 3	8.056e-05	3.130e-01	15.740	79.008	19.822
set 4	4.053e-04	5.708e-01	106.846	122.819	63.396
set 5	3.164e-04	3.903e-01	139.577	98.677	91.613
set 6	8.379e-04	4.699e-01	156.880	124.592	143.713
set 7	7.870e-04	1.140e-02	25.731	51.631	51.858
set 8	3.923e-04	2.540e-01	97.656	125.724	23.552
set 9	4.746e-05	3.121e-01	109.038	137.538	115.013
set 10	7.529e-04	5.458e-01	13.058	21.762	102.001
set 11	3.142e-04	1.186e-01	100.494	151.715	67.139
set 12	4.166e-04	4.047e-01	16.801	109.722	78.695
set 13	3.105e-04	1.000e-01	148.187	169.372	36.946
set 14	6.393e-05	2.737e-01	112.892	18.225	95.869
set 15	7.556e-04	1.102e-02	108.974	34.654	68.109
set 16	3.866e-04	4.241e-01	139.306	105.166	174.307
set 17	6.235e-04	5.474e-01	97.284	134.667	74.761
set 18	5.779e-04	4.344e-01	64.341	59.185	27.119
set 19	8.060e-04	1.201e-01	77.509	105.948	14.444
set 20	6.347e-04	6.223e-01	124.753	25.287	82.279

Table S-6: Orientational data of IPC **1** obtained by TITANIA on the last optimization iteration of run **1-A31**.

Set	$\boldsymbol{A}_{zz}$	$\boldsymbol{R}$	$\boldsymbol{\alpha}/^\circ$	$\boldsymbol{\beta}/^\circ$	$\boldsymbol{\gamma}/^\circ$
set 1	6.190e-04	2.811e-01	13.017	30.870	89.129
set 2	7.992e-05	2.262e-01	139.312	62.830	154.086
set 3	8.364e-05	3.134e-01	15.105	80.683	20.210
set 4	4.125e-04	5.521e-01	108.291	123.393	65.004
set 5	3.227e-04	3.929e-01	142.675	99.528	92.638
set 6	8.156e-04	4.773e-01	159.481	124.356	145.477
set 7	7.676e-04	2.125e-03	126.045	52.395	51.820
set 8	3.918e-04	2.516e-01	97.559	125.949	25.152
set 9	4.639e-05	2.922e-01	110.659	138.006	115.806
set 10	7.618e-04	5.721e-01	15.238	22.999	100.518
set 11	3.107e-04	1.059e-01	110.160	152.268	68.564
set 12	4.223e-04	3.985e-01	15.312	110.826	79.999
set 13	3.054e-04	1.247e-01	141.816	170.547	36.014
set 14	6.320e-05	2.628e-01	115.528	19.124	93.566
set 15	7.486e-04	2.382e-02	84.084	35.278	68.484
set 16	3.946e-04	4.158e-01	141.338	103.733	176.264
set 17	6.258e-04	5.190e-01	98.737	135.059	75.673
set 18	5.745e-04	4.025e-01	64.180	60.459	26.946
set 19	8.290e-04	1.175e-01	73.393	106.150	15.491
set 20	6.221e-04	6.258e-01	126.260	26.241	80.907

Table S-7: Orientational data of IPC **1** obtained by TITANIA on the last optimization iteration of run **1-A39**.

Set	$\boldsymbol{A}_{zz}$	$\boldsymbol{R}$	$\boldsymbol{\alpha}/^\circ$	$\boldsymbol{\beta}/^\circ$	$\boldsymbol{\gamma}/^\circ$
set 1	6.214e-04	2.645e-01	13.041	30.120	90.406
set 2	7.904e-05	2.375e-01	138.195	62.436	154.814
set 3	8.340e-05	3.220e-01	16.744	79.902	20.496
set 4	4.130e-04	5.483e-01	107.672	122.359	64.690
set 5	3.220e-04	3.914e-01	141.730	98.213	92.767
set 6	8.254e-04	4.833e-01	157.970	124.428	144.468
set 7	7.727e-04	1.184e-02	103.052	51.495	51.989
set 8	3.957e-04	2.374e-01	98.850	125.046	26.086
set 9	4.671e-05	3.037e-01	110.708	137.287	115.432
set 10	7.640e-04	5.643e-01	13.978	22.442	102.834
set 11	3.104e-04	1.169e-01	103.444	151.370	67.952
set 12	4.174e-04	3.896e-01	15.513	109.408	79.920
set 13	3.053e-04	9.968e-02	146.212	169.491	37.517
set 14	6.325e-05	2.725e-01	111.862	18.260	95.724
set 15	7.509e-04	3.716e-02	89.311	34.377	68.987
set 16	3.894e-04	4.392e-01	139.903	104.546	175.895
set 17	6.266e-04	5.300e-01	97.707	134.203	75.327
set 18	5.734e-04	4.141e-01	65.209	59.596	26.902
set 19	8.262e-04	1.166e-01	72.375	105.585	16.560
set 20	6.232e-04	6.364e-01	125.130	25.316	81.669

Note that the Euler angles differ due to the different reference frames. Thus a comparison can here only be based on A_{ZZ} and R, which shows a good agreement for the runs **1-A17** to **1-A39** between the input orientations used to back-calculate the artificial RDCs and the final orientations determined by TITANIA. The comparison of orientations with using a common reference frame is found in section 2.2.4.

1-B

Input orientations

The RDCs of setup **1-B** were calculated by the orientations summarized in table S-8.

Table S-8: Orientational data used for the synthetic RDC sets of setup **1-B** and **1-E**.

Set	$\boldsymbol{A}_{zz}$	$\boldsymbol{R}$	$\boldsymbol{\alpha}/^\circ$	$\boldsymbol{\beta}/^\circ$	$\boldsymbol{\gamma}/^\circ$
set 1	-8.166e-04	4.731e-01	62.238	154.576	121.551
set 2	9.519e-04	4.642e-01	76.734	78.357	140.473
set 3	-1.583e-03	3.447e-01	148.367	118.389	150.530
set 4	6.259e-04	6.557e-01	165.587	54.317	77.300
set 5	6.454e-04	5.588e-01	164.877	71.897	73.177
set 6	-8.756e-04	4.057e-01	42.558	122.051	136.107

Output orientations

All orientiations of setup **1-B** (**11**-**39**) obtained from the full TITANIA optimization runs are listed in the following section. Changes of the Euler angles compared to the literature data listed above are due to the change of the reference frames (TITANIA used the principle axis system of the molecule). The comparison of the input and output data is summarized in table S-36 (section 2.2.4).

Table S-9: Orientational data of IPC **1** obtained by TITANIA on the last optimization iteration for the run **1-B11**.

Set	$\boldsymbol{A}_{zz}$	$\boldsymbol{R}$	$\boldsymbol{\alpha}/^\circ$	$\boldsymbol{\beta}/^\circ$	$\boldsymbol{\gamma}/^\circ$
set 1	-8.244e-04	5.073e-01	99.505	37.190	147.052
set 2	1.002e-03	4.400e-01	95.072	115.134	162.170
set 3	-1.619e-03	3.989e-01	168.306	83.003	140.187
set 4	-7.062e-04	5.614e-01	160.472	99.745	137.362
set 5	7.119e-04	5.892e-01	174.633	87.953	47.321
set 6	-7.918e-04	2.987e-01	61.637	72.685	153.102

Table S-10: Orientational data of IPC **1** obtained by TITANIA on the last optimization iteration of run **1-B17**.

Set	$\boldsymbol{A}_{zz}$	$\boldsymbol{R}$	$\boldsymbol{\alpha}/^\circ$	$\boldsymbol{\beta}/^\circ$	$\boldsymbol{\gamma}/^\circ$
set 1	-8.108e-04	4.409e-01	99.643	34.298	144.649
set 2	9.064e-04	5.071e-01	95.256	110.676	163.366
set 3	-1.505e-03	3.608e-01	163.909	74.951	141.586
set 4	6.048e-04	6.488e-01	176.158	67.332	49.982
set 5	6.081e-04	5.628e-01	178.879	84.302	48.337
set 6	-8.311e-04	3.977e-01	63.102	66.832	151.953

Table S-11: Orientational data of IPC **1** obtained by TITANIA on the last optimization iteration of run **1-B23**.

Set	$\boldsymbol{A}_{zz}$	$\boldsymbol{R}$	$\boldsymbol{\alpha}/^\circ$	$\boldsymbol{\beta}/^\circ$	$\boldsymbol{\gamma}/^\circ$
set 1	-8.042e-04	4.571e-01	96.528	31.560	149.039
set 2	9.047e-04	4.945e-01	92.854	108.102	164.157
set 3	-1.527e-03	3.440e-01	161.588	71.675	144.470
set 4	6.048e-04	6.509e-01	179.884	65.253	50.975
set 5	6.104e-04	5.683e-01	2.499	83.064	50.439
set 6	-8.505e-04	3.968e-01	62.457	63.994	154.884

Table S-12: Orientational data of IPC **1** obtained by TITANIA on the last optimization iteration of run **1-B31**.

Set	$\boldsymbol{A}_{zz}$	$\boldsymbol{R}$	$\boldsymbol{\alpha}/^\circ$	$\boldsymbol{\beta}/^\circ$	$\boldsymbol{\gamma}/^\circ$
set 1	-7.644e-04	4.726e-01	98.228	31.031	149.711
set 2	8.819e-04	4.809e-01	92.649	107.750	165.933
set 3	-1.468e-03	3.562e-01	163.680	71.780	144.397
set 4	5.857e-04	6.520e-01	179.713	66.985	51.253
set 5	6.025e-04	5.575e-01	2.748	84.854	50.808
set 6	-7.994e-04	4.049e-01	62.748	64.052	155.672

Table S-13: Orientational data of IPC **1** obtained by TITANIA on the last optimization iteration of run **1-B39**.

Set	$\boldsymbol{A}_{zz}$	$\boldsymbol{R}$	$\boldsymbol{\alpha}/^\circ$	$\boldsymbol{\beta}/^\circ$	$\boldsymbol{\gamma}/^\circ$
set 1	-7.947e-04	4.634e-01	97.953	34.319	144.673
set 2	9.067e-04	4.808e-01	95.439	110.469	162.358
set 3	-1.522e-03	3.504e-01	163.308	74.337	141.465
set 4	6.066e-04	6.455e-01	176.995	66.514	49.234
set 5	6.213e-04	5.514e-01	0.137	84.036	47.788
set 6	-8.415e-04	4.056e-01	62.515	66.982	152.650

Note that as before the Euler angles differ due to the different reference frames. Thus a comparison can here only be based on A_{ZZ} and R, which again show a good agreement between the input orientations used for back-calculation and the final orientations for the runs utilizing 17 to 39 RDCs. The comparison of orientations with using a common reference frame is found in section 2.2.4.

1-C

Input orientations

The RDCs of setup **1-C** were calculated by the orientations summarized in table S-14.

Table S-14: Orientational used for the synthetic RDC sets of setup **1-C** and **1-F**.

Set	$\boldsymbol{A}_{zz}$	$\boldsymbol{R}$	$\boldsymbol{\alpha}/^\circ$	$\boldsymbol{\beta}/^\circ$	$\boldsymbol{\gamma}/^\circ$
set 1	-8.166e-04	4.731e-01	62.238	154.576	121.551
set 2	9.519e-04	4.642e-01	76.734	78.357	140.473
set 7	-6.930e-04	6.207e-01	67.088	140.025	118.143
set 8	9.806e-04	5.071e-01	77.192	81.428	137.636
set 9	1.036e-03	5.134e-01	72.293	80.309	139.775
set 10	9.246e-04	4.815e-01	77.352	77.964	140.567

Output orientations

All orientations of setup **1-C** (**11-39**) obtained from the full TITANIA optimization runs are listed in the following section. Changes of the Euler angles compared to the literature data listed above are due to the change of the reference frames (TITANIA used the principle axis system of the molecule). The comparison of the input and output data is summarized in table S-37 (section 2.2.4).

Table S-15: Orientational data of IPC **1** obtained by TITANIA on the last optimization iteration for the runs **1-C11**.

Set	$\boldsymbol{A}_{zz}$	$\boldsymbol{R}$	$\boldsymbol{\alpha}/^\circ$	$\boldsymbol{\beta}/^\circ$	$\boldsymbol{\gamma}/^\circ$
set 1	-7.943e-04	5.097e-01	102.085	37.179	143.291
set 2	9.609e-04	4.326e-01	100.119	113.990	162.818
set 7	-6.135e-04	6.637e-01	98.069	48.535	160.754
set 8	9.945e-04	4.811e-01	101.804	110.641	164.537
set 9	1.050e-03	4.726e-01	96.439	112.234	163.051
set 10	9.343e-04	4.500e-01	100.587	114.356	162.903

Table S-16: Orientational data of IPC **1** obtained by TITANIA on the last optimization iteration of run **1-C17**.

Set	$\boldsymbol{A}_{zz}$	$\boldsymbol{R}$	$\boldsymbol{\alpha}/^\circ$	$\boldsymbol{\beta}/^\circ$	$\boldsymbol{\gamma}/^\circ$
set 1	-6.630e-04	5.320e-01	92.012	27.294	149.210
set 2	6.131e-04	4.682e-01	81.440	102.747	153.765
set 7	6.536e-04	6.242e-01	92.776	128.778	165.380
set 8	5.919e-04	5.567e-01	82.873	96.917	153.684
set 9	6.396e-04	5.731e-01	74.931	98.582	151.072
set 10	5.998e-04	4.847e-01	82.711	103.363	153.929

Table S-17: Orientational data of IPC **1** obtained by TITANIA on the last optimization iteration of run **1-C23**.

Set	$\boldsymbol{A}_{zz}$	$\boldsymbol{R}$	$\boldsymbol{\alpha}/^\circ$	$\boldsymbol{\beta}/^\circ$	$\boldsymbol{\gamma}/^\circ$
set 1	-8.047e-04	4.573e-01	96.356	31.573	149.123
set 2	9.060e-04	4.933e-01	92.842	108.112	164.115
set 7	-6.871e-04	5.963e-01	93.761	43.221	162.469
set 8	9.305e-04	5.356e-01	93.201	104.329	165.855
set 9	9.846e-04	5.441e-01	88.538	105.973	164.218
set 10	8.806e-04	5.106e-01	93.458	108.524	164.143

Table S-18: Orientational data of IPC **1** obtained by TITANIA on the last optimization iteration of run **1-C31**.

Set	$\boldsymbol{A}_{zz}$	$\boldsymbol{R}$	$\boldsymbol{\alpha}/^\circ$	$\boldsymbol{\beta}/^\circ$	$\boldsymbol{\gamma}/^\circ$
set 1	-7.950e-04	4.621e-01	97.104	31.388	149.865
set 2	9.152e-04	4.760e-01	93.208	108.092	165.652
set 7	-6.720e-04	6.171e-01	93.379	42.998	164.303
set 8	9.408e-04	5.198e-01	93.779	104.373	167.514
set 9	9.951e-04	5.254e-01	88.804	106.031	165.771
set 10	8.891e-04	4.935e-01	93.852	108.487	165.691

Table S-19: Orientational data of IPC **1** obtained by TITANIA on the last optimization iteration of run **1-C39**.

Set	$\boldsymbol{A}_{zz}$	$\boldsymbol{R}$	$\boldsymbol{\alpha}/^\circ$	$\boldsymbol{\beta}/^\circ$	$\boldsymbol{\gamma}/^\circ$
set 1	-7.839e-04	4.699e-01	96.697	31.199	149.514
set 2	8.978e-04	4.811e-01	93.376	107.944	165.281
set 7	-6.608e-04	6.242e-01	92.838	42.771	164.059
set 8	9.221e-04	5.260e-01	93.844	104.220	167.183
set 9	9.754e-04	5.309e-01	88.906	105.870	165.412
set 10	8.726e-04	4.984e-01	93.995	108.343	165.304

Note that as before the Euler angles differ due to the different reference frames. Thus a comparison can here only be based on A_{ZZ} and R, which again show a good agreement between the input orientations used for back-calculation and the final orientations for the runs utilizing 17 to 39 RDCs. The comparison of orientations with using a common reference frame is found in section 2.2.4.

1-D

Input orientations

The RDCs of run **1-D** were calculated by adding random Gaussian error to the RDCs of **1-A** (for more information see the start of section 2). Therefore the orientation data are reported in table S-2.

Output orientations

All orientiations of run **1-D** (**11-39**) obtained from the full TITANIA optimization runs are listed in the following section. Changes of the Euler angles compared to the literature data listed above are due to the change of the reference frames (TITANIA used the principle axis system of the molecule) and the added errors. The comparison of the input and output data is summarized in table S-38 (section 2.2.4).

Table S-20: Orientational data of IPC **1** obtained by TITANIA on the last optimization iteration for the runs **1-D11**.

Set	$\boldsymbol{A}_{zz}$	$\boldsymbol{R}$	$\boldsymbol{\alpha}/^\circ$	$\boldsymbol{\beta}/^\circ$	$\boldsymbol{\gamma}/^\circ$
set 1	6.563e-04	1.709e-01	17.261	34.845	91.053
set 2	-5.517e-05	3.735e-01	87.915	26.830	9.600
set 3	-9.313e-05	9.125e-02	171.939	98.010	98.051
set 4	4.663e-04	5.462e-01	93.750	121.115	64.374
set 5	3.359e-04	3.032e-01	133.863	104.485	88.760
set 6	7.921e-04	4.444e-01	166.107	124.691	143.805
set 7	7.918e-04	1.332e-01	147.979	49.227	54.222
set 8	3.386e-04	3.093e-01	71.237	122.130	20.822
set 9	-6.140e-05	2.967e-01	105.865	34.709	133.496
set 10	8.866e-04	4.802e-01	11.296	28.311	108.368
set 11	2.675e-04	1.420e-01	98.058	149.404	64.884
set 12	4.638e-04	1.826e-01	10.888	114.606	78.810
set 13	2.887e-04	1.143e-01	168.817	13.701	165.191
set 14	8.921e-05	2.601e-01	37.800	23.631	136.646
set 15	8.573e-04	1.154e-01	92.175	34.978	73.255
set 16	4.080e-04	3.538e-01	137.808	107.276	176.617
set 17	6.827e-04	5.409e-01	92.825	132.102	73.204
set 18	5.554e-04	2.171e-01	49.083	55.873	29.584
set 19	8.126e-04	2.133e-01	55.817	101.724	14.943
set 20	7.043e-04	6.064e-01	108.558	27.698	88.831

Table S-21: Orientational data of IPC **1** obtained by TITANIA on the last optimization iteration of run **1-D17**.

Set	$\boldsymbol{A}_{zz}$	$\boldsymbol{R}$	$\boldsymbol{\alpha}/^\circ$	$\boldsymbol{\beta}/^\circ$	$\boldsymbol{\gamma}/^\circ$
set 1	6.059e-04	3.268e-01	13.221	33.839	89.181
set 2	8.460e-05	3.694e-01	129.989	70.139	140.494
set 3	-1.176e-04	6.150e-01	164.392	86.995	117.859
set 4	4.040e-04	4.402e-01	96.585	130.964	59.756
set 5	2.841e-04	4.845e-01	156.371	104.724	98.880
set 6	8.591e-04	4.121e-01	165.522	129.724	150.550
set 7	8.145e-04	6.008e-02	11.020	56.983	56.894
set 8	4.182e-04	1.440e-01	81.533	126.561	20.323
set 9	7.065e-05	2.541e-01	123.750	146.150	161.212
set 10	7.675e-04	5.517e-01	15.325	21.610	99.638
set 11	3.710e-04	2.226e-01	43.364	158.730	65.707
set 12	4.143e-04	4.879e-01	14.950	119.941	83.078
set 13	3.195e-04	1.952e-01	166.385	168.871	10.701
set 14	7.742e-05	4.860e-01	111.691	10.102	93.346
set 15	7.571e-04	5.801e-02	178.908	40.032	71.258
set 16	4.329e-04	3.027e-01	33.782	72.276	2.236
set 17	6.593e-04	4.945e-01	93.732	142.102	72.712
set 18	6.516e-04	3.550e-01	50.779	61.785	35.678
set 19	8.827e-04	8.288e-02	77.402	103.840	16.179
set 20	-6.316e-04	5.429e-01	110.204	115.878	122.231

Table S-22: Orientational data of IPC **1** obtained by TITANIA on the last optimization iteration of run **1-D23**.

Set	$\boldsymbol{A}_{zz}$	$\boldsymbol{R}$	$\boldsymbol{\alpha}/^\circ$	$\boldsymbol{\beta}/^\circ$	$\boldsymbol{\gamma}/^\circ$
set 1	5.426e-04	2.362e-01	11.316	32.424	88.929
set 2	7.098e-05	2.009e-01	109.314	70.870	152.829
set 3	-9.066e-05	5.977e-01	159.380	70.140	116.061
set 4	4.470e-04	3.137e-01	97.587	127.566	57.891
set 5	2.761e-04	3.854e-01	140.338	105.367	88.578
set 6	7.891e-04	4.065e-01	172.713	124.737	147.775
set 7	7.637e-04	3.626e-02	178.086	53.274	50.632
set 8	4.147e-04	1.731e-01	85.358	128.168	25.998
set 9	-6.384e-05	5.674e-01	114.262	46.157	128.209
set 10	7.141e-04	5.443e-01	9.243	22.310	105.819
set 11	3.569e-04	1.704e-01	36.869	156.062	61.174
set 12	4.286e-04	4.063e-01	15.881	115.892	75.844
set 13	3.301e-04	9.256e-02	160.233	167.061	13.655
set 14	8.555e-05	4.025e-01	73.338	6.196	134.808
set 15	7.036e-04	5.993e-02	120.607	36.416	67.786
set 16	4.320e-04	2.289e-01	131.685	109.974	176.345
set 17	6.525e-04	4.270e-01	90.678	138.119	67.640
set 18	6.318e-04	3.737e-01	61.248	58.735	28.034
set 19	7.326e-04	1.426e-01	55.639	103.787	15.440
set 20	-5.794e-04	6.602e-01	102.764	113.157	117.951

Table S-23: Orientational data of IPC **1** obtained by TITANIA on the last optimization iteration of run **1-D31**.

Set	$\boldsymbol{A}_{zz}$	$\boldsymbol{R}$	$\boldsymbol{\alpha}/^\circ$	$\boldsymbol{\beta}/^\circ$	$\boldsymbol{\gamma}/^\circ$
set 1	8.047e-04	3.336e-01	25.222	61.033	95.877
set 2	-8.554e-05	6.285e-01	5.810	60.847	87.329
set 3	-1.565e-04	5.936e-01	3.039	51.339	115.432
set 4	4.875e-04	3.627e-01	77.128	157.071	53.823
set 5	2.976e-04	1.638e-01	148.088	137.136	106.951
set 6	1.004e-03	4.777e-01	155.895	59.952	0.334
set 7	8.694e-04	1.285e-01	2.828	86.872	71.023
set 8	4.560e-04	4.040e-02	56.083	144.047	12.286
set 9	8.979e-05	5.555e-01	71.705	21.314	96.499
set 10	-9.124e-04	6.013e-01	38.910	122.316	30.387
set 11	3.752e-04	1.111e-01	72.986	10.509	106.165
set 12	4.872e-04	3.780e-01	23.796	143.958	94.570
set 13	4.100e-04	6.639e-02	145.202	32.008	103.647
set 14	-9.756e-05	3.743e-01	144.083	110.067	148.322
set 15	9.326e-04	1.250e-01	36.552	68.904	85.908
set 16	4.417e-04	4.748e-01	176.989	90.463	10.252
set 17	-6.937e-04	6.565e-01	87.432	78.067	93.327
set 18	6.253e-04	6.106e-01	46.556	89.597	46.569
set 19	1.034e-03	1.708e-01	22.402	124.759	16.561
set 20	7.612e-04	5.575e-01	134.633	56.445	93.873

Table S-24: Orientational data of IPC **1** obtained by TITANIA on the last optimization iteration of run **1-D39**.

Set	$\boldsymbol{A}_{zz}$	$\boldsymbol{R}$	$\boldsymbol{\alpha}/^\circ$	$\boldsymbol{\beta}/^\circ$	$\boldsymbol{\gamma}/^\circ$
set 1	6.137e-04	2.661e-01	11.846	33.966	86.087
set 2	1.069e-04	2.113e-01	115.186	85.384	125.380
set 3	-1.376e-04	6.411e-01	10.793	50.272	101.518
set 4	4.296e-04	5.611e-01	104.454	130.564	51.757
set 5	2.668e-04	4.541e-01	135.754	111.709	81.312
set 6	8.533e-04	4.253e-01	163.643	127.678	143.549
set 7	7.836e-04	3.283e-02	3.277	58.422	46.265
set 8	4.234e-04	2.592e-01	106.522	131.223	15.142
set 9	-9.219e-05	3.046e-01	90.650	69.495	30.447
set 10	6.654e-04	5.674e-01	26.150	22.286	86.476
set 11	3.389e-04	9.875e-02	80.190	157.003	48.210
set 12	4.771e-04	1.638e-01	172.144	120.901	75.174
set 13	3.494e-04	2.126e-01	89.884	3.648	111.646
set 14	8.111e-05	4.186e-01	155.709	15.863	62.243
set 15	7.576e-04	1.021e-01	127.889	40.833	62.219
set 16	3.193e-04	4.718e-01	149.408	97.659	168.665
set 17	6.339e-04	5.178e-01	106.807	138.658	76.344
set 18	5.853e-04	4.836e-01	56.279	68.670	23.333
set 19	8.351e-04	1.388e-01	82.687	111.111	9.466
set 20	-6.623e-04	6.587e-01	111.998	113.253	112.885

In contrast to the setups **1-A** to **1-C** the Euler angles not only differ due to the different reference frames but also due to the heterogeneity added purposefully. This heterogeneity will also have an impact on A_{ZZ} and R, which is why larger differences between the input orientations used for back-calculation and the final orientations are found. These differences show variations between the respective sets of one run. The reason for this finding is the different magnitudes of A_{ZZ} used for the back-calculation of the data (see table S-2). This circumstance is discussed below in more detail (see table S-41). The comparison of the orientations using a common reference frame as discussed before is found in section 2.2.4.

1-E

Input orientations

The RDCs of run **1-E** were calculated by adding random Gaussian error to the RDCs of **1-B** (for more information see the start of section 2). Therefore the orientation data are reported in table S-8.

Output orientations

All orientiations of setup **1-E** (**11**-**39**) obtained from the full TITANIA optimization runs are listed in the following section. Changes of the Euler angles compared to the literature data listed above are due to the change of the reference frames (TITANIA used the principle axis system of the molecule) and the added errors. The comparison of the input and output data is summarized in table S-39 (section 2.2.4).

Table S-25: Orientational data of IPC **1** obtained by TITANIA on the last optimization iteration for the runs **1-E11**.

Set	$\boldsymbol{A}_{zz}$	$\boldsymbol{R}$	$\boldsymbol{\alpha}/^\circ$	$\boldsymbol{\beta}/^\circ$	$\boldsymbol{\gamma}/^\circ$
set 1	-7.950e-04	4.150e-01	98.308	39.844	148.548
set 2	1.075e-03	3.454e-01	95.275	110.848	170.903
set 3	-1.715e-03	2.654e-01	166.563	81.713	150.363
set 4	6.906e-04	5.243e-01	174.590	61.131	62.663
set 5	-6.504e-04	6.572e-01	171.204	92.325	148.200
set 6	-1.112e-03	4.359e-01	57.118	78.351	160.360

Table S-26: Orientational data of IPC **1** obtained by TITANIA on the last optimization iteration of run **1-E17**.

Set	$\boldsymbol{A}_{zz}$	$\boldsymbol{R}$	$\boldsymbol{\alpha}/^\circ$	$\boldsymbol{\beta}/^\circ$	$\boldsymbol{\gamma}/^\circ$
set 1	-8.416e-04	4.807e-01	104.721	32.283	145.280
set 2	1.028e-03	4.582e-01	93.978	109.339	167.592
set 3	-1.505e-03	3.815e-01	171.934	74.350	138.887
set 4	6.274e-04	5.836e-01	177.183	69.383	50.276
set 5	6.333e-04	5.853e-01	1.499	89.880	48.709
set 6	-8.158e-04	3.788e-01	64.006	66.422	148.850

Table S-27: Orientational data of IPC **1** obtained by TITANIA on the last optimization iteration of run **1-E23**.

Set	$\boldsymbol{A}_{zz}$	$\boldsymbol{R}$	$\boldsymbol{\alpha}/^\circ$	$\boldsymbol{\beta}/^\circ$	$\boldsymbol{\gamma}/^\circ$
set 1	-7.845e-04	5.005e-01	111.550	33.680	133.099
set 2	9.726e-04	4.230e-01	103.895	107.315	165.964
set 3	-1.378e-03	3.799e-01	167.469	76.387	142.910
set 4	6.171e-04	5.638e-01	174.011	63.799	53.724
set 5	5.885e-04	5.784e-01	176.935	83.091	50.360
set 6	-8.206e-04	3.945e-01	62.038	68.148	152.355

Table S-28: Orientational data of IPC **1** obtained by TITANIA on the last optimization iteration of run **1-E31**.

Set	$\boldsymbol{A}_{zz}$	$\boldsymbol{R}$	$\boldsymbol{\alpha}/^\circ$	$\boldsymbol{\beta}/^\circ$	$\boldsymbol{\gamma}/^\circ$
set 1	-7.148e-04	4.847e-01	111.265	34.675	139.686
set 2	8.980e-04	4.268e-01	96.474	108.629	170.759
set 3	-1.481e-03	3.565e-01	174.799	79.481	140.420
set 4	-5.675e-04	6.589e-01	165.145	96.850	141.009
set 5	5.897e-04	6.332e-01	174.093	95.134	48.894
set 6	-8.324e-04	3.884e-01	71.951	70.827	148.756

Table S-29: Orientational data of IPC **1** obtained by TITANIA on the last optimization iteration of run **1-E39**.

Set	$\boldsymbol{A}_{zz}$	$\boldsymbol{R}$	$\boldsymbol{\alpha}/^\circ$	$\boldsymbol{\beta}/^\circ$	$\boldsymbol{\gamma}/^\circ$
set 1	-7.372e-04	4.911e-01	101.629	34.887	153.570
set 2	9.537e-04	4.505e-01	91.551	112.601	176.219
set 3	-1.408e-03	4.446e-01	174.426	81.373	150.820
set 4	-6.019e-04	6.482e-01	164.776	98.050	146.706
set 5	6.340e-04	6.218e-01	172.237	91.176	55.083
set 6	-8.176e-04	3.882e-01	63.855	72.320	157.256

1-F

Input orientations

The RDCs of run **1-F** were calculated by adding random Gaussian error to the RDCs of **1-C** (for more information see the start of section 2). Therefore the orientation data are reported in table S-14.

Output orientations

All orientiations of run **1-F** (**11-39**) obtained from the full TITANIA optimization runs are listed in the following section. Changes of the Euler angles compared to the literature data listed above are due to the change of the reference frames (TITANIA used the principle axis system of the molecule) and the added errors. Of high impact for this setup is the missing convergence and thereby large distortions of the structure. This leads to wrong orientation parameters. The comparison of the input and output data is summarized in table S-40 (section 2.2.4).

Table S-30: Orientational data of IPC **1** obtained by TITANIA on the last optimization iteration for the runs **1-F11**.

Set	$\boldsymbol{A}_{zz}$	$\boldsymbol{R}$	$\boldsymbol{\alpha}/^\circ$	$\boldsymbol{\beta}/^\circ$	$\boldsymbol{\gamma}/^\circ$
set 1	-7.323e-04	1.757e-01	21.959	53.078	131.176
set 2	-7.112e-04	5.412e-01	9.253	46.213	103.567
set 7	-6.834e-04	2.104e-01	134.133	64.583	133.945
set 8	-7.553e-04	5.281e-01	10.523	32.605	100.127
set 9	-7.792e-04	6.015e-01	14.527	36.754	103.745
set 10	-7.135e-04	4.771e-01	8.645	42.312	105.833

Table S-31: Orientational data of IPC **1** obtained by TITANIA on the last optimization iteration of run **1-F17**.

Set	$\boldsymbol{A}_{zz}$	$\boldsymbol{R}$	$\boldsymbol{\alpha}/^\circ$	$\boldsymbol{\beta}/^\circ$	$\boldsymbol{\gamma}/^\circ$
set 1	-5.315e-04	4.740e-01	108.017	51.100	147.127
set 2	6.644e-04	3.148e-01	56.389	64.107	0.762
set 7	-5.094e-04	6.181e-01	114.681	59.992	160.917
set 8	6.937e-04	4.115e-01	47.726	69.585	3.639
set 9	7.393e-04	4.202e-01	61.175	66.555	2.115
set 10	6.356e-04	4.076e-01	54.700	64.377	0.618

Table S-32: Orientational data of IPC **1** obtained by TITANIA on the last optimization iteration of run **1-F23**.

Set	$\boldsymbol{A}_{zz}$	$\boldsymbol{R}$	$\boldsymbol{\alpha}/^\circ$	$\boldsymbol{\beta}/^\circ$	$\boldsymbol{\gamma}/^\circ$
set 1	1.595e-03	2.485e-01	28.009	54.848	28.371
set 2	2.116e-03	1.006e-01	23.912	61.662	12.787
set 7	1.510e-03	2.810e-01	18.880	53.793	40.299
set 8	2.033e-03	1.485e-01	24.423	64.106	11.306
set 9	2.362e-03	1.640e-01	21.980	63.071	14.331
set 10	1.989e-03	1.162e-01	20.411	61.822	13.466

Table S-33: Orientational data of IPC **1** obtained by TITANIA on the last optimization iteration of run **1-F31**.

Set	$\boldsymbol{A}_{zz}$	$\boldsymbol{R}$	$\boldsymbol{\alpha}/^\circ$	$\boldsymbol{\beta}/^\circ$	$\boldsymbol{\gamma}/^\circ$
set 1	-6.765e-04	4.767e-01	87.261	37.011	148.785
set 2	7.922e-04	5.650e-01	106.172	110.947	177.261
set 7	-5.425e-04	4.219e-01	79.068	48.417	169.225
set 8	8.220e-04	6.492e-01	67.184	74.229	0.356
set 9	8.507e-04	6.143e-01	106.840	108.146	176.660
set 10	7.558e-04	6.047e-01	111.864	109.909	177.867

Table S-34: Orientational data of IPC **1** obtained by TITANIA on the last optimization iteration of run **1-F39**.

Set	$\boldsymbol{A}_{zz}$	$\boldsymbol{R}$	$\boldsymbol{\alpha}/^\circ$	$\boldsymbol{\beta}/^\circ$	$\boldsymbol{\gamma}/^\circ$
set 1	-7.593e-04	4.385e-01	156.619	68.190	122.764
set 2	9.258e-04	3.843e-01	24.901	86.472	21.230
set 7	-5.855e-04	6.374e-01	162.446	64.609	138.184
set 8	9.469e-04	5.005e-01	21.550	90.237	16.287
set 9	9.947e-04	4.520e-01	27.344	88.479	18.041
set 10	8.596e-04	4.968e-01	18.928	90.301	19.966

2.2.3 Optimization Trajectories

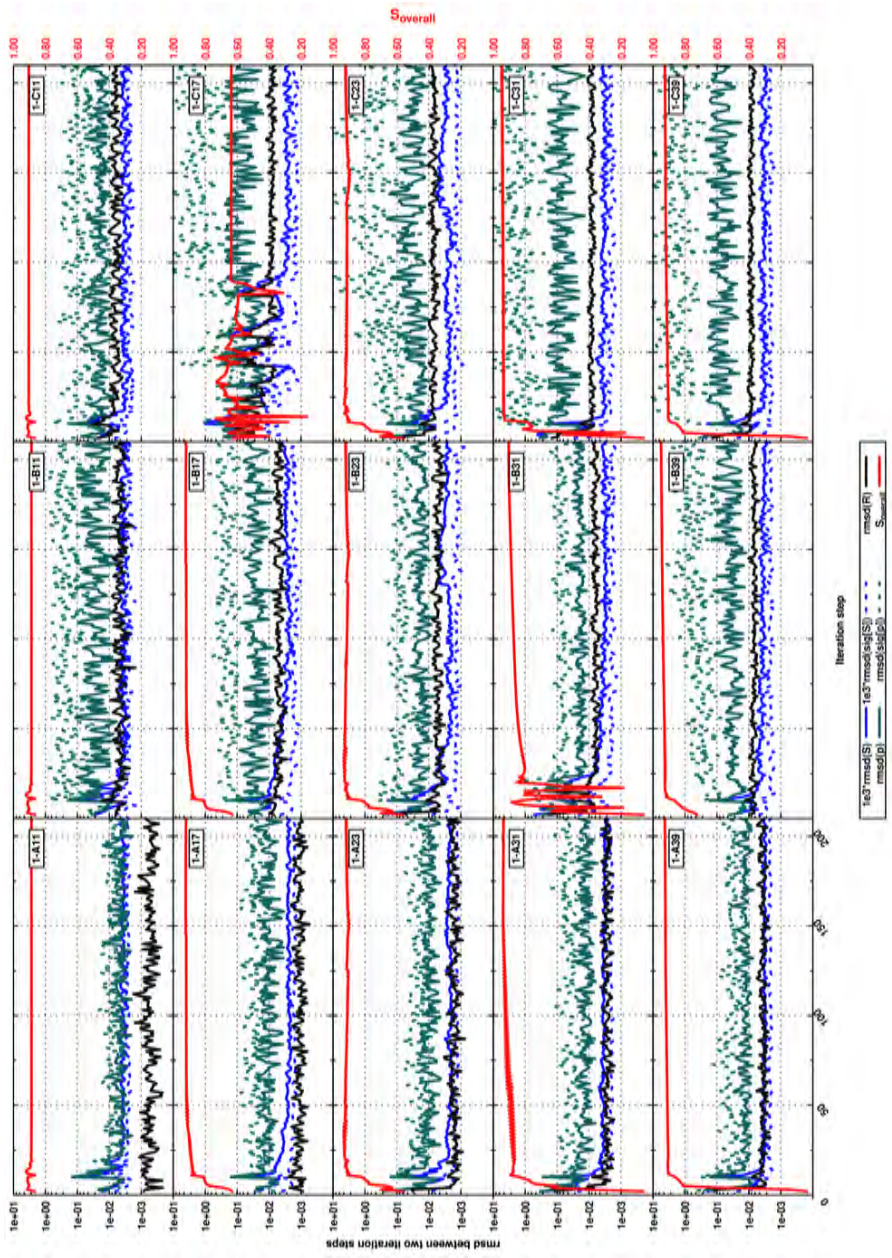

Figure S-10: Trajectory of the Monte-Carlo *rmsd*s obtained for the individual runs of the setups **1-A**, **B** and **C**. Shown are the data obtained by the default redundant internal coordinates algorithm.

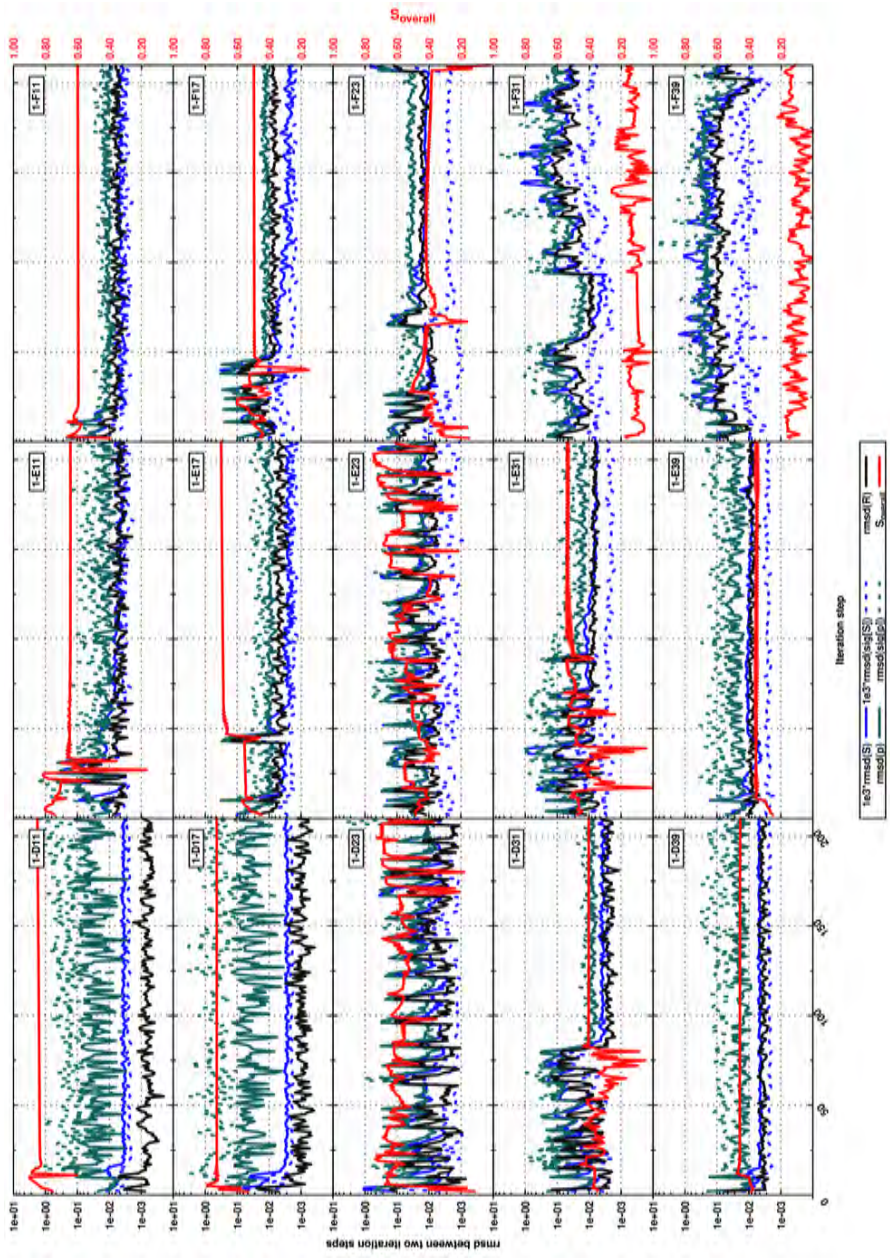

Figure S-11: Trajectory of the Monte-Carlo *rmsd*s obtained for the individual runs of the setups **1-D**, **E** and **F**. Shown are the data obtained by the default redundant internal coordinates algorithm.

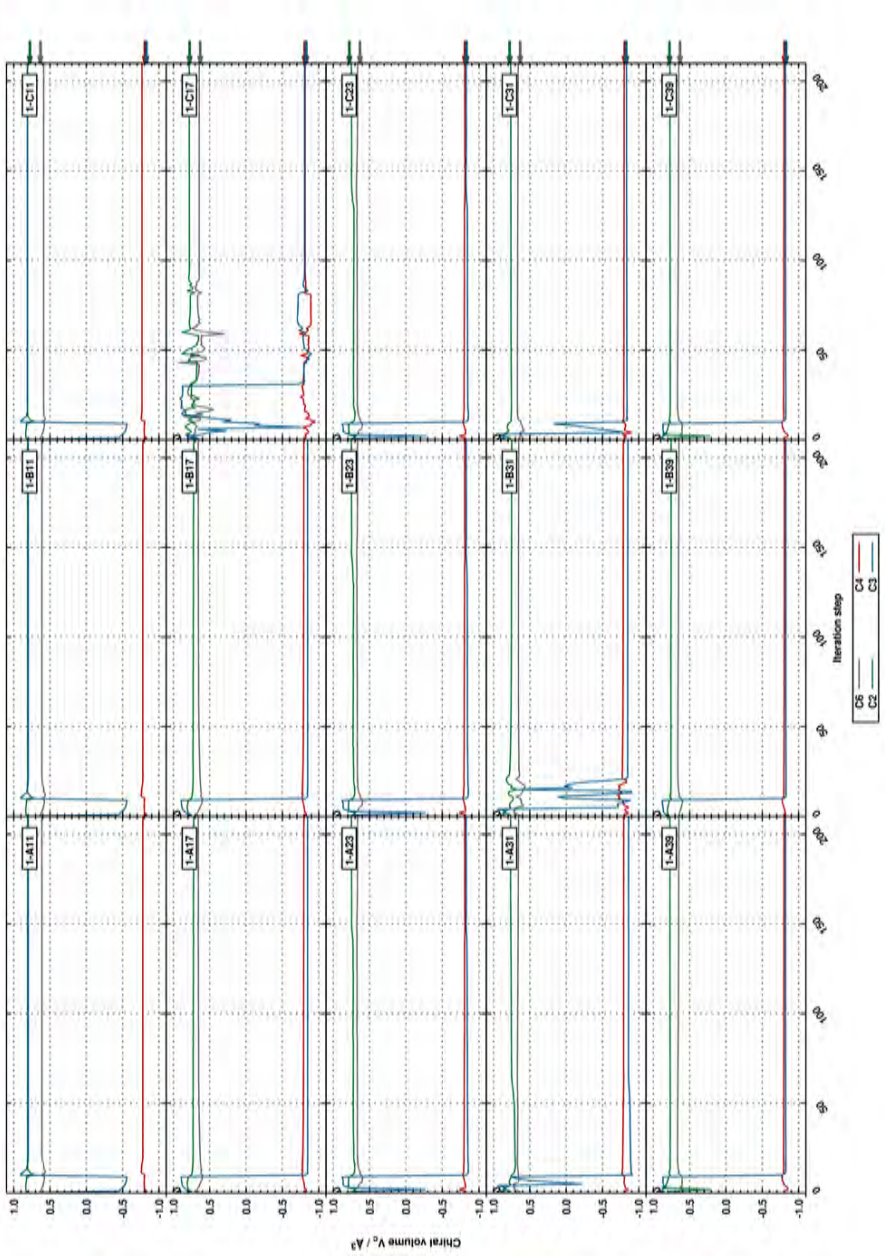

Figure S-12: Trajectory of the normalized chiral volumes obtained for the individual runs of the setups **1-A**, **B** and **C**. Shown are the data obtained by the default redundant internal coordinates algorithm. The arrows at the top indicate the values of the reference structure (correct configuration).

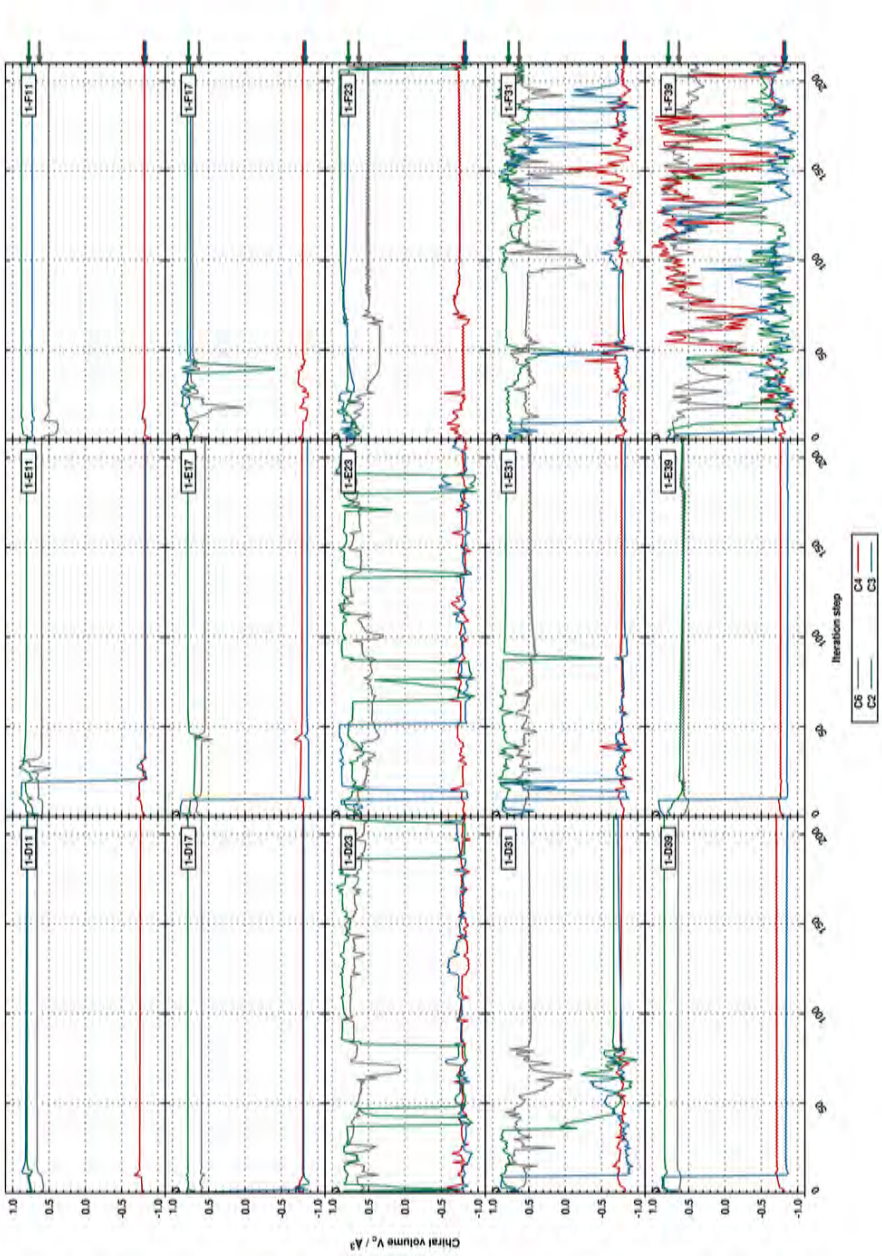

Figure S-13: Trajectory of the normalized chiral volumes obtained for the individual runs of the setups **1-D**, **E** and **F**. Shown are the data obtained by the default redundant internal coordinates algorithm. The arrows at the top indicate the values of the reference structure (correct configuration).

The iterative progression of TITANIA is assessed by a Monte-Carlo bootstrap after every iteration step. In this bootstrap all RDCs are varied simultaneously by normal distributed random numbers, with the user estimated experimental errors of the individual RDCs as standard deviation, and used for the determination of the alignment (tensor shape and Euler angles) and from that the resulting structure parameters (spherical harmonics and spherical coordinates). The parameters monitored (which can be used as stop criteria, for respective flags see section 1.2.1) are the change (*rmsd*) in the reduced Saupe matrix (S_{zz}, S_{xx}-S_{yy}, S_{xy}, S_{xz}, S_{yz}), the trigonometric functions of the polar angles p (e.g. $\cos(\theta)$) and the standard deviation of the respective values. The fifth parameter monitored is the change of the mean length R_s of the averaged Monte-Carlo RDC direction vectors (see eq. (34)). In the present runs the thresholds for the convergence were set to zero to show the full trajectories of the runs **1-A** to **1-F** (stop criteria not used).

Of special interest in fig. S-10 is the behavior of the structure related parameters. As expected the *rmsd* of R_s shows less fluctuation when increasing the number of RDCs per set. If convergence is not achieved large spikes in the Monte-Carlo trajectories (see first steps in fig. S-10) and significant changes in the chiral volumes throughout the whole optimization would be observed. All trajectories except **1-C17** show the last significant spike in S_{overall} around iteration 10, which is the point at which the final configurations are reached. As expected the trajectories **1-X17** to **1-X39** (with **X** equals **A** to **C**) clearly show convergence to the correct structure. Convergence is also achieved in **1-A11**, but the wrong configuration is obtained with a distorted geometry at the center C3.

Compared to the Monte-Carlo plots of setup **1-A** the runs of **1-B** and **1-C** show larger fluctuations in the parameters monitored. This is due to the fact that here fewer RDC sets are used. S_{overall} is not as strongly affected by the number of sets as the Monte-Carlo results, as it is determined from the experimental RDCs instead of the Monte-Carlo bootstrap. Only **1-C17** seems to show an unexpected behavior due to a rather low S_{overall} parameter and high fluctuations in the orientations of the RDC vector obtained from the Monte-Carlo bootstrap (*rmsd*[p] and *rmsd*(sig[p])).

These instabilities are based on the linear dependence and the number of RDC sets. This can be seen in the comparison of all runs in fig. S-10. Here the fluctuations of the vector orientations increases when reducing the number of sets (**1-A** to **1-B**) and again when increasing the linear dependence of the sets (**1-B** to **1-C**).

This trend seems to change when adding heterogeneity. Here **1-F** shows fast convergence with comparably low S_{overall} values. By investigation of the geometries it becomes clear that this a random local minimum. This will be

discussed in more detail on the chiral volume plots. The two last runs (**1-F31** and **39**) in fig. S-11 show instabilities in the full course of the optimization. This is a hint towards random inversions. This will also be discussed below.

The runs with 11 and 17 RDCs for **1-D** and **1-E** show an increase in the fluctuations compared to the homogeneous data, with **1-D** being more affected. The reason might be the large variety of axial components for **1-D** (see table S-41 for more details). This fluctuation is reduced with the number of RDCs, demonstrating that larger set sizes lead to a higher error tolerance. An exception are the runs using 23 RDC, which show no convergence at all. A close look on the xyz coordinates (see supplementary materials section 5) and the chiral volume trajectories allows a better assessment of these two runs. By this it becomes clear that **1-E23** undergoes several inversions of different centers accompanied by large distortions of the geometry (including large variations in the bond lengths of the ring scaffold). **1-D23** on the other hand only shows large fluctuations at C6 which influences the whole trajectory, especially the center C2. C2 and C6 have in common that $^1D_{\mathrm{CC}}$ couplings are used to define the configuration. These are lower in magnitude than $^1D_{\mathrm{CH}}$ RDCs. Furthermore no long-range RDCs are available to further define or confirm the configuration. Additionally the S_{overall} is reduced in size, especially when long-range RDCs are added in the larger setups with 31 or 39 RDCs.

The trajectories of the **1-F** runs with 11 to 23 RDCs imply a fast convergence. This behavior is due to the convergence into a local minimum barely optimizing the structure at all (see below). The runs **1-F31** and **1-F39** show the other scenario where no convergence is achieved at all. Here only random inversions occur during the optimization. Additionally the lowest S_{overall} for IPC are found in these runs. This shows that the MFA is neither capable to determine structure parameters for heterogeneous, dependent alignment conditions nor to properly determine any dynamic parameters in this scenario.

The chiral volume plots of the homogeneous data (fig. S-12) show, as expected from the main text discussion, very stable configurations. Therefore the trajectories of the heterogeneous setups **1-D** to **1-F** are of larger interest. It is noteworthy that **1-E11** converged into the correct relative configuration. This is unexpected and should not be over-interpreted. More important is that the setups with long-range couplings show a reduction in stability compared to the homogeneous data while still achieving the correct relative configuration. An exception are the runs using 23 RDCs. The trajectories of both the chiral volume and the *rmsd*s shown above, are not stable at any point of the optimization. In such a case the number of RDCs per set should be varied (in a real scenario lowered) or the vector addition algorithm should

be used. The reduction of the number of RDCs would allows to identify RDCs that disturb the trajectories, most likely due to high local heterogeneity. The alternative vector addition algorithm is more robust and thereby could help to find the correct configurations. This algorithm is discussed later for the heterogeneous setups.

The setup **1-F** shows very interesting results. Here the first three trajectories converge very fast without a change in any configurations. If the set size is increased further (**1-F31** and **39**) rapid inversion without any pattern can be observed. This demonstrates how linear dependence in combination with heterogeneity does not allow to obtain correct vector orientations by using TITANIA.

2.2.4 Change in Orientation

To quantify the similarity of the input and the output orientations a common reference frame has to be used. Therefore an all atom *rmsd* structure alignment was performed to match the TITANIA output structure with the reference structure (or its enantiomer). The alignment tensors of the transformed structures are recalculated and the differences in the orientations (TITANIA vs. reference) are expressed by the β angle.

1-A

Table S-35: Generalized angle β enclosed by the reference structure of IPC and the structure obtained by TITANIA from the last optimization step of the runs **1-A**. The data were obtained by transformation of the respective structures to a common reference frame, followed by recalculating the alignment tensors with the in-house software `RDC@hotFCHT`.[9]

	$\boldsymbol{\beta}/^\circ$				
Set	**1-A11**	**1-A17**	**1-A23**	**1-A31**	**1-A39**
set 1	5.923	3.185	2.991	5.292	1.331
set 2	8.151	1.968	2.981	5.732	1.067
set 3	3.245	2.592	0.915	4.253	1.597
set 4	9.843	2.437	1.429	2.718	0.754
set 5	12.561	2.022	1.855	3.214	1.393
set 6	11.638	2.107	2.136	4.630	0.637
set 7	8.578	1.787	1.701	5.329	0.848
set 8	5.394	3.385	3.354	3.429	1.138
set 9	8.501	2.442	2.134	4.568	0.714
set 10	5.250	3.403	2.512	4.475	1.362
set 11	7.617	1.904	1.687	3.285	0.802
set 12	11.348	1.805	2.673	2.424	1.115
set 13	9.771	2.135	1.961	4.408	0.776
set 14	6.866	3.345	2.227	5.294	0.604
set 15	8.051	3.053	2.651	5.344	1.000
set 16	7.947	2.034	2.853	5.279	1.558
set 17	7.454	2.524	1.594	3.482	0.716
set 18	4.324	1.631	1.313	5.337	0.731
set 19	6.208	2.596	3.187	3.588	1.730
set 20	7.094	2.881	2.136	5.383	0.438

It can be seen that only **1-A11** shows β angles of larger magnitude. The reason is the incorrect configuration on C3. All other runs only have very small deviations between the reference and output structures. This confirms the agreement of the TITANIA structure and the reference.

1-B

Table S-36: Generalized angle β enclosed by the reference structure of IPC and the structure obtained by TITANIA from the last optimization step of the runs **1-B**. The data were obtained by transformation of the respective structures to a common reference frame, followed by recalculating the alignment tensors with the in-house software `RDC@hotFCHT`.[9]

	$\beta/^\circ$				
Set	**1-B11**	**1-B17**	**1-B23**	**1-B31**	**1-B39**
set 1	2.994	2.709	2.424	2.520	2.034
set 2	5.193	2.339	2.763	2.234	1.953
set 3	7.820	1.842	2.553	4.310	2.417
set 4	7.238	1.254	2.075	3.899	2.373
set 5	6.125	2.185	1.767	3.641	2.174
set 6	6.159	2.707	3.605	3.559	2.338

All runs of the setup **1-B** show excellent agreement between the TITANIA and reference structure.

1-C

Table S-37: Generalized angle β enclosed by the reference structure of IPC and the structure obtained by TITANIA from the last optimization step of the runs **1-C**. The data were obtained by transformation of the respective structures to a common reference frame, followed by recalculating the alignment tensors with the in-house software `RDC@hotFCHT`.[9]

	$\beta/^\circ$				
Set	**1-C11**	**1-C17**	**1-C23**	**1-C31**	**1-C39**
set 1	2.418	10.222	2.362	1.492	0.611
set 2	4.152	20.642	2.716	1.466	1.028
set 7	2.550	10.907	2.679	1.669	0.715
set 8	4.793	23.999	2.816	1.463	1.129
set 9	4.662	23.865	2.699	1.377	1.023
set 10	4.029	20.034	2.702	1.457	1.021

The high β angle found for **1-C17** shows a large value due to distortions of the methyl vectors C6-C8 and C6-C9.

1-D

Table S-38: Generalized angle β enclosed by the reference structure of IPC and the structure obtained by TITANIA from the last optimization step of the runs **1-D**. The data were obtained by transformation of the respective structures to a common reference frame, followed by recalculating the alignment tensors with the in-house software `RDC@hotFCHT`.[9] The mean contribution of the random noise to the β angles is reported in table S-41.

	$\boldsymbol{\beta}/^\circ$				
Set	**1-D11**	**1-D17**	**1-D23**	**1-D31**	**1-D39**
set 1	10.116	7.150	5.541	39.437	15.202
set 2	13.430	16.208	14.208	45.302	13.448
set 3	11.460	12.745	10.916	27.275	15.252
set 4	9.075	9.924	4.270	58.423	12.129
set 5	5.162	10.557	7.233	57.837	8.629
set 6	12.618	4.166	9.068	57.086	9.181
set 7	9.845	7.009	4.444	57.993	16.812
set 8	11.790	4.946	10.780	32.610	13.318
set 9	11.158	11.279	17.303	52.909	16.708
set 10	6.207	7.644	5.606	44.127	13.986
set 11	14.393	5.905	4.101	52.062	8.597
set 12	8.996	7.016	9.430	39.717	10.459
set 13	9.181	9.410	7.701	42.717	8.083
set 14	7.418	15.582	12.608	47.711	10.091
set 15	9.178	8.688	4.663	52.551	15.287
set 16	6.976	5.430	9.705	33.347	15.209
set 17	13.728	9.042	4.330	60.949	10.506
set 18	7.528	7.684	3.738	40.481	15.600
set 19	7.279	4.436	4.824	31.517	14.840
set 20	10.886	7.651	7.978	51.570	9.160

Apart from **1-D31**, which did not converge using redundant internal coordinates, the β angles show good agreement. The values are a combination of the errors added and the deviations in the final compared to the reference structure. The separation of these two effects is addressed later.

1-E

Table S-39: Generalized angle β enclosed by the reference structure of IPC and the structure obtained by TITANIA from the last optimization step of the runs **1-E**. The data were obtained by transformation of the respective structures to a common reference frame, followed by recalculating the alignment tensors with the in-house software `RDC@hotFCHT`.[9] The mean contribution of the random noise to the β angles is reported in table S-42.

	$\boldsymbol{\beta}/^\circ$				
Set	**1-E11**	**1-E17**	**1-E23**	**1-E31**	**1-E39**
set 1	1.031	5.365	12.059	4.732	11.162
set 2	8.733	2.112	10.428	2.994	11.562
set 3	12.759	8.271	3.496	7.317	14.976
set 4	13.415	5.349	6.096	4.400	16.701
set 5	13.848	6.355	4.570	4.474	16.945
set 6	11.343	8.382	4.536	10.023	7.351

The β angles are a combination of the errors added and the deviations in the final compared to the reference structure. The separation of this two effects is addressed later.

1-F

Table S-40: Generalized angle β enclosed by the reference structure of IPC and the structure obtained by TITANIA from the last optimization step of the runs **1-F**. The data were obtained by transformation of the respective structures to a common reference frame, followed by recalculating the alignment tensors with the in-house software `RDC@hotFCHT`.[9] The mean contribution of the random noise to the β angles is reported in table S-43.

	$\boldsymbol{\beta}/^\circ$				
Set	**1-F11**	**1-F17**	**1-F23**	**1-F31**	**1-F39**
set 1	37.217	22.950	103.611	57.157	55.099
set 2	58.962	19.781	108.086	58.470	55.278
set 7	36.418	25.518	115.432	63.649	61.063
set 8	51.858	28.486	104.242	63.774	56.893
set 9	58.467	21.751	103.605	60.611	55.627
set 10	55.075	21.936	105.504	60.508	58.774

In the setup **1-F** the error now shows the importance of linear independence in the alignment media when experimental error is present. None of

the runs shown has converged.

2.2.5 Change induced by error

When adding error to the RDCs a change in the orientation is induced. This change is addressed in this section. In the following tables the generalized β angle β is calculated for the individual sets. Since a change in the orientation can be induced by the change of RDCs as well as by structural changes the following β angles contain this information simultaneously. To address the pure change due to the variation of RDCs, the mean β angle (and the corresponding standard deviation) of the individual runs is calculated using the reference structure.

1-A
Some β-angles in the **1-A** vs. **1-D** comparison have rather large magnitudes. This is especially true for the sets with small A_{zz} values (see table S-2). Therefore the rows of table S-41 have a grayscale filling according to their A_{zz} value with smaller values being brighter and larger values being darker.

Table S-41: Generalized angle β enclosed by the orientations of IPC **1** obtained by TITANIA in the last optimization step of the runs **1-A** and **1-D**. The last column contains the input A_{zz} values. Since the alignment parameters (see table S-2) were generated from random numbers some of the A_{zz} values are much lower than others. This in combination with the artificial error added in setup **1-D** to larger deviations compared to the results of **1-A**. Therefore the grayscale of the rows are used for faster recognition of the respective A_{zz} (brighter: lower value).

			$\beta/^\circ$			
Set	**1-X11**	**1-X17**	**1-X23**	**1-X31**	**1-X39**	$\boldsymbol{A_{zz}}$
set 1	13.754	8.389	4.391	37.700	8.956	6.502e-04
set 2	56.361	24.603	13.036	73.498	52.239	8.426e-05
set 3	45.596	19.352	21.619	31.226	40.387	8.788e-05
set 4	7.884	11.785	12.640	58.093	15.019	4.350e-04
set 5	9.210	15.631	4.966	62.720	18.800	3.411e-04
set 6	7.223	5.349	10.551	57.126	7.043	8.659e-04
set 7	7.014	4.296	6.884	58.397	16.848	8.074e-04
set 8	7.611	5.447	12.093	30.660	17.325	4.177e-04
set 9	62.542	42.149	48.853	103.289	66.291	4.881e-05
set 10	10.053	8.561	5.996	43.642	14.567	7.993e-04
set 11	18.252	15.942	12.937	55.436	10.125	3.255e-04
set 12	18.496	9.949	3.941	39.637	19.294	4.468e-04
set 13	16.268	10.687	8.240	50.801	21.353	3.196e-04
set 14	22.749	27.244	36.312	49.772	27.672	6.600e-05
set 15	13.067	5.993	7.141	53.089	14.881	7.857e-04
set 16	12.608	7.207	11.477	38.565	25.334	4.146e-04
set 17	8.950	7.007	7.185	59.096	10.198	6.562e-04
set 18	6.602	6.626	4.010	40.255	23.232	5.977e-04
set 19	4.636	2.425	8.698	29.789	16.583	8.809e-04
set 20	13.965	7.359	8.405	54.562	14.024	6.492e-04
$\langle\beta\rangle$[a)]	12.648	9.251	8.501	14.399	14.142	
σ	16.649	10.110	8.877	18.626	15.591	

[a)] To separate the impact of the final structure from the variation of the RDCs, the β angle was calculated from the reference structure using the RDC sets of setups **1-A** and **1-D**. The mean angle of all 20 sets (and the respective standard deviation σ) was calculated for the individual set sizes and is reported here.

1-B

Table S-42: Generalized angle β enclosed by the orientations of IPC **1** obtained by TITANIA in the last optimization step of the runs **1-B** (see tables S-9 to S-13) and **1-E** (see tables S-25 to S-29).

	$\boldsymbol{\beta}/^\circ$				
Set	**1-X11**	**1-X17**	**1-X23**	**1-X31**	**1-X39**
set 1	4.969	3.238	10.145	3.410	8.860
set 2	13.312	3.264	9.710	6.011	14.149
set 3	16.851	10.181	5.003	7.905	17.732
set 4	22.522	4.413	7.169	5.435	15.439
set 5	19.989	7.013	3.581	8.476	13.816
set 6	11.654	8.756	4.523	11.833	5.536
$\langle\beta\rangle$[a)]	2.826	2.347	2.068	3.334	4.802
σ	0.961	0.863	0.516	1.371	1.628

[a)] To separate the impact of the final structure from the variation of the RDCs, the β angle was calculated from the reference structure using the RDC sets of setups **1-B** and **1-E**. The mean angle of all 6 sets (and the respective standard deviation σ) was calculated for the individual set sizes and is reported here.

1-C

Table S-43: Generalized angle β enclosed by the orientations of IPC **1** obtained by TITANIA in the last optimization step of the runs **1-C** (see tables S-15 to S-19) and **1-F** (see tables S-30 to S-34).

	$\boldsymbol{\beta}/^\circ$				
Set	**1-X11**	**1-X17**	**1-X23**	**1-X31**	**1-X39**
set 1	39.620	37.102	101.492	60.392	58.817
set 2	57.278	40.919	105.975	63.705	62.843
set 7	37.742	41.943	114.199	64.808	63.499
set 8	49.962	49.684	102.378	64.122	58.861
set 9	59.757	44.155	102.100	61.099	59.238
set 10	54.290	38.990	104.644	62.866	58.941
$\langle\beta\rangle$[a)]	3.329	2.416	2.070	2.868	4.384
σ	1.279	0.775	0.613	0.732	0.770

[a)] To separate the impact of the final structure from the variation of the RDCs, the β angle was calculated from the reference structure using the RDC sets of setups **1-C** and **1-F**. The mean angle of all 6 sets (and the respective standard deviation σ) was calculated for the individual set sizes and is reported here.

2.3 Random coordinates structure

2.3.1 Keyword adjustments

The runs using random coordinates as input structure were adjusted by the TITANIA keywords as follows:

Table S-44: Keywords for the standard IPC runs (using redundant internal coordinates, **stan**) that changed when using random coordinates as input (**rnd #**). Some keywords had to be adjusted for the individual runs to achieve convergence. This is especially true for the damping constants (see **rnd 3** and **4**) and the convergence threshold (**rnd 2**).

Keyword	**stan**	**rnd 1**	**rnd 2**	**rnd 3**	**rnd 4**
`useInitialHolonomics`	1	0	0	0	0
`MaxTITANIAiterations`	200	1000	1000	1000	1000
`overoptimizationsteps`	10	0	0	0	0
`MeanAlignmentConvergence`	0	1e-6	**1e-5**	1e-6	1e-6
`SigmaAlignmentConvergence`	0	1e-6	1e-6	1e-6	1e-6
`MeanAngleConvergence`	0	1e-3	1e-3	1e-3	1e-3
`SigmaAngleConvergence`	0	1e-3	1e-3	1e-3	1e-3
`SpreadAngleConvergence`	0	1e-5	1e-5	1e-5	1e-5
`useRedundantsOnlyAfter`	10	25	25	25	25
`redundantsDamping`	0	50	50	**5**	**5**
`StaticBondWeighting`	-	2.0	2.0	2.0	**-**
`StaticRDCWeighting`	-	2.0	2.0	2.0	**-**
`floatingRDCangles`	0	1	1	1	1

The change in **rnd 2** was done to prevent instabilities in late iteration steps. When the initial holonomical terms (internal coordinates) cannot be used (no proper initial structure was defined) the MMFF94 equilibrium parameters are used. These do not contain the optimal values for IPC and thereby can lead to instabilities in the late optimization steps. The second changes to the damping / weighting of the redundant internal coordinates (**rnd 3/4**) are due to slow progression in the structure generation overall. Since no proper input structure is used, the structure generation algorithm needs not only to update the coordinates according to RDC information but also to build a chemically meaningful structure. For some structures this was not possible due to high damping constants.

2.3.2 Output orientations

Isopinocampheol run 1-A

Random start coordinates
The orientations when starting from random coordinates are summarized in the tables below. Note that the Euler angles might again be different due to completely different molecular frames as random coordinates are used. An additional change is observed when (+)-IPC is obtained instead of the reference structure ((−)IPC). These differences are addressed in table S-60 (section 2.2.4).

Table S-45: Orientational data of IPC **1** obtained by TITANIA on the last optimization iteration for the runs **1-A11** starting from random coordinates.

Set	$\boldsymbol{A}_{zz}$	$\boldsymbol{R}$	$\boldsymbol{\alpha}/^\circ$	$\boldsymbol{\beta}/^\circ$	$\boldsymbol{\gamma}/^\circ$
set 1	4.839e-04	4.592e-01	118.016	54.440	167.509
set 2	6.072e-05	5.690e-01	36.003	91.575	31.163
set 3	8.278e-05	3.771e-01	89.705	46.222	60.765
set 4	2.986e-04	3.379e-01	167.382	96.818	81.982
set 5	3.295e-04	1.487e-01	125.607	141.502	74.481
set 6	7.976e-04	3.053e-01	82.157	115.741	151.396
set 7	5.172e-04	2.636e-01	40.703	24.521	134.680
set 8	3.827e-04	3.915e-01	125.158	74.802	69.539
set 9	4.189e-05	2.190e-01	50.612	101.735	124.954
set 10	-6.537e-04	6.091e-01	39.394	40.145	41.577
set 11	3.437e-04	5.113e-01	101.841	79.313	111.505
set 12	-3.720e-04	1.885e-01	147.554	72.250	16.675
set 13	-3.539e-04	6.249e-01	119.260	159.058	154.246
set 14	-5.881e-05	5.639e-01	82.922	150.163	136.916
set 15	5.238e-04	3.291e-02	22.832	49.074	159.015
set 16	3.679e-04	5.108e-01	93.376	48.331	16.745
set 17	5.279e-04	2.085e-01	77.281	91.186	99.244
set 18	4.404e-04	5.078e-01	106.080	20.323	34.049
set 19	8.224e-04	5.358e-02	159.485	60.825	54.351
set 20	-6.506e-04	4.306e-01	81.562	141.746	126.907

Table S-46: Orientational data of IPC **1** obtained by TITANIA on the last optimization iteration of run **1-A17** starting from random coordinates.

Set	$\boldsymbol{A}_{zz}$	$\boldsymbol{R}$	$\boldsymbol{\alpha}/^\circ$	$\boldsymbol{\beta}/^\circ$	$\boldsymbol{\gamma}/^\circ$
set 1	6.954e-04	2.925e-01	55.852	45.461	92.973
set 2	7.192e-05	3.067e-01	63.428	87.206	49.690
set 3	8.369e-05	3.467e-01	88.792	136.879	32.374
set 4	4.394e-04	5.280e-01	76.282	128.625	113.355
set 5	3.096e-04	4.440e-01	83.525	140.058	165.625
set 6	8.205e-04	3.652e-01	100.024	84.337	171.141
set 7	7.679e-04	6.009e-02	85.965	24.599	123.780
set 8	4.368e-04	2.228e-01	55.951	118.123	82.199
set 9	4.315e-05	3.677e-01	127.728	99.390	148.306
set 10	8.236e-04	5.626e-01	62.944	52.580	94.645
set 11	2.988e-04	8.436e-02	91.269	102.299	116.056
set 12	3.924e-04	4.363e-01	18.298	138.857	140.021
set 13	2.906e-04	1.559e-01	10.538	80.777	109.112
set 14	6.557e-05	2.034e-01	153.116	55.799	101.029
set 15	8.246e-04	9.017e-02	79.230	38.832	103.451
set 16	4.197e-04	4.848e-01	60.351	117.667	18.093
set 17	6.405e-04	5.571e-01	99.292	118.392	121.652
set 18	5.426e-04	3.757e-01	175.003	34.915	174.085
set 19	9.052e-04	2.190e-01	68.135	123.906	59.326
set 20	6.510e-04	5.326e-01	151.801	49.558	100.747

Table S-47: Orientational data of IPC **1** obtained by TITANIA on the last optimization iteration of run **1-A23** starting from random coordinates.

Set	$\boldsymbol{A}_{zz}$	$\boldsymbol{R}$	$\boldsymbol{\alpha}/^\circ$	$\boldsymbol{\beta}/^\circ$	$\boldsymbol{\gamma}/^\circ$
set 1	6.033e-04	2.867e-01	99.829	92.800	172.167
set 2	5.710e-05	3.844e-01	47.847	49.606	30.652
set 3	7.409e-05	3.771e-01	171.832	25.581	127.866
set 4	3.917e-04	5.529e-01	31.508	148.272	88.814
set 5	2.641e-04	4.018e-01	31.760	115.606	54.323
set 6	6.652e-04	4.241e-01	41.383	78.696	96.816
set 7	6.525e-04	1.111e-01	62.783	62.530	165.362
set 8	4.005e-04	2.210e-01	83.485	162.710	138.647
set 9	3.439e-05	3.918e-01	10.578	103.737	100.210
set 10	7.593e-04	5.503e-01	94.367	99.391	169.314
set 11	2.654e-04	1.425e-01	50.969	131.943	125.173
set 12	3.195e-04	2.656e-01	97.557	132.151	63.327
set 13	2.704e-04	8.378e-02	133.997	119.266	146.055
set 14	5.835e-05	1.896e-01	6.372	101.064	162.659
set 15	6.978e-04	1.381e-01	68.681	83.013	167.492
set 16	3.333e-04	5.258e-01	0.205	43.602	99.840
set 17	5.499e-04	5.853e-01	25.915	138.686	101.145
set 18	5.014e-04	4.104e-01	112.684	48.102	140.910
set 19	7.785e-04	2.432e-01	28.363	6.408	54.599
set 20	5.526e-04	5.397e-01	4.534	95.004	164.913

Table S-48: Orientational data of IPC **1** obtained by TITANIA on the last optimization iteration of run **1-A31** starting from random coordinates.

Set	$\boldsymbol{A}_{zz}$	$\boldsymbol{R}$	$\boldsymbol{\alpha}/^\circ$	$\boldsymbol{\beta}/^\circ$	$\boldsymbol{\gamma}/^\circ$
set 1	5.816e-04	2.622e-01	128.497	140.473	127.589
set 2	6.657e-05	3.357e-01	109.515	86.475	120.877
set 3	7.503e-05	3.132e-01	163.076	40.204	79.321
set 4	4.083e-04	5.320e-01	99.437	89.367	48.098
set 5	2.866e-04	4.141e-01	78.630	85.431	10.624
set 6	7.250e-04	4.594e-01	108.136	42.574	172.090
set 7	7.079e-04	7.607e-02	149.386	24.014	1.585
set 8	3.996e-04	2.401e-01	86.601	84.302	74.384
set 9	3.837e-05	3.540e-01	124.136	126.470	25.324
set 10	7.200e-04	5.582e-01	126.070	137.606	115.109
set 11	2.834e-04	1.036e-01	119.228	114.256	61.285
set 12	3.610e-04	3.491e-01	21.212	85.312	27.877
set 13	2.799e-04	9.792e-02	32.208	127.620	79.352
set 14	5.843e-05	2.693e-01	24.481	140.351	109.510
set 15	7.053e-04	1.168e-01	175.364	150.632	138.425
set 16	3.401e-04	4.516e-01	112.591	39.681	118.886
set 17	5.858e-04	5.259e-01	116.788	101.720	48.082
set 18	5.262e-04	4.133e-01	124.178	18.500	63.275
set 19	7.706e-04	1.749e-01	108.004	66.201	82.070
set 20	5.686e-04	6.139e-01	36.801	144.694	120.895

Table S-49: Orientational data of IPC **1** obtained by TITANIA on the last optimization iteration of run **1-A39** starting from random coordinates.

Set	$\boldsymbol{A}_{zz}$	$\boldsymbol{R}$	$\boldsymbol{\alpha}/^\circ$	$\boldsymbol{\beta}/^\circ$	$\boldsymbol{\gamma}/^\circ$
set 1	5.891e-04	2.767e-01	124.469	95.506	94.653
set 2	7.370e-05	3.083e-01	146.883	121.502	144.053
set 3	8.000e-05	3.692e-01	9.604	41.840	41.012
set 4	3.734e-04	6.173e-01	29.536	162.189	5.752
set 5	3.042e-04	3.889e-01	159.437	54.078	149.638
set 6	7.730e-04	4.809e-01	40.553	95.076	18.405
set 7	7.396e-04	4.554e-02	125.614	65.652	80.895
set 8	3.975e-04	2.062e-01	161.735	163.330	127.964
set 9	4.088e-05	3.344e-01	14.808	118.521	23.686
set 10	7.327e-04	5.647e-01	112.000	104.634	93.147
set 11	2.841e-04	1.503e-01	60.778	142.216	58.064
set 12	3.699e-04	3.622e-01	96.588	36.266	154.075
set 13	2.937e-04	7.459e-02	171.093	127.724	75.773
set 14	6.029e-05	2.910e-01	18.774	106.474	87.298
set 15	7.092e-04	2.583e-02	98.649	85.551	86.981
set 16	3.625e-04	4.759e-01	6.220	61.131	20.463
set 17	5.491e-04	6.128e-01	32.972	150.627	27.701
set 18	5.574e-04	4.539e-01	130.699	59.096	57.961
set 19	7.986e-04	1.237e-01	178.354	24.726	2.195
set 20	5.839e-04	6.620e-01	18.101	97.941	87.799

Isopinocampheol run 1-B

Random start coordinates

The the orientations when starting from random coordinates are summarized in the tables below. Note that the Euler angles might again be different due to completely different molecular frames as random coordinates are used. An additional change is observed when (+)-IPC is obtained instead of the reference structure ((−)IPC). These differences are addressed in table S-61 (section 2.2.4).

Table S-50: Orientational data of IPC **1** obtained by TITANIA on the last optimization iteration for the runs **1-B11** starting from random coordinates.

Set	$\boldsymbol{A}_{zz}$	$\boldsymbol{R}$	$\boldsymbol{\alpha}/^\circ$	$\boldsymbol{\beta}/^\circ$	$\boldsymbol{\gamma}/^\circ$
set 1	8.761e-04	1.028e-01	147.085	100.577	114.383
set 2	1.070e-03	3.061e-01	87.256	105.065	94.030
set 3	-1.620e-03	3.932e-01	104.900	91.068	62.665
set 4	7.724e-04	5.369e-01	171.971	155.873	165.391
set 5	-6.737e-04	4.671e-01	119.095	83.488	81.372
set 6	-1.028e-03	4.308e-01	35.464	95.488	48.392

Table S-51: Orientational data of IPC **1** obtained by TITANIA on the last optimization iteration of run **1-B17** starting from random coordinates.

Set	$\boldsymbol{A}_{zz}$	$\boldsymbol{R}$	$\boldsymbol{\alpha}/^\circ$	$\boldsymbol{\beta}/^\circ$	$\boldsymbol{\gamma}/^\circ$
set 1	-7.681e-04	4.511e-01	52.180	79.659	137.478
set 2	8.362e-04	5.444e-01	1.126	149.778	38.602
set 3	-1.536e-03	3.932e-01	99.348	57.215	177.915
set 4	6.410e-04	6.529e-01	99.700	37.107	8.100
set 5	6.322e-04	5.876e-01	76.542	37.249	35.177
set 6	-8.246e-04	3.698e-01	22.922	54.446	160.331

Table S-52: Orientational data of IPC **1** obtained by TITANIA on the last optimization iteration of run **1-B23** starting from random coordinates.

Set	$\boldsymbol{A}_{zz}$	$\boldsymbol{R}$	$\boldsymbol{\alpha}/^\circ$	$\boldsymbol{\beta}/^\circ$	$\boldsymbol{\gamma}/^\circ$
set 1	-7.930e-04	3.734e-01	5.657	67.226	174.047
set 2	8.394e-04	5.928e-01	23.021	99.508	75.947
set 3	1.412e-03	6.666e-01	73.765	38.931	65.043
set 4	6.853e-04	4.852e-01	90.762	36.795	67.020
set 5	7.149e-04	3.957e-01	104.323	38.666	48.798
set 6	-7.124e-04	1.450e-01	7.410	114.197	32.245

Table S-53: Orientational data of IPC **1** obtained by TITANIA on the last optimization iteration of run **1-B31** starting from random coordinates.

Set	$\boldsymbol{A}_{zz}$	$\boldsymbol{R}$	$\boldsymbol{\alpha}/^\circ$	$\boldsymbol{\beta}/^\circ$	$\boldsymbol{\gamma}/^\circ$
set 1	-7.388e-04	4.551e-01	173.016	104.800	66.725
set 2	8.174e-04	5.442e-01	17.093	103.766	148.573
set 3	-1.362e-03	4.058e-01	120.420	91.006	107.575
set 4	5.493e-04	6.586e-01	9.564	35.637	26.572
set 5	5.732e-04	5.565e-01	16.734	17.548	15.394
set 6	-6.977e-04	3.266e-01	28.779	103.340	100.809

Table S-54: Orientational data of IPC **1** obtained by TITANIA on the last optimization iteration of run **1-B39** starting from random coordinates.

Set	$\boldsymbol{A}_{zz}$	$\boldsymbol{R}$	$\boldsymbol{\alpha}/^\circ$	$\boldsymbol{\beta}/^\circ$	$\boldsymbol{\gamma}/^\circ$
set 1	-7.563e-04	4.713e-01	37.021	109.846	128.910
set 2	8.074e-04	5.659e-01	149.439	115.065	16.169
set 3	-1.246e-03	4.302e-01	162.465	75.020	149.525
set 4	5.184e-04	6.173e-01	33.891	74.574	60.898
set 5	5.356e-04	5.123e-01	35.672	59.957	48.165
set 6	-6.684e-04	3.549e-01	64.153	89.393	152.698

Isopinocampheol run 1-C

Random start coordinates

The the orientations when starting from random coordinates are summarized in the tables below. Note that the Euler angles might again be different due to completely different molecular frames as random coordinates are used. An additional change is observed when (+)-IPC is obtained instead of the reference structure ((−)IPC). These differences are addressed in table S-62 (section 2.2.4).

Table S-55: Orientational data of IPC **1** obtained by TITANIA on the last optimization iteration for the runs **1-C11** starting from random coordinates.

Set	$\boldsymbol{A}_{zz}$	$\boldsymbol{R}$	$\boldsymbol{\alpha}/^\circ$	$\boldsymbol{\beta}/^\circ$	$\boldsymbol{\gamma}/^\circ$
set 1	-8.138e-04	5.915e-01	154.862	100.130	157.192
set 2	1.164e-03	3.456e-01	177.718	73.079	78.584
set 7	-5.766e-04	3.076e-01	146.160	110.585	142.667
set 8	1.286e-03	3.201e-01	2.008	75.336	79.152
set 9	1.339e-03	2.998e-01	1.006	73.883	77.707
set 10	1.133e-03	3.579e-01	177.227	72.971	78.373

Table S-56: Orientational data of IPC **1** obtained by TITANIA on the last optimization iteration of run **1-C17** starting from random coordinates.

Set	$\boldsymbol{A}_{zz}$	$\boldsymbol{R}$	$\boldsymbol{\alpha}/^\circ$	$\boldsymbol{\beta}/^\circ$	$\boldsymbol{\gamma}/^\circ$
set 1	-7.702e-04	4.737e-01	64.511	81.273	130.223
set 2	9.101e-04	5.175e-01	36.811	140.863	71.257
set 7	-6.302e-04	6.271e-01	58.117	88.763	116.314
set 8	9.454e-04	5.545e-01	38.761	137.280	73.684
set 9	9.951e-04	5.617e-01	43.329	139.714	73.651
set 10	8.845e-04	5.322e-01	35.748	141.047	70.758

Table S-57: Orientational data of IPC **1** obtained by TITANIA on the last optimization iteration of run **1-C23** starting from random coordinates.

Set	$\boldsymbol{A}_{zz}$	$\boldsymbol{R}$	$\boldsymbol{\alpha}/^\circ$	$\boldsymbol{\beta}/^\circ$	$\boldsymbol{\gamma}/^\circ$
set 1	-7.716e-04	3.711e-01	49.994	71.696	124.149
set 2	8.494e-04	5.940e-01	43.828	134.097	71.188
set 7	-6.154e-04	5.683e-01	45.892	78.545	112.278
set 8	8.794e-04	6.532e-01	44.086	130.952	72.765
set 9	-9.314e-04	6.665e-01	54.650	56.982	125.656
set 10	8.252e-04	6.120e-01	42.917	134.094	70.534

Table S-58: Orientational data of IPC **1** obtained by TITANIA on the last optimization iteration of run **1-C31** starting from random coordinates.

Set	$\boldsymbol{A}_{zz}$	$\boldsymbol{R}$	$\boldsymbol{\alpha}/^\circ$	$\boldsymbol{\beta}/^\circ$	$\boldsymbol{\gamma}/^\circ$
set 1	-7.127e-04	4.347e-01	66.768	93.187	144.325
set 2	7.422e-04	6.212e-01	17.020	151.744	71.691
set 7	-5.896e-04	6.126e-01	56.044	100.473	132.928
set 8	-7.607e-04	6.520e-01	60.696	79.329	148.973
set 9	-8.116e-04	6.491e-01	63.640	78.859	144.652
set 10	7.235e-04	6.365e-01	15.911	151.761	70.907

Table S-59: Orientational data of IPC **1** obtained by TITANIA on the last optimization iteration of run **1-C39** starting from random coordinates.

Set	$\boldsymbol{A}_{zz}$	$\boldsymbol{R}$	$\boldsymbol{\alpha}/^\circ$	$\boldsymbol{\beta}/^\circ$	$\boldsymbol{\gamma}/^\circ$
set 1	-7.491e-04	4.611e-01	57.038	105.795	168.339
set 2	8.255e-04	5.360e-01	163.157	153.147	71.950
set 7	-6.307e-04	6.278e-01	66.413	119.704	169.448
set 8	8.396e-04	5.873e-01	170.099	155.721	78.907
set 9	8.940e-04	5.913e-01	163.086	153.570	76.169
set 10	8.035e-04	5.522e-01	162.967	153.085	71.148

2.3.3 Change in Orientation

1-A

Table S-60: Generalized angle β enclosed by the reference structure of IPC and the structure obtained by TITANIA from the last optimization step of the runs **1-A** using random start coordinates. The data were obtained by transformation of the respective structures to a common reference frame, followed by recalculating the alignment tensors with the in-house software `RDC@hotFCHT`.[9]

	$\beta/^\circ$				
Set	**1-A11**	**1-A17**	**1-A23**	**1-A31**	**1-A39**
set 1	54.278	3.333	2.103	8.992	2.518
set 2	33.157	7.799	3.040	5.246	0.623
set 3	44.832	5.824	7.441	7.603	1.603
set 4	67.560	3.752	5.225	3.246	2.627
set 5	114.715	6.124	2.802	4.747	2.401
set 6	17.816	9.912	5.349	7.789	0.994
set 7	39.553	11.291	6.148	6.288	2.845
set 8	15.250	7.295	4.019	3.667	2.447
set 9	12.462	9.949	4.959	6.350	2.163
set 10	54.355	2.660	4.665	8.359	1.921
set 11	46.911	8.392	4.098	4.104	2.232
set 12	48.198	6.275	3.873	2.715	2.152
set 13	84.427	4.763	2.814	6.104	1.421
set 14	107.470	4.669	3.671	7.301	3.134
set 15	72.467	6.875	2.946	7.378	3.417
set 16	18.298	6.513	6.743	10.020	1.128
set 17	21.621	8.970	4.400	4.014	3.573
set 18	26.787	7.159	5.825	7.009	2.015
set 19	16.181	7.160	5.214	6.231	1.532
set 20	97.894	6.811	3.671	6.642	3.426

The β angles of **1-A17** to **1-A39** enclosed by the alignment tensors obtained from the two structures (TITANIA optimized and reference) in a common frame are comparable to those reported in table S-35 (C3 epimer starting structure). The small differences are due to structural changes elicited by experimental errors and the change of holonomic terms. The standard approach is to extract them from the input structure. This is not possible for random coordinates.

1-B

Table S-61: Generalized angle β enclosed by the reference structure of IPC and the structure obtained by TITANIA from the last optimization step of the runs **1-B** using random start coordinates. The data were obtained by transformation of the respective structures to a common reference frame, followed by recalculating the alignment tensors with the in-house software `RDC@hotFCHT`.[9]

	$\boldsymbol{\beta}/^\circ$				
Set	**1-B11**	**1-B17**	**1-B23**	**1-B31**	**1-B39**
set 1	81.835	5.163	15.189	5.888	7.866
set 2	73.678	6.842	20.081	5.335	7.010
set 3	76.385	4.555	27.076	2.144	6.420
set 4	82.391	3.093	37.250	2.605	4.194
set 5	94.694	4.626	32.549	1.936	4.072
set 6	48.408	5.425	20.847	3.985	9.193

As in **1-A11** the example **1-B11** shows large differences (large β angles) when using 11 RDCs. In addition **1-B23** shows large β angles since the inverse C2-C10 RDC vector is found for the final structure. The β angles of all other runs originate from the use of different holonomic terms (see above).

1-C

Table S-62: Generalized angle β enclosed by the reference structure of IPC and the structure obtained by TITANIA from the last optimization step of the runs **1-C** using random start coordinates. The data were obtained by transformation of the respective structures to a common reference frame, followed by recalculating the alignment tensors with the in-house software `RDC@hotFCHT`.[9]

	$\boldsymbol{\beta}/^\circ$				
Set	**1-C11**	**1-C17**	**1-C23**	**1-C31**	**1-C39**
set 1	46.844	8.346	14.694	3.082	8.199
set 2	84.687	7.423	15.061	3.329	8.165
set 7	41.721	6.795	10.885	3.281	8.517
set 8	84.353	7.065	12.458	3.510	8.208
set 9	86.778	6.977	20.640	3.813	8.081
set 10	83.159	7.470	14.322	3.213	8.183

As before run **1-C11** shows large differences (large β angles) when using 11 RDCs. In addition **1-C23** shows large β angles, for the same reason as in **1-B23**. The inverse C2-C10 RDC vector is found for the final structure. The β angles of all other runs originate from the use of different holonomic terms (see above).

2.3.4 Optimization Trajectories

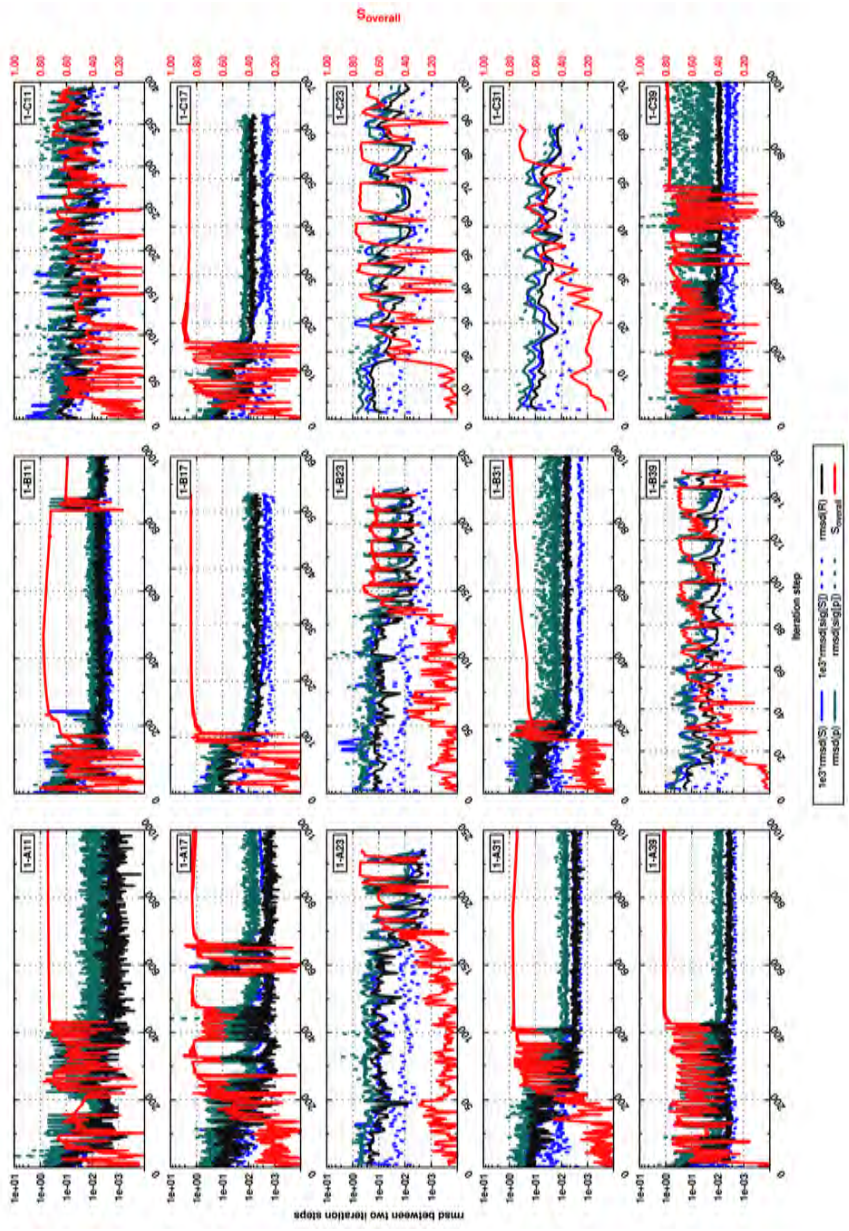

Figure S-14: Trajectory of the Monte-Carlo *rmsd*s obtained for the individual runs of the setups **1-A**, **B** and **C**. Shown are the data obtained by the default redundant internal coordinates algorithm starting from random coordinates.

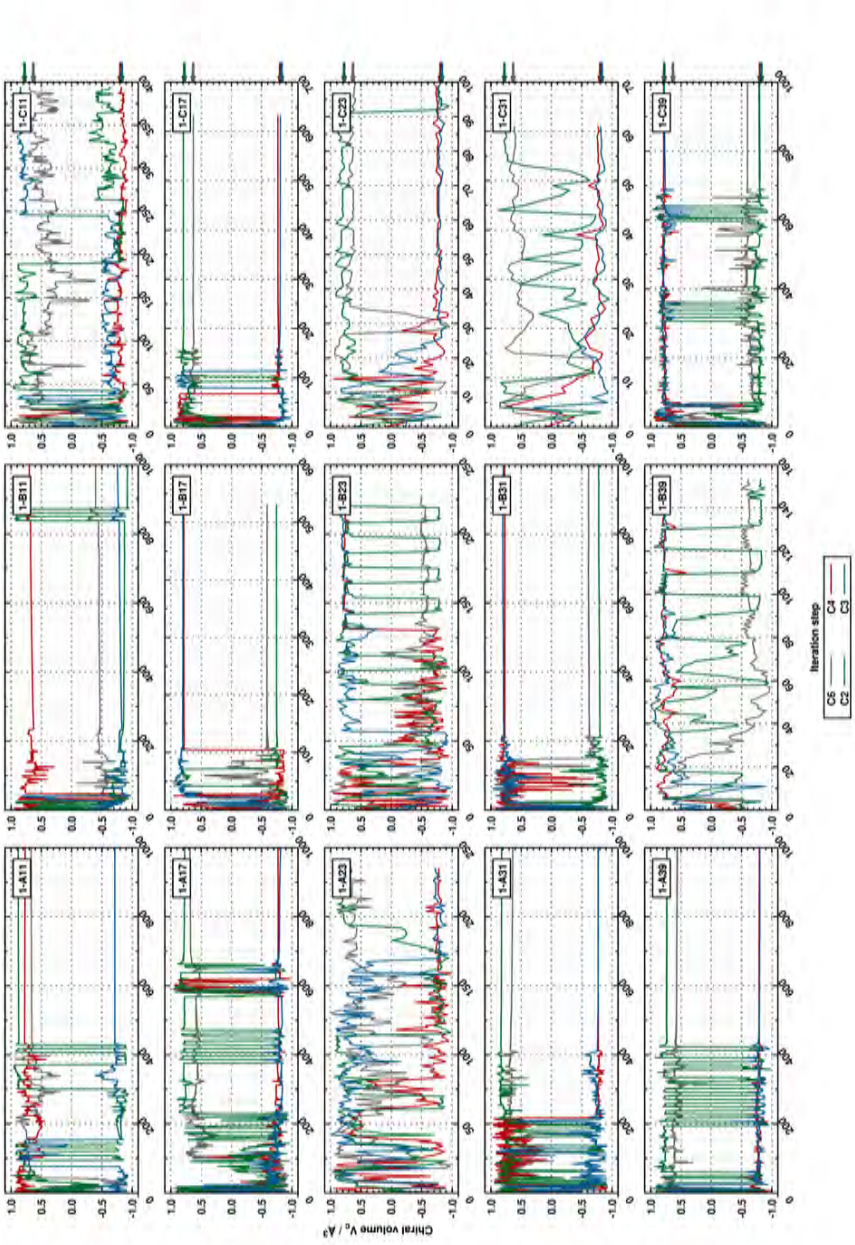

Figure S-15: Trajectory of the normalized chiral volumes obtained for the individual runs of the setups **1-A**, **B** and **C**. Shown are the data obtained by the default redundant internal coordinates algorithm starting from random coordinates. The arrows at the top indicate the values of the reference structure (correct configuration). Note that in contrast to the runs starting from the C3 epimer also the enantiomeric solution is obtained (**1-B17**, **31**, **39** and **1-C39**).

As before none of the runs with 11 RDCs converges to the correct relative configuration in all cases. This behavior is discussed in the main text. The two runs **1-B23** and **1-B39** do not show a stable configuration on C2 and the final structure has the wrong configuration at this center. **1-B23** can easily be recognized as inverse vector solution (see fig. S-16).

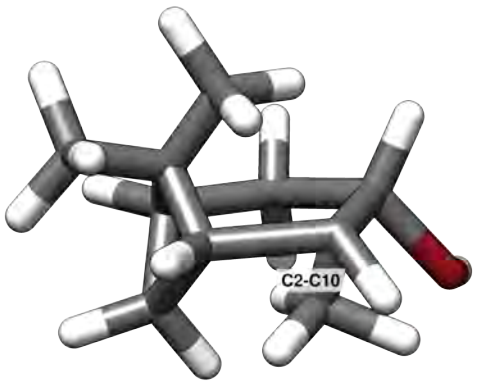

Figure S-16: Final 3D structure for the run **1-B23**. The C2-C10 bond is represented by the inverse RDC solution. This can be identified with some basic chemistry knowledge.

The wrong configuration of **1-B39** can be identified by the very short C2-C10 bond (1.13Å). Both structures were rerun while forcing 1 000 iteration steps, ending in a stable trajectory with the correct relative configuration.

2.4 Vector addition algorithm

2.4.1 Output orientations

Isopinocampheol run 1-D

Structure generation *via* vector addition
Additionally to the redundant internal coordinates algorithm the optimization was performed using the non-default vector addition algorithm. The orientations obtained are summarized in the tables below. Changes of the Euler angles compared to the literature data listed above are due to the change of the initial reference frames (TITANIA used the principle axis system of the molecule) and the added errors. These differences are addressed in table S-78 (section 2.4.2).

Table S-63: Orientational data of IPC **1** obtained by TITANIA on the last optimization iteration for the run **1-D11** when using the non-default vector addition algorithm.

Set	$\boldsymbol{A}_{zz}$	$\boldsymbol{R}$	$\boldsymbol{\alpha}/^\circ$	$\boldsymbol{\beta}/^\circ$	$\boldsymbol{\gamma}/^\circ$
set 1	5.373e-04	2.042e-01	174.491	39.947	75.871
set 2	1.038e-04	2.681e-01	133.318	75.386	133.293
set 3	-1.221e-04	3.855e-01	23.708	87.733	109.974
set 4	-5.633e-04	1.638e-01	105.955	44.595	30.299
set 5	2.840e-04	6.189e-01	144.284	97.006	97.110
set 6	9.636e-04	4.520e-01	156.527	143.191	152.451
set 7	9.946e-04	1.361e-01	39.369	62.490	52.623
set 8	-4.378e-04	6.335e-01	54.994	42.280	33.234
set 9	-8.343e-05	6.136e-01	142.655	138.007	16.961
set 10	7.712e-04	1.712e-01	134.452	13.446	108.690
set 11	3.913e-04	3.432e-01	81.937	150.351	32.083
set 12	4.075e-04	4.888e-01	152.925	119.223	73.971
set 13	3.653e-04	1.550e-01	27.367	155.243	0.254
set 14	9.404e-05	2.873e-01	36.080	27.308	174.843
set 15	8.313e-04	1.613e-01	174.945	48.744	55.599
set 16	4.463e-04	1.898e-01	112.773	116.491	170.623
set 17	-8.387e-04	4.194e-01	92.152	54.816	43.156
set 18	7.629e-04	4.672e-01	45.210	62.128	36.137
set 19	7.171e-04	5.343e-01	105.610	77.381	169.026
set 20	-5.477e-04	4.438e-01	110.761	121.855	117.043

Table S-64: Orientational data of IPC **1** obtained by TITANIA on the last optimization iteration of run **1-D17** when using the non-default vector addition algorithm.

Set	$\boldsymbol{A}_{zz}$	$\boldsymbol{R}$	$\boldsymbol{\alpha}/^\circ$	$\boldsymbol{\beta}/^\circ$	$\boldsymbol{\gamma}/^\circ$
set 1	5.419e-04	2.683e-01	9.021	36.607	90.171
set 2	9.144e-05	4.008e-01	138.048	80.914	136.202
set 3	-1.167e-04	5.925e-01	158.072	92.805	114.997
set 4	4.143e-04	4.151e-01	88.219	128.259	45.551
set 5	2.706e-04	3.798e-01	145.308	106.148	89.560
set 6	8.609e-04	5.053e-01	170.674	137.355	146.594
set 7	7.984e-04	1.426e-01	28.327	57.799	56.824
set 8	4.434e-04	1.455e-01	80.734	122.264	12.327
set 9	7.443e-05	2.305e-01	124.121	150.843	150.070
set 10	7.200e-04	4.211e-01	10.869	24.973	105.082
set 11	3.641e-04	2.843e-01	25.436	155.844	36.503
set 12	4.131e-04	5.149e-01	8.788	116.895	70.597
set 13	3.238e-04	2.873e-01	17.705	20.404	174.540
set 14	7.652e-05	5.849e-01	85.755	12.407	109.289
set 15	7.089e-04	3.531e-02	5.030	41.847	71.173
set 16	3.885e-04	3.207e-01	150.003	117.563	173.687
set 17	6.435e-04	5.210e-01	77.645	142.149	51.667
set 18	6.205e-04	4.784e-01	45.213	57.659	36.705
set 19	7.955e-04	1.423e-01	70.305	101.398	10.529
set 20	-5.876e-04	4.930e-01	104.722	121.034	114.784

Table S-65: Orientational data of IPC **1** obtained by TITANIA on the last optimization iteration of run **1-D23** when using the non-default vector addition algorithm.

Set	$\boldsymbol{A}_{zz}$	$\boldsymbol{R}$	$\boldsymbol{\alpha}/^\circ$	$\boldsymbol{\beta}/^\circ$	$\boldsymbol{\gamma}/^\circ$
set 1	5.422e-04	2.953e-01	6.547	40.663	93.785
set 2	7.777e-05	3.952e-01	137.781	81.261	141.378
set 3	1.192e-04	5.651e-01	2.096	70.688	22.769
set 4	4.288e-04	3.641e-01	84.188	125.257	40.916
set 5	2.845e-04	3.795e-01	137.694	109.125	82.773
set 6	8.685e-04	4.910e-01	166.888	140.944	138.662
set 7	7.966e-04	1.002e-01	14.489	56.143	52.502
set 8	4.357e-04	1.245e-01	90.698	117.437	9.536
set 9	7.061e-05	3.380e-01	94.943	143.508	128.948
set 10	7.164e-04	5.193e-01	2.455	30.800	109.095
set 11	3.439e-04	2.539e-01	17.640	153.142	29.169
set 12	4.369e-04	4.309e-01	7.727	116.793	65.726
set 13	3.089e-04	1.993e-01	22.045	22.709	163.635
set 14	-8.449e-05	4.659e-01	86.259	104.079	109.945
set 15	7.079e-04	2.872e-02	97.047	41.276	71.833
set 16	3.968e-04	3.593e-01	143.684	120.315	170.488
set 17	6.474e-04	5.077e-01	74.058	139.950	47.386
set 18	6.324e-04	4.819e-01	41.151	56.150	31.643
set 19	8.226e-04	7.408e-02	71.928	96.851	8.674
set 20	-6.087e-04	5.421e-01	100.258	124.743	106.130

Table S-66: Orientational data of IPC **1** obtained by TITANIA on the last optimization iteration of run **1-D31** when using the non-default vector addition algorithm.

Set	$\boldsymbol{A}_{zz}$	$\boldsymbol{R}$	$\boldsymbol{\alpha}/^\circ$	$\boldsymbol{\beta}/^\circ$	$\boldsymbol{\gamma}/^\circ$
set 1	5.808e-04	3.500e-01	152.618	36.719	129.517
set 2	8.500e-05	3.771e-01	84.661	81.637	3.749
set 3	-8.143e-05	3.999e-01	150.775	44.056	152.961
set 4	3.267e-04	5.536e-01	91.801	116.906	80.228
set 5	2.282e-04	2.315e-01	105.807	108.839	105.951
set 6	8.329e-04	5.664e-01	144.445	149.298	164.489
set 7	6.220e-04	5.170e-02	162.979	54.598	105.010
set 8	2.573e-04	4.079e-01	100.349	106.334	41.365
set 9	6.041e-05	1.480e-01	100.168	176.397	45.151
set 10	6.206e-04	4.546e-01	150.536	21.461	145.007
set 11	2.886e-04	2.668e-01	137.185	147.350	63.502
set 12	4.487e-04	3.509e-01	163.675	113.105	97.211
set 13	2.899e-04	3.908e-01	109.262	156.869	13.863
set 14	-7.818e-05	4.865e-01	99.147	112.849	156.148
set 15	7.136e-04	1.681e-01	160.598	41.065	117.970
set 16	3.379e-04	3.937e-01	14.660	58.488	14.345
set 17	5.650e-04	4.201e-01	69.620	131.382	84.382
set 18	-3.220e-04	3.770e-01	52.916	127.830	17.946
set 19	7.162e-04	2.887e-01	90.691	88.466	25.740
set 20	5.993e-04	5.382e-01	98.260	39.378	132.572

Table S-67: Orientational data of IPC **1** obtained by TITANIA on the last optimization iteration of run **1-D39** when using the non-default vector addition algorithm.

Set	$\boldsymbol{A}_{zz}$	$\boldsymbol{R}$	$\boldsymbol{\alpha}/^\circ$	$\boldsymbol{\beta}/^\circ$	$\boldsymbol{\gamma}/^\circ$
set 1	6.537e-04	1.980e-01	176.084	57.511	103.435
set 2	1.168e-04	1.209e-01	131.923	115.122	128.867
set 3	1.329e-04	6.661e-01	21.177	91.627	20.967
set 4	4.322e-04	5.670e-01	64.569	128.320	28.137
set 5	2.641e-04	3.147e-01	110.795	125.524	70.914
set 6	9.346e-04	4.090e-01	171.640	154.657	153.294
set 7	8.031e-04	5.941e-02	176.832	66.736	65.927
set 8	4.661e-04	2.270e-01	91.020	113.544	1.088
set 9	-8.924e-05	2.382e-01	59.742	67.508	47.813
set 10	6.985e-04	5.202e-01	6.170	47.530	108.602
set 11	3.230e-04	1.719e-01	164.057	34.955	178.525
set 12	4.940e-04	1.481e-01	149.735	131.613	61.722
set 13	3.401e-04	2.454e-01	64.761	33.170	129.886
set 14	8.389e-05	4.301e-01	114.177	37.535	90.348
set 15	8.199e-04	1.158e-01	97.962	57.061	86.443
set 16	3.179e-04	6.111e-01	164.189	117.542	175.132
set 17	6.448e-04	5.742e-01	62.558	148.610	46.049
set 18	-5.197e-04	6.493e-01	155.032	65.944	142.232
set 19	9.158e-04	1.450e-01	61.396	96.706	5.354
set 20	-7.089e-04	6.287e-01	96.120	141.355	105.311

Isopinocampheol run 1-E

Structure generation *via* vector addition

Additionally to the redundant internal coordinates algorithm the optimization was performed using the non-default vector addition algorithm. The orientations obtained are summarized in the tables below. Changes of the Euler angles compared to the literature data listed above are due to the change of the initial reference frames (TITANIA used the principle axis system of the molecule) and the added errors. These differences are addressed in table S-79 (section 2.4.2).

Table S-68: Orientational data of IPC **1** obtained by TITANIA on the last optimization iteration for the run **1-E11**.

Set	$\boldsymbol{A}_{zz}$	$\boldsymbol{R}$	$\boldsymbol{\alpha}/^\circ$	$\boldsymbol{\beta}/^\circ$	$\boldsymbol{\gamma}/^\circ$
set 1	-8.045e-04	4.224e-01	96.654	45.307	141.473
set 2	9.842e-04	3.760e-01	102.637	119.671	163.307
set 3	-1.559e-03	4.380e-01	0.144	86.486	141.153
set 4	6.483e-04	5.398e-01	164.882	72.865	55.053
set 5	7.506e-04	5.074e-01	165.107	94.059	51.050
set 6	-8.986e-04	3.824e-01	60.266	78.975	150.058

Table S-69: Orientational data of IPC **1** obtained by TITANIA on the last optimization iteration of run **1-E17**.

Set	$\boldsymbol{A}_{zz}$	$\boldsymbol{R}$	$\boldsymbol{\alpha}/^\circ$	$\boldsymbol{\beta}/^\circ$	$\boldsymbol{\gamma}/^\circ$
set 1	-7.506e-04	4.306e-01	95.625	44.765	138.420
set 2	9.079e-04	4.336e-01	101.463	118.080	164.331
set 3	-1.433e-03	3.668e-01	172.173	83.773	137.762
set 4	6.241e-04	4.948e-01	164.533	65.655	53.280
set 5	6.060e-04	5.223e-01	167.754	84.704	48.102
set 6	-8.748e-04	5.243e-01	59.604	76.589	145.749

Table S-70: Orientational data of IPC **1** obtained by TITANIA on the last optimization iteration of run **1-E23**.

Set	$\boldsymbol{A}_{zz}$	$\boldsymbol{R}$	$\boldsymbol{\alpha}/^\circ$	$\boldsymbol{\beta}/^\circ$	$\boldsymbol{\gamma}/^\circ$
set 1	-7.473e-04	4.975e-01	100.985	42.990	139.459
set 2	9.475e-04	4.088e-01	97.794	116.732	163.104
set 3	-1.476e-03	3.611e-01	168.306	85.335	138.283
set 4	6.407e-04	5.536e-01	166.678	65.822	51.849
set 5	6.173e-04	5.787e-01	169.087	83.561	46.772
set 6	-8.716e-04	4.251e-01	62.549	78.948	149.451

Table S-71: Orientational data of IPC **1** obtained by TITANIA on the last optimization iteration of run **1-E31**.

Set	$\boldsymbol{A}_{zz}$	$\boldsymbol{R}$	$\boldsymbol{\alpha}/^\circ$	$\boldsymbol{\beta}/^\circ$	$\boldsymbol{\gamma}/^\circ$
set 1	-7.730e-04	5.076e-01	105.411	46.667	138.334
set 2	9.805e-04	3.926e-01	104.582	120.649	167.947
set 3	-1.415e-03	3.527e-01	171.479	90.805	139.949
set 4	-5.611e-04	6.561e-01	160.802	109.762	139.541
set 5	5.613e-04	6.531e-01	159.936	90.942	46.574
set 6	-8.536e-04	3.913e-01	69.350	81.978	148.908

Table S-72: Orientational data of IPC **1** obtained by TITANIA on the last optimization iteration of run **1-E39**.

Set	$\boldsymbol{A}_{zz}$	$\boldsymbol{R}$	$\boldsymbol{\alpha}/^\circ$	$\boldsymbol{\beta}/^\circ$	$\boldsymbol{\gamma}/^\circ$
set 1	-7.039e-04	4.508e-01	106.614	54.081	132.169
set 2	8.750e-04	5.101e-01	104.966	126.999	161.873
set 3	-1.280e-03	3.819e-01	173.038	101.759	132.569
set 4	-5.380e-04	5.827e-01	170.093	118.722	130.653
set 5	-5.554e-04	5.716e-01	3.628	117.657	126.624
set 6	-7.847e-04	2.740e-01	82.142	91.507	139.637

Isopinocampheol run 1-F

Structure generation *via* vector addition
Additionally to the redundant internal coordinates algorithm the optimization was performed using the non-default vector addition algorithm. The orientations obtained are summarized in the tables below. Changes of the Euler angles compared to the literature data listed above are due to the change of the initial reference frames (TITANIA used the principle axis system of the molecule) and the added errors. These differences are addressed in table S-80 (section 2.4.2).

Table S-73: Orientational data of IPC **1** obtained by TITANIA on the last optimization iteration for the run **1-F11** when using the non-default vector addition algorithm.

Set	$\boldsymbol{A}_{zz}$	$\boldsymbol{R}$	$\boldsymbol{\alpha}/^\circ$	$\boldsymbol{\beta}/^\circ$	$\boldsymbol{\gamma}/^\circ$
set 1	-7.986e-04	3.230e-01	2.066	137.336	110.782
set 2	1.001e-03	3.944e-01	101.511	87.663	6.560
set 7	-7.037e-04	2.935e-01	166.537	124.515	109.441
set 8	1.025e-03	4.540e-01	73.463	90.888	176.144
set 9	1.028e-03	4.314e-01	69.241	88.352	178.191
set 10	9.506e-04	4.538e-01	106.320	88.585	5.534

Table S-74: Orientational data of IPC **1** obtained by TITANIA on the last optimization iteration of run **1-F17** when using the non-default vector addition algorithm.

Set	$\boldsymbol{A}_{zz}$	$\boldsymbol{R}$	$\boldsymbol{\alpha}/^\circ$	$\boldsymbol{\beta}/^\circ$	$\boldsymbol{\gamma}/^\circ$
set 1	5.172e-04	3.569e-01	100.110	168.760	103.421
set 2	-4.900e-04	6.643e-01	114.304	71.029	126.469
set 7	4.518e-04	3.707e-01	115.334	175.073	82.319
set 8	-6.387e-04	3.458e-01	116.715	66.886	135.240
set 9	-6.327e-04	4.583e-01	108.846	65.639	135.803
set 10	-5.175e-04	5.732e-01	110.411	70.972	127.709

Table S-75: Orientational data of IPC **1** obtained by TITANIA on the last optimization iteration of run **1-F23** when using the non-default vector addition algorithm.

Set	$\boldsymbol{A}_{zz}$	$\boldsymbol{R}$	$\boldsymbol{\alpha}/^\circ$	$\boldsymbol{\beta}/^\circ$	$\boldsymbol{\gamma}/^\circ$
set 1	-7.187e-04	3.226e-01	44.621	30.151	72.340
set 2	8.070e-04	6.100e-01	64.226	105.260	28.398
set 7	-4.776e-04	5.014e-01	80.383	37.385	58.352
set 8	8.589e-04	6.540e-01	67.644	101.645	25.270
set 9	8.942e-04	6.283e-01	68.959	103.619	24.495
set 10	7.606e-04	6.647e-01	65.988	104.884	27.058

Table S-76: Orientational data of IPC **1** obtained by TITANIA on the last optimization iteration of run **1-F31** when using the non-default vector addition algorithm.

Set	$\boldsymbol{A}_{zz}$	$\boldsymbol{R}$	$\boldsymbol{\alpha}/^\circ$	$\boldsymbol{\beta}/^\circ$	$\boldsymbol{\gamma}/^\circ$
set 1	-6.325e-04	1.540e-01	164.453	57.070	135.066
set 2	6.561e-04	4.912e-01	39.950	85.192	31.400
set 7	-4.383e-04	1.960e-01	134.982	69.883	146.908
set 8	6.903e-04	6.131e-01	48.772	89.446	33.466
set 9	6.647e-04	5.898e-01	48.406	85.773	31.000
set 10	6.459e-04	5.499e-01	40.665	86.226	31.143

Table S-77: Orientational data of IPC **1** obtained by TITANIA on the last optimization iteration of run **1-F39** when using the non-default vector addition algorithm.

Set	$\boldsymbol{A}_{zz}$	$\boldsymbol{R}$	$\boldsymbol{\alpha}/^\circ$	$\boldsymbol{\beta}/^\circ$	$\boldsymbol{\gamma}/^\circ$
set 1	-6.493e-04	2.931e-01	83.540	45.197	133.570
set 2	7.685e-04	4.741e-01	107.215	120.702	156.138
set 7	-5.236e-04	3.958e-01	89.022	59.785	145.760
set 8	8.758e-04	4.584e-01	106.274	116.057	156.547
set 9	8.684e-04	4.575e-01	103.184	116.835	158.978
set 10	7.645e-04	5.018e-01	110.056	117.807	159.900

2.4.2 Change in Orientation

1-D

Table S-78: Generalized angle β enclosed by the reference structure of IPC and the structure obtained by TITANIA (using the non-default vector addition algorithm) from the last optimization step of the runs **1-D**. The data were obtained by transformation of the respective structures to a common reference frame, followed by recalculating the alignment tensors with the in-house software `RDC@hotFCHT`.[9]

	$\beta/^\circ$				
Set	**1-D11**	**1-D17**	**1-D23**	**1-D31**	**1-D39**
set 1	30.946	15.144	9.845	9.685	7.362
set 2	50.402	20.464	29.090	20.140	14.040
set 3	33.763	12.271	4.070	25.837	8.092
set 4	39.991	7.758	6.975	15.387	8.185
set 5	15.312	7.121	7.499	13.342	9.721
set 6	17.512	5.726	8.002	25.098	8.446
set 7	24.971	11.795	12.735	36.093	6.718
set 8	41.949	6.681	3.395	14.813	10.582
set 9	60.050	23.234	16.183	56.141	9.593
set 10	38.598	15.734	8.275	19.042	6.990
set 11	22.213	8.194	5.626	23.012	10.864
set 12	17.809	8.714	11.250	17.496	8.847
set 13	12.005	15.378	7.849	23.905	11.418
set 14	23.741	25.161	18.718	24.281	12.408
set 15	38.101	16.293	13.371	15.462	6.005
set 16	18.983	11.337	10.441	8.505	9.386
set 17	37.170	8.983	8.302	12.882	6.654
set 18	17.004	7.385	6.051	29.541	11.212
set 19	44.102	11.605	5.659	12.636	8.456
set 20	13.838	13.730	10.206	19.869	10.911

1-E

Table S-79: Generalized angle β enclosed by the reference structure of IPC and the structure obtained by TITANIA (using the non-default vector addition algorithm) from the last optimization step of the runs **1-E**. The data were obtained by transformation of the respective structures to a common reference frame, followed by recalculating the alignment tensors with the in-house software `RDC@hotFCHT`.[9]

	$\beta/^\circ$				
Set	**1-E11**	**1-E17**	**1-E23**	**1-E31**	**1-E39**
set 1	6.038	10.846	4.915	4.829	12.146
set 2	4.647	11.171	7.822	5.393	8.713
set 3	9.215	9.386	2.881	2.354	15.258
set 4	7.580	5.549	4.465	3.928	17.104
set 5	11.577	3.545	4.774	2.920	11.867
set 6	7.147	11.098	2.417	1.879	16.664

1-F

Table S-80: Generalized angle β enclosed by the reference structure of IPC and the structure obtained by TITANIA (using the non-default vector addition algorithm) from the last optimization step of the runs **1-F**. The data were obtained by transformation of the respective structures to a common reference frame, followed by recalculating the alignment tensors with the in-house software `RDC@hotFCHT`.[9]

	$\beta/^\circ$				
Set	**1-F11**	**1-F17**	**1-F23**	**1-F31**	**1-F39**
set 1	123.585	83.564	81.269	30.297	23.402
set 2	72.325	59.705	80.800	64.861	23.772
set 7	113.151	82.807	99.972	38.546	22.152
set 8	64.246	64.948	73.213	57.898	18.615
set 9	75.126	62.949	80.406	58.654	21.404
set 10	75.531	63.720	78.106	60.904	21.482

As before for the redundant internal coordinates algorithm **1-F** also does not converge when using the non-default vector addition algorithm.

The shown β angles describe the difference of the alignment tensors calculated using the reference structure and the final structure of the TITANIA runs. When comparing the results to the β angles obtained from the redundant internal coordinates algorithm it becomes clear that the angles are

larger for the vector addition algorithms. The reason for this behavior are the missing restraints for the vector addition algorithms. This can lead to a collective motion of the RDC vector orientations as discussed in the main text for run **1-E39**. In such a case the differences in the orientations of the structures compared will always be larger due to structural distortions.

2.4.3 Optimization Trajectories

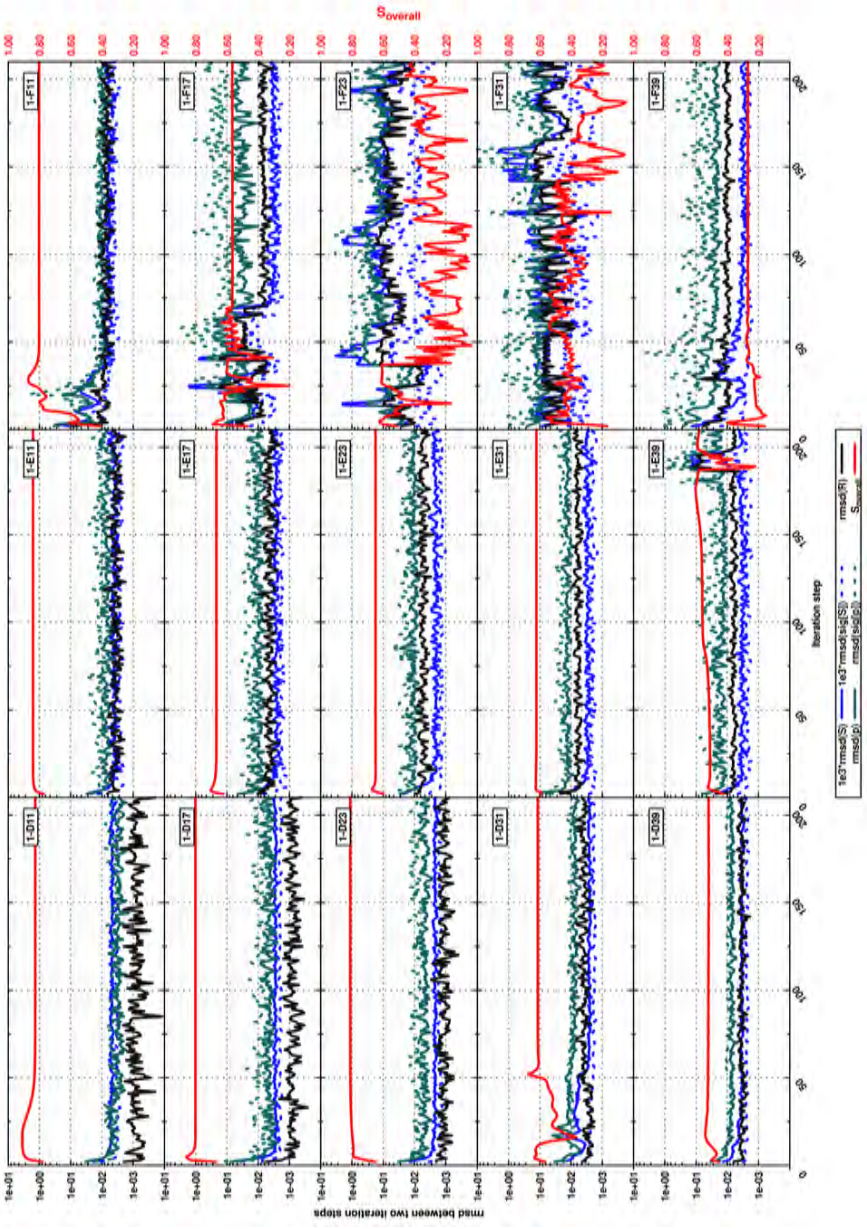

Figure S-17: Trajectory of the Monte-Carlo *rmsd*s obtained for the individual runs of the setups **1-D**, **E** and **F**. Shown are the data obtained by the vector addition algorithm.

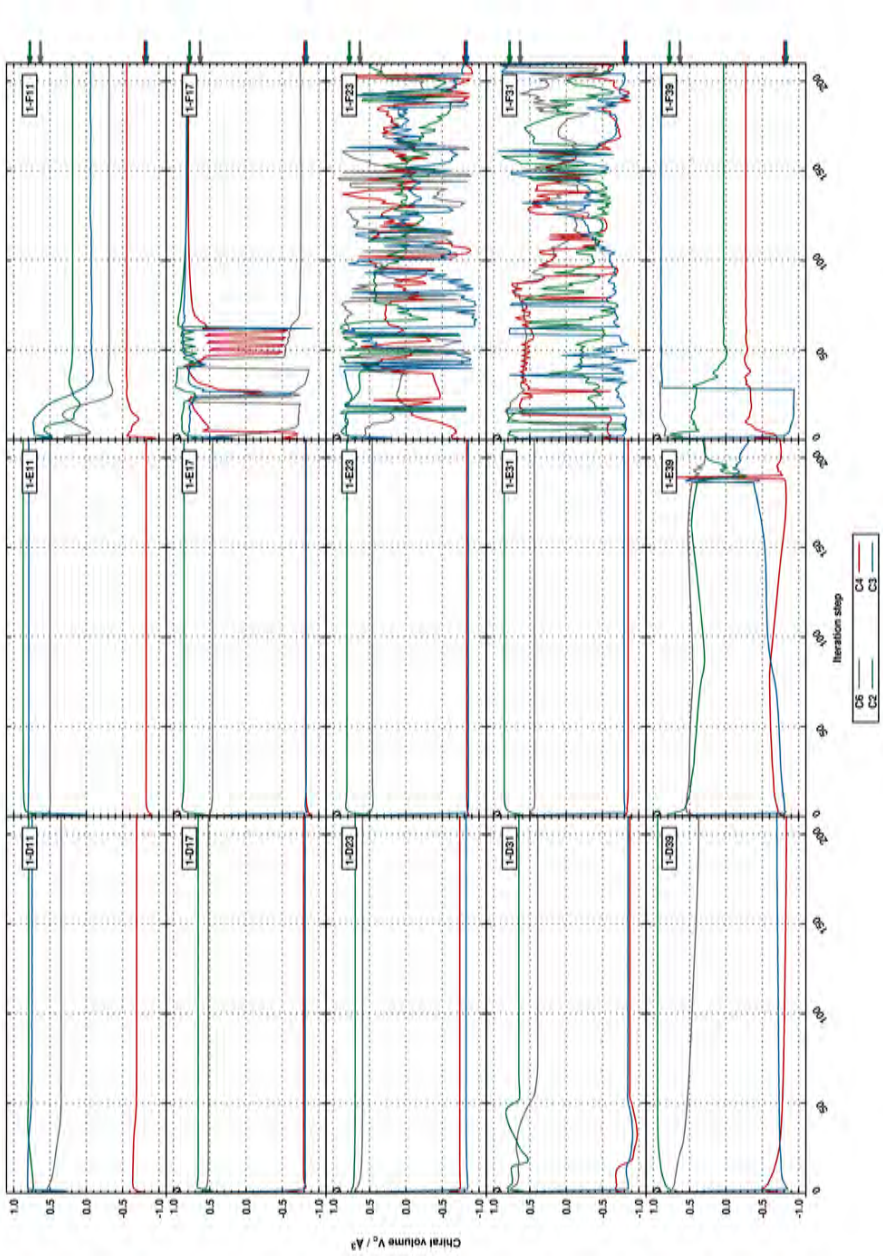

Figure S-18: Trajectory of the normalized chiral volumes obtained for the individual runs of the setups **1-D**, **E** and **F**. Shown are the data obtained by the vector addtion algorithm. The arrows at the top indicate the values of the reference structure (correct configuration).

The vector addition algorithm shows rather smooth trajectories for the setups **1-D** and **1-E**. The reason for this is that only RDC vectors are optimized and the scaffold is retained. In the case of **1-E39** this can lead to a strange behavior, where the RDC vectors show a collective movement around the fixed structure. At some point (around iteration 190) this leads to an instant rearrangement. Still the correct relative configuration was found for this run.

As expected the setup **1-F** does not show convergence. A change of algorithms cannot help if the data quality is not sufficient.

2.5 RDC list

Table S-81: List of all RDCs used in the runs of **1-A**, **B** and **C**.

RDC pair	11 RDCs	17 RDCs	23 RDCs	31 RDCs	39 RDCs
C1-H1	x	x	x	x	x
C2-H2	x	x	x	x	x
C3-H3	x	x	x	x	x
C4-H4a	x	x	x	x	x
C4-H4s	x	x	x	x	x
C5-H5	x	x	x	x	x
C7-H7a	x	x	x	x	x
C7-H7s	x	x	x	x	x
C10-C2	x	x	x	x	x
C6-C8	x	x	x	x	x
C6-C9	x	x	x	x	x
H1-H2		x	x	x	x
H1-H3				x	x
H1-H4a					x
H1-H4s				x	x
H1-H5				x	x
H1-H7a			x		x
H1-H7s		x	x	x	x
H2-H3		x	x	x	x
H2-H4a				x	x
H2-H4s					x
H2-H5					x
H2-H7a					x
H2-H7s				x	x
H3-H4a			x	x	x
H3-H4s		x	x	x	x
H3-H5					x
H3-H7a				x	x
H3-H7s					x
H4a-H4s			x	x	x
H4a-H5			x	x	x
H4a-H7a				x	x
H4a-H7s					x
H4s-H5		x	x	x	x
H4s-H7a				x	x
H4s-H7s				x	x
H5-H7a		x	x	x	x
H5-H7s			x	x	x
H7a-H7s			x	x	x

2.6 Final structures

1-A11

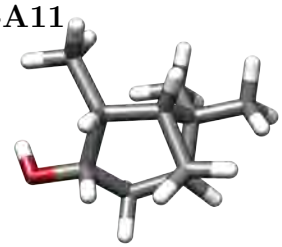

1-B11

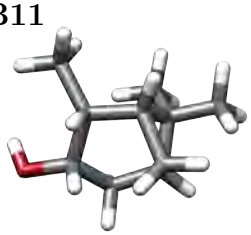

1-C11

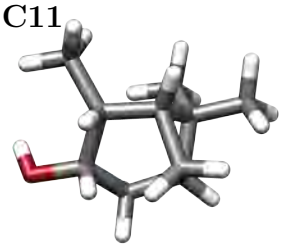

1-A17

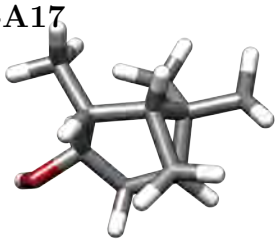

1-B17

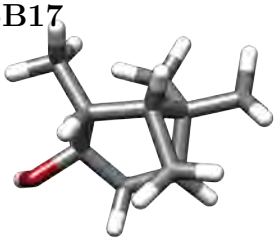

1-C17

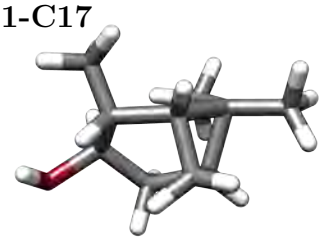

1-A23

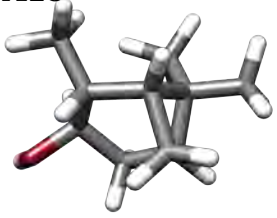

1-B23

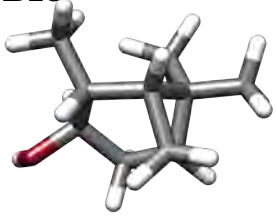

1-C23

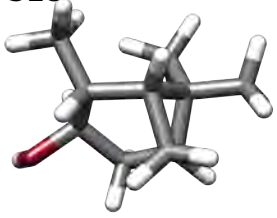

1-A31

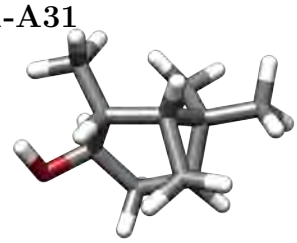

1-B31

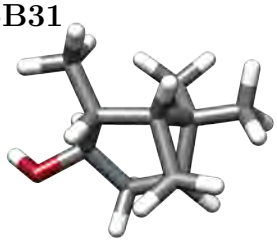

1-C31

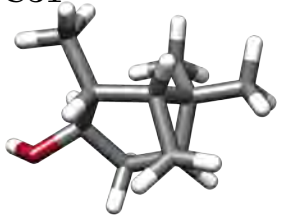

1-A39

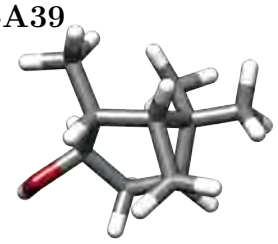

1-B39

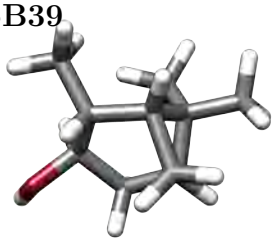

1-C39

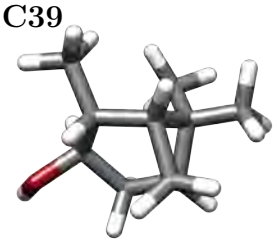

1-D11

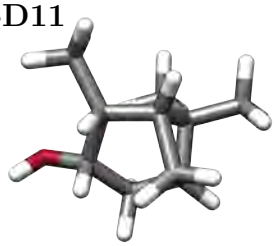

1-E11

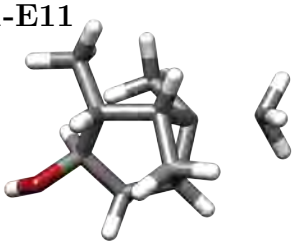

1-F11

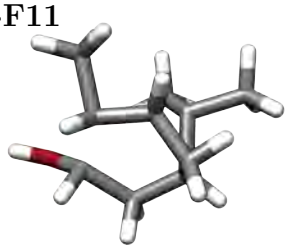

1-D17

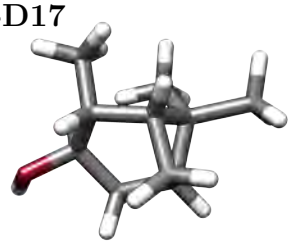

1-E17

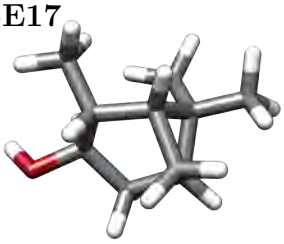

1-F17

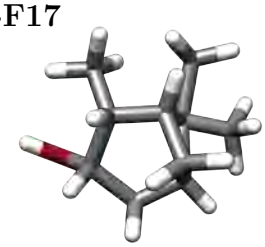

1-D23

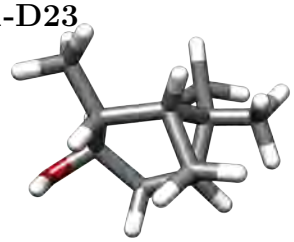

1-E23

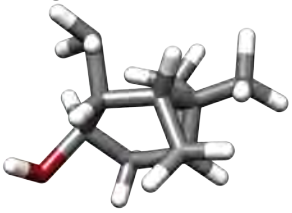

1-F23

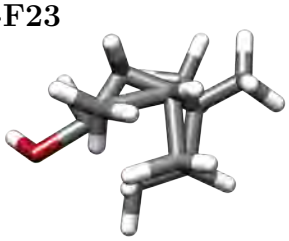

1-D31

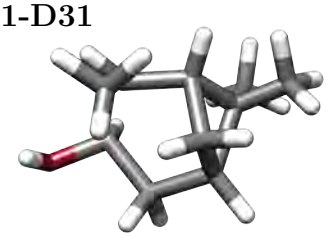

1-E31

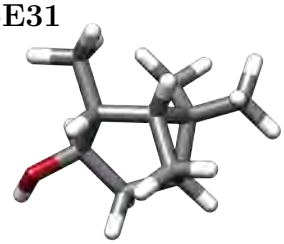

1-F31

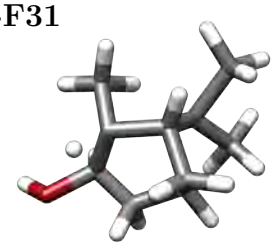

1-D39

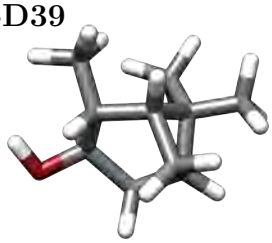

1-E39

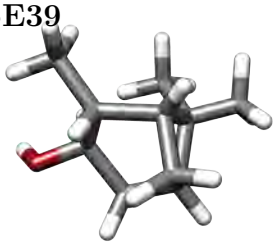

1-F39

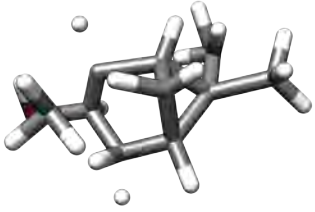

The xyz coordinates of the final structures are all available in the supplementary material.

3 Tubocurarine (2)

Tubocurarine was optimized in two setups, which were built on the same eight randomly generated alignment tensors. The goal was to investigate the possibility of optimizing a rather complex structure with conformational flexibility and to investigate the impact of heterogeneities on the result. Therefore the data will differ from those in section 2. For a better understanding the structure containing all RDCs (in addition to the respective RDC list in section 3.3) is given here.

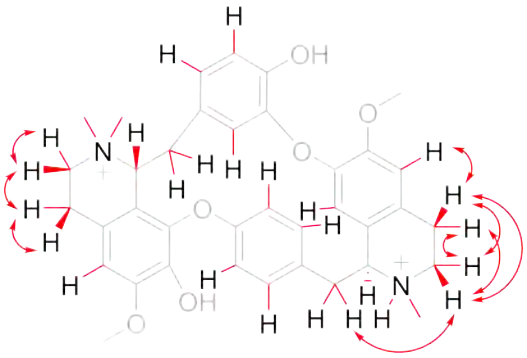

2

Figure S-19: Structure of tubocurarine **2** with all RDCs used for the TITANIA optimization marked in red.

3.1 SECONDA eigenmodes

The eigenmodes of **2-A** and **2-B** give additional insights into the homogeneity and heterogeneity of the RDC data. As expected from literature the eigenmodes 1 to 5 obtained from the homogeneous setup **2-A** have equally distributed elements with no spikes. This is also expected from figure 10 in the main text showing the SECONDA plot of **2-A** and **2-B**, in which the collectivities of **2-A** are all larger than 50 %. This behavior is changed drastically by adding heterogeneity in setup **2-B**. Here most eigenmodes contain large spikes, which can all be assigned to ${}^1D_{\mathrm{CN}}$ couplings. These couplings have the largest relative error in the data set. This is due to the fact that the added random numbers were not scaled down for these RDCs despite the low magnitude of the corresponding D_{max}. The effect of the heterogeneity is even large enough that the principle variance $\lambda_{4,\mathbf{2-A}}$ and the corresponding eigenmode $|4_{\mathbf{2-A}}\rangle$ coincide with $\lambda_{5,\mathbf{2-B}}$ and $|5_{\mathbf{2-B}}\rangle$ (see gray trace in fig. S-20). This means that a principle variance and eigenmode which is mainly elicited by the synthetic error ($\lambda_{4,\mathbf{2-B}}$) is within the first five eigenvalues, thus implying a shift of eigenvalues. Additionally $\lambda_{5,\mathbf{2-A}}$ and $|5_{\mathbf{2-A}}\rangle$ are very similar to $\lambda_{7,\mathbf{2-B}}$ and $|7_{\mathbf{2-B}}\rangle$ (see gray trace in fig. S-20).

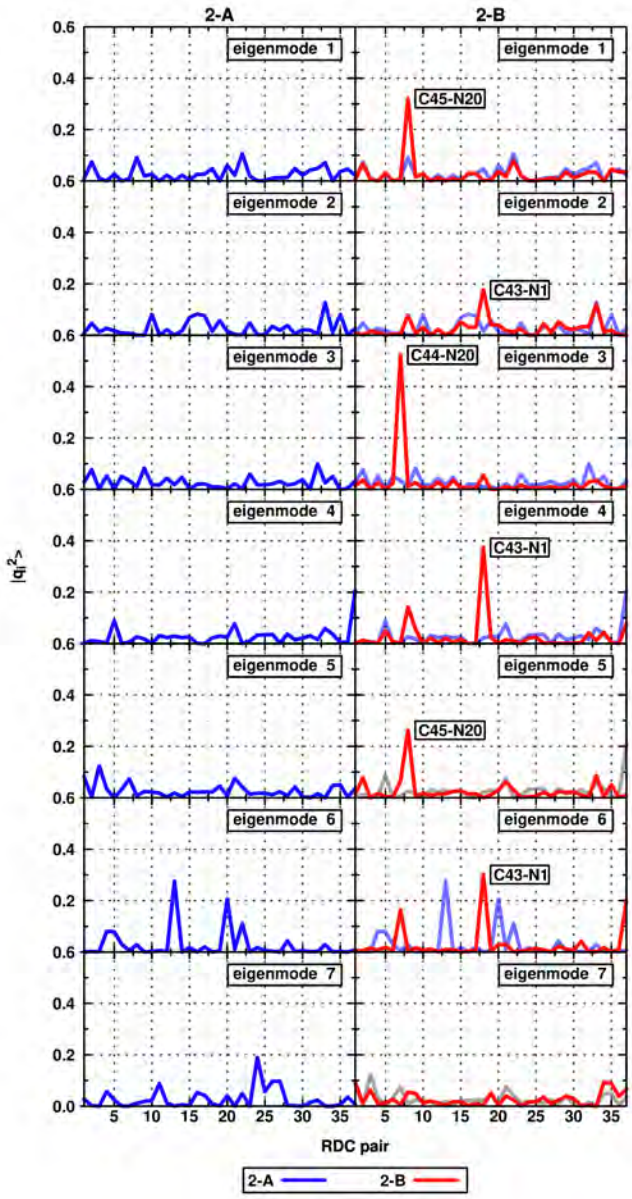

Figure S-20: Eigenmodes of the setups **2-A** (blue) and **2-B** (red) obtained from SECONDA. Note that in the panel on the right (**2-B**) a superposition with the corresponding eigenmodes of **2-A** is shown. For eigenmodes $|5_{\mathbf{2-B}}\rangle$ and $|7_{\mathbf{2-B}}\rangle$ the corresponding eigenmode of **2-A** is $|4_{\mathbf{2-A}}\rangle$ and $|5_{\mathbf{2-A}}\rangle$, respectively. These are shown in gray.

3.2 Orientations

3.2.1 Tubocurarine run 2-A

The RDCs of run **2-A** were calculated by the orientations summarized in table S-82. These orientations were generated from random numbers, where A_{zz} was constrained to be lower than 1e-2.

Table S-82: Orientational data used for the artifical RDC sets of run **2-A** and **2-B**.

Set	$\boldsymbol{A}_{zz}$	$\boldsymbol{R}$	$\boldsymbol{\alpha}/^\circ$	$\boldsymbol{\beta}/^\circ$	$\boldsymbol{\gamma}/^\circ$
set 1	-2.522e-03	2.534e-01	19.620	117.810	39.700
set 2	7.391e-04	4.661e-01	71.810	75.570	146.000
set 3	-7.096e-04	6.177e-01	66.370	138.590	116.000
set 4	-8.076e-04	5.195e-01	61.600	154.440	119.000
set 5	-1.580e-03	3.812e-01	148.030	117.480	149.500
set 6	-8.315e-04	6.143e-01	142.480	103.210	156.400
set 7	-7.961e-04	3.370e-01	45.600	118.300	131.000
set 8	6.659e-04	5.547e-01	164.010	71.820	72.200

Output orientations
All orientiations of setup **2-A** obtained from the full TITANIA optimization runs are listed in the following section. Changes of the Euler angles, compared to the input data listed above, are due to the change of the reference frames (TITANIA used the principle axis system of the molecule). The comparison of the input and output data is summarized in table S-85 (section 3.2.3).

Table S-83: Orientational data of tubocurarine **2** obtained by TITANIA on the last optimization iteration for the runs **2-A**.

Set	$\boldsymbol{A}_{zz}$	$\boldsymbol{R}$	$\boldsymbol{\alpha}/^\circ$	$\boldsymbol{\beta}/^\circ$	$\boldsymbol{\gamma}/^\circ$
set 1	-2.645e-03	3.105e-01	27.927	60.902	131.974
set 2	7.445e-04	4.327e-01	67.523	112.378	33.395
set 3	6.992e-04	6.290e-01	69.164	135.421	34.727
set 4	-7.588e-04	5.840e-01	64.918	33.967	59.359
set 5	-1.457e-03	4.094e-01	139.165	70.484	30.973
set 6	7.758e-04	6.192e-01	171.343	134.193	107.367
set 7	-7.646e-04	3.274e-01	49.797	70.676	46.730
set 8	6.092e-04	5.309e-01	172.420	115.822	109.699

3.2.2 Tubocurarine run 2-B

The RDCs of run **2-B** were generated from the **2-A** RDCs with addition of Gaussian error (σ = 0.5 Hz). All orientiations of setup **2-B** obtained from the full TITANIA optimization runs are listed in the following section. Changes of the Euler angles compared to the literature data listed above are due to the change of the reference frames (TITANIA used the principle axis system of the molecule). The comparison of the input and output data is summarized in table S-85 (section 3.2.3).

Table S-84: Orientational data of tubocurarine **2** obtained by TITANIA on the last optimization iteration of run **2-B**.

Set	$\boldsymbol{A}_{zz}$	$\boldsymbol{R}$	$\boldsymbol{\alpha}/^\circ$	$\boldsymbol{\beta}/^\circ$	$\boldsymbol{\gamma}/^\circ$
set 1	-2.822e-03	3.615e-01	17.286	88.193	145.503
set 2	6.736e-04	4.686e-01	34.365	92.548	32.461
set 3	6.277e-04	6.485e-01	40.373	115.349	21.292
set 4	-6.981e-04	6.483e-01	17.325	30.906	105.648
set 5	-1.792e-03	4.060e-01	123.030	52.257	38.777
set 6	9.544e-04	6.394e-01	137.002	141.092	78.246
set 7	-7.975e-04	2.826e-01	24.163	64.957	64.493
set 8	7.868e-04	5.060e-01	147.746	137.159	90.780

3.2.3 Change in Orientations

To quantify the similarity of the input and the output orientations a common reference frame has to be used. Therefore an all atom *rmsd* structure alignment was performed to match the TITANIA output structure with the reference structure (or its enantiomer). The alignment tensors of the transformed structures are recalculated and the differences in the orientations (TITANIA vs. reference) are expressed by the β angle.

Table S-85: Generalized angle β enclosed by the reference structure of tubocurarine and the structure obtained by TITANIA from the last optimization step of the runs **2-A** and **2-B**. The data were obtained by transformation of the respective structures to a common reference frame, followed by recalculating the alignment tensors with the in-house software `RDC@hotFCHT`.[9]

	$\boldsymbol{\beta}/^\circ$	
Set	**2-A**	**2-B**
set 1	8.986	26.982
set 2	14.368	43.365
set 3	10.712	40.292
set 4	14.001	48.061
set 5	5.750	23.571
set 6	9.489	36.148
set 7	9.769	35.040
set 8	12.558	30.525

The β angles for comparison of the reference and final structure in run **2-A** are induced by structural change. Additionally to fluctuations of the spherical angles (angular part of the RDC definition) the bond lengths and distances (radial part of the RDC definition) show deviations from the reference structure. These changes lead to differences in the alignment parameters. **2-B** shows even higher β angles, which are caused by the same fluctuations, but additionally heterogeneities in the RDCs come into play. This is even more pronounced by the fact, that the final **2-B** structure shows large distortions in the methoxy groups, leading to a change in the process of finding a proper common reference frame. These distortions are marked in fig. S-21.

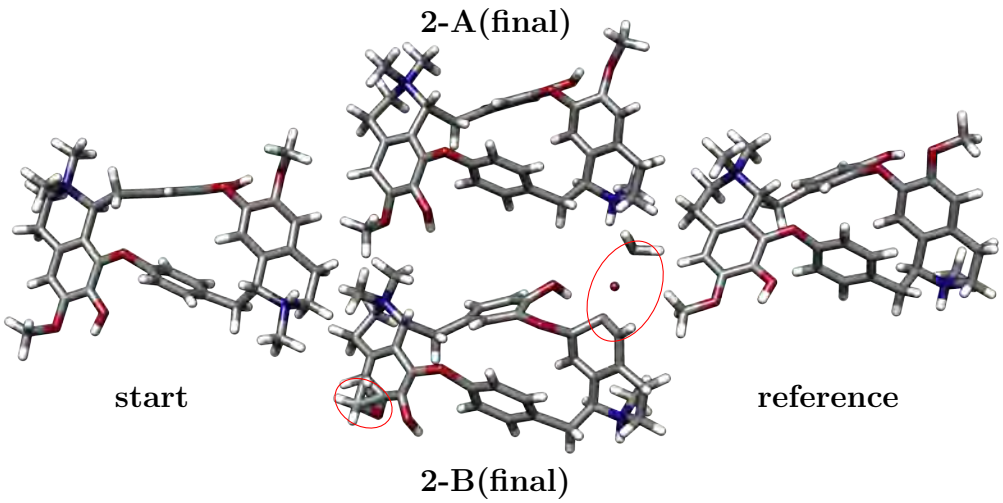

Figure S-21: Comparison of tubocurarine **2** structures. Shown are the start structure of the optimizations (left), the reference structure used of the prediction of the RDCs (right) and the final structures obtained from the TITANIA optimization runs (middle). In the structure of **2-B** the methoxy groups marked showed large distortions which did not disturb the overall structure optimization.

Table S-86: Generalized angle β enclosed by the orientations of tubocurarine **2** obtained by TITANIA in the last optimization step of the runs **2-A** and **2-B**. The structures were transformed into a common reference frame by all atom *rmsd* alignment. Additionally the β angle was calculated from the reference structure to separate the change induced by errors.

	$\boldsymbol{\beta}/^\circ$	
Set	**TITANIA**	**Reference**
set 1	27.9157	10.545
set 2	40.1463	12.704
set 3	34.3988	6.933
set 4	31.1403	14.173
set 5	23.0264	2.6737
set 6	33.5241	6.9610
set 7	32.2838	4.0627
set 8	18.0189	3.0128

The previously discussed β angles in table S-85 (**2-B**) can again be found in table S-86 when comparing the final TITANIA structures. Separating the influence of the structure, as above, from the heterogeneities by using the

reference structure (see column **Reference** in table S-86) relatively small β angles are found. This means, that the difference of the individual **2-A** and **2-B** sets is mainly elicited by the changes in the mean structure.
Comparing the final structure of **2-A** and the reference structure it becomes clear, that TITANIA is capable of a simultaneous interpretation of the RDC data in the context of conformational and configurational structure determination, as long as sufficient data is available.

3.3 RDC list

The RDC lists of the IPC **2** runs were equal for the respective sets of alignment media. All RDCs used for **2-A** and **2-B** are listed in table S-81.

Table S-87: List of all RDCs used in the runs of **2-A** and **B**.

RDC pair	RDC pair
C21-H21a	**C21-H21e**
C22-H22a	**C22-H22e**
C25-H25	**C19-H19**
C44-N20	**C45-N20**
C18-H18r	**C18-H18s**
C31-H31	**C32-H32**
C34-H34	**C35-H35**
C36-H36r	**C36-H36s**
C6-H6	**C43-N1**
H1-N1	**C2-H2a**
C2-H2e	**C3-H3a**
C3-H3e	**C10-H10**
C7-H7	**C17-H17**
C15-H15	**C14-H14**
H21a-H21e	**H22a-H22e**
H21e-H22a	**H3e-H7**
H2e-H3e	**H2e-H3a**
H2a-H3e	**H2a-H3a**
H2a-H36r	

4 Strychnine (3)

Strychnine **3** is an example used to demonstrate the optimization of a highly fused carbon scaffold. Since previous examples already have shown that optimizations can still be performed when heterogeneities are present in the RDC data, we refrain from repeating to take this discussion again and perform the optimization only with artificial RDCs.

4.1 SECONDA plot

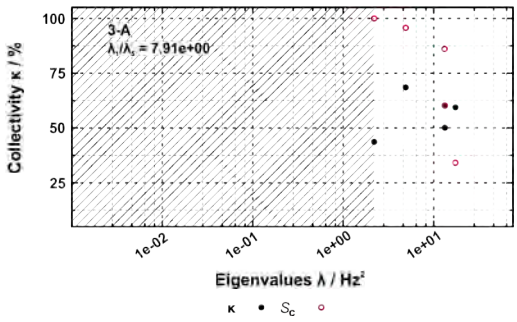

Figure S-22: SECONDA plot of strychnine run **3-A**. Plotted are the collectivities κ in respect to the eigenvalues λ (black) of the RDC covariance matrix. In addition the cumulative sum (red) of the eigenvalues were plotted to measure the participation of the principle variances to the overall variance of the RDC matrix.

The SECONDA plot shows a linear independence of the setup, which is comparable to **1-A** ($\lambda_{1,\mathbf{1-A}}/\lambda_{5,\mathbf{1-A}}$ between 5 and 9). As expected no additional non-zero eigenvalues λ_n (n $>$ 5) are observed since homogeneous back-calculated RDC data was used.

4.2 Orientations

4.2.1 Strychnine run 3-A

Input orientations
The RDCs of run **3-A** were calculated by the orientations summarized in table S-88.

Table S-88: Orientational data used for the artifical RDC sets of run **3-A**.

Set	$\boldsymbol{A}_{zz}$	$\boldsymbol{R}$	$\boldsymbol{\alpha}/^\circ$	$\boldsymbol{\beta}/^\circ$	$\boldsymbol{\gamma}/^\circ$
set 1	4.702e-04	249e-01	101.85	-126.97	-138.66
set 2	5.529e-04	281e-01	90.67	-11.21	87.58
set 3	1.761e-04	478e-01	148.27	-63.18	110.96
set 4	9.310e-04	408e-01	22.86	122.49	-12.90
set 5	2.507e-04	329e-01	178.66	-142.29	136.69
set 6	2.094e-04	517e-01	132.02	62.69	-147.29
set 7	2.134e-04	246e-01	140.50	-45.14	-84.16
set 8	4.079e-04	628e-01	115.52	-87.76	-135.31
set 9	4.750e-04	578e-01	142.36	106.33	-25.05
set 10	5.166e-04	486e-01	71.08	173.66	91.56
set 11	2.898e-04	310e-01	159.43	-1.56	-35.12

Output orientations
All orientiations of run **3-A** obtained from the full TITANIA optimization runs. The orientations differ from table S-88 due to the change of the reference frame (TITANIA used the PAS of the inertia tensor). The comparison in the same reference frame can be found in table S-90 (section 4.2.2).

Table S-89: Orientational data of strychnine **3** obtained by TITANIA on the last optimization iteration for the runs **3-A**.

Set	$\boldsymbol{A}_{zz}$	$\boldsymbol{R}$	$\boldsymbol{\alpha}/^\circ$	$\boldsymbol{\beta}/^\circ$	$\boldsymbol{\gamma}/^\circ$
set 1	5.681e-04	3.097e-01	100.083	127.472	126.526
set 2	4.648e-04	2.561e-01	135.899	97.251	86.745
set 3	1.724e-04	4.639e-01	21.351	76.388	140.959
set 4	9.215e-04	3.958e-01	75.032	126.756	47.192
set 5	2.600e-04	3.487e-01	79.325	153.659	57.116
set 6	2.064e-04	5.263e-01	82.353	93.409	75.199
set 7	2.105e-04	2.432e-01	118.222	4.328	148.826
set 8	4.264e-04	5.862e-01	150.163	62.968	67.569
set 9	4.755e-04	5.694e-01	3.303	124.333	24.379
set 10	5.356e-04	4.846e-01	79.299	132.038	128.516
set 11	2.938e-04	3.565e-01	145.537	139.275	125.117

4.2.2 Change in Orientations

To quantify the similarity of the input orientations with the output orientations a common reference frame is defined by an all atom rmsd structure alignment. The differences in the respective orientations are quantified by the generalized β angle.

Table S-90: Generalized angle β enclosed by the orientations of strychnine **3** obtained by TITANIA in the last optimization iteration of the runs **3-A** (see table S-89) and the orientations of RDC@HOTFCHT (see table S-88).[9]

	$\beta/^\circ$
Set	**3-A**
set 1	12.852
set 2	3.791
set 3	9.654
set 4	7.449
set 5	12.323
set 6	8.967
set 7	18.427
set 8	11.460
set 9	8.322
set 10	13.211
set 11	11.352

The β angles show rather low differences in between the reference and final structure of TITANIA. The main reason for deviations can be found in the strychnine structures shown in the main text figure 14. Here the plane of the aromatic ring is tilted. This leads to the differences in the calculated alignment tensors.

4.3 RDC list

The RDC list of the strychnine **3** run are listed in table S-91.

Table S-91: List of all RDCs used in the runs of **3-A**.

RDC pair	RDC pair
C1-H1	**C2-H2**
C3-H3	**C4-H4**
H1-H2	**H2-H3**
H3-H4	**C8-H8**
C11-H11a	**C11-H11b**
H11a-H11b	**C12-H12**
H11a-H12	**H11b-H12**
C13-H13	**H12-H13**
C14-H14	**H13-H14**
C15-H15a	**C15-H15b**
H15a-H15b	**H14-H15a**
H14-H15b	**C16-H16**
H15a-H16	**H15b-H16**
C17-H17a	**C17-H17b**
H17a-H17b	**C18-H18a**
C18-H18b	**H18a-H18b**
H17a-H18a	**H17b-H18a**
H17b-H18b	**C20-H20a**
C20-H20b	**H20a-H20b**
C22-H22	**C23-H23a**
C23-H23b	**H23a-H23b**
H22-H23a	

5 Content of Supplementary Material

The supplementary material is available as a zip-archive which contains all information used to perform the TITANIA runs with the respective outputs. A `README.md` file was added to the archive using the markdown syntax. This is also added here:

```
# TITANIA: Model Free Interpretation of Residual
    Dipolar Couplings in the context of Organic
       Compounds - Supplementary Material
## Felix A. Roth, Volker Schmidts and
           Christina M. Thiele

## Top Level Directories
- 1-A_IPC_20_sets
- 1-B_IPC_6_indep_sets
- 1-C_IPC_6_dep_sets
- 1-D_IPC_20_sets_err
- 1-E_IPC_6_indep_sets_err
- 1-F_IPC_6_dep_sets_err

All directories listed above (IPC setups) contain
individual subdirectories for the individual runs:
- ipc_xx_rdcs
- yy_ipc_xx_rdcs

where xx is the number of RDCs (11, 17, 23, 31 and 39)
and yy are are variations of the runs with different
settings (random [coordinates] for the input structure
and non_redundant for the structure generation algorithm).
The individual subdirectories contain the input files
(input.tna), output files (input.tna.out), files for alignment
media specific information (input.tna.out.medium_label.ali),
the trajectory file (input.tna.out.trj) and the Cartesian
coordinates of every iteration step (input.tna.out.xyz).
Additional directories for tubocurarine and strychnine
directly contain the respective files mentioned above.
These directories are:
-  2-A_tubocurarine_8_sets
-  2-B_tubocurarine_8_sets_err
-  3-A_strychnine_11_sets
```

Some individual runs use different keywords, RDC data and structures. These are located in the remaining directories:

- keywords
- rdcs
- structures

For more information on the syntax of the input and output files see Supporting Information section 1.2

References

[1] T. A. Halgren, *Journal of Computational Chemistry* **1996**, *17*, 490–519.

[2] J. R. Tolman, *Journal of the American Chemical Society* **2002**, *124*, 12020–12030.

[3] V. Bakken, T. Helgaker, *Journal of Chemical Physics* **2002**, *117*, 9160–9174.

[4] C. Peng, P. Y. Ayala, H. B. Schlegel, M. J. Frisch, *Journal of Computational Chemistry* **1996**, *17*, 49–56.

[5] K. V. Mardia in *Statistics of Directional Data*, (Ed.: K. V. Mardia), Probability and Mathematical Statistics: A Series of Monographs and Textbooks, Academic Press, **1972**, pp. 18–38.

[6] S. Hansmann, T. Larem née Montag, C. M. Thiele, *European Journal of Organic Chemistry* **2016**, *2016*, 1324–1329.

[7] M. Schwab, D. Herold, C. M. Thiele, *Chemistry – A European Journal* **2017**, *23*, 14576–14584.

[8] A. Marx, V. Schmidts, C. M. Thiele, *Magnetic Resonance in Chemistry* **2009**, *47*, 734–740.

[9] R. Berger, C. Fischer, M. Klessinger, *Journal of Physical Chemistry A* **1998**, *102*, 7157–7167.

[10] J.-C. Hus, R. Brüschweiler, *Journal of Biomolecular NMR* **2002**, *24*, 123–132.